ABSTRACT

DUKE, KATHERINE SUE HLAVINKA. A Tale of Two Carbon Nanotubes: Inflammatory, Fibrogenic, and Immune Responses to Tangled and Rod-like Multi-Walled Carbon Nanotubes in Genetically Susceptible Mouse Models. (Under the direction of Dr. James C. Bonner).

Engineered nanomaterials (ENMs) are currently incorporated into numerous consumer goods and have several beneficial uses. However, the safety of these emerging materials is not fully understood. One class of ENM, multi-walled carbon nanotubes (MWCNTs), have a fiber-like shape and similar properties to asbestos and thus potentially pose similar health risks. Physicochemical characteristics differ between different types of MWCNTs and determine their pulmonary toxicity. The extent of MWCNT-induced toxicity and resultant disease in the lung can be worsened by genetic susceptibility factors. For example, mice lacking the signal transducer and activator of transcription 1 (STAT1) are more susceptible to injury-induced pulmonary fibrosis and mice heterozygous deficient in the tumor suppressor p53 are highly susceptible to sarcomas and mesothelioma development from exposure via intraperitoneal injection of asbestos or MWCNTs. Pulmonary exposure of both wild type or genetically susceptible mouse models to tangled (t-) or rod-like (r-) MWCNTs was hypothesized to result in differing pulmonary immune, fibrotic, and neoplastic responses that would be exaggerated STAT1- and p53-deficient susceptible mouse models. A measurement of rigidity was determined for these MWCNTs, and the rMWCNTs were found to be 7-fold more rigid than the tMWCNTs. Oropharyngeal aspiration of vehicle, 4mg/kg tMWCNTs or 4mg/kg rMWCNTs in wild type and STAT1 knockout (*Stat1*$^{-/-}$) mice was completed and samples collected one- and 21 days later. We found that exposure to rMWCNTs results in larger granulomas, mucous cell metaplasia and more inflammogenic and fibrogenic responses compared to tMWCNTs. Increased rMWCNT-induced airway fibrosis was measured and

found to be significant in wild type mice, and significantly greater in *Stat1*$^{-/-}$ mice. Increased airway fibrosis was found to be due to a mechanism involving STAT1-dependent suppression of transforming growth factor (TGF) -β1 and reduced activation of its downstream signaling molecule, Smad2/3. Oropharyngeal aspiration of vehicle, 1 mg/kg tMWCNTs, or 1 mg/kg rMWCNTs once a week for a total of 4 mg/kg over 4 weeks was completed in wild type and p53 heterozygous knockout mice. Lung tissues were collected from mice 11 months following the initial exposure. MWCNTs were found in singlet and aggregate forms in the lung tissue after chronic exposure and rMWCNTs were found to result in larger granulomas, increased inducible lymphoid tissue, greater proliferation of granulomatous associated cells, and greater epithelial cell hyperplasia compared to tMWCNTs. We also found vehicle-treated p53 heterozygous mice to have significantly higher area of endogenous inducible lymphoid tissue in the lung compared to wild type mice. These studies highlight the mechanism of MWCNT-mediated fibrosis and the hyperplastic and immunogenic differences these materials pose in the lung. These results cumulatively demonstrate the importance of physicochemical properties of MWCNTs and genetic susceptibility in determining immunologic, fibrogenic or neoplastic disease.

© Copyright 2017 by Katherine Sue Hlavinka Duke

All Rights Reserved

A tale of two carbon nanotubes: Inflammatory, fibrogenic, and immune responses to tangled and rod-like multi-walled carbon nanotubes in genetically susceptible mouse models

by
Katherine Sue Hlavinka Duke

A dissertation submitted to the Graduate Faculty of
North Carolina State University
in partial fulfillment of the
requirements for the degree of
Doctor of Philosophy

Toxicology

Raleigh, North Carolina

2017

APPROVED BY:

_____	_____
James C. Bonner, Ph. D Committee Chair	Rob Smart, Ph. D
_____	_____
Jun Ninomiya-Tsuji, Ph. D	Philip Sannes, Ph. D

DEDICATION

I would like to dedicate my dissertation to my loving and supportive family and friends who continuously support me through life's endeavors.

BIOGRAPHY

Katherine Duke began her scientific journey early in life, with a great appreciation and wonderment of nature and how things worked. She began her first research project as a high school senior in a synthetic biology laboratory. It was during this early experience that Katherine's passion for scientific inquiry grew as did her understanding and methodology of molecular biology. Following high school graduation she continue her education completing a bachelor of science degree in Biology from Elon University while also pursuing undergraduate research on the cardiotoxic effects of a flame retardant in fish models. This toxicologic research ignited the motivation for Katherine to continue this research after graduation while also working in the clinical trials department in a diagnostic laboratory. Katherine's passion for research drove her to quickly apply to graduate programs and that following fall she joined the graduate program in Biology at the University of North Carolina at Greensboro. There she completed her Master of Science degree on the role of reactive oxygen species on the development of insulin resistance. This drove Katherine to continue her education specializing in Toxicology at North Carolina State University where she works under the mentorship of Dr. Bonner on the pulmonary fibrotic and immune effects of carbon nanotubes in genetically susceptible mouse models for her PhD. Her drive and passion for pulmonary research has flourished in this program and continues to drive her interest in scientific inquiry.

ACKNOWLEDGMENTS

I would like to begin by first thanking my advisor, Dr. James C. Bonner. A stable pillar of support and encouragement through each step of every endeavor I chased. His continual support of my career advancement and professional development has provided me opportunities to partake in to further both my professional and personal growth as a scientist and as a person. I am extremely grateful for his guidance and could not define a better mentor for myself. I am forever thankful for the lessons learned from Dr. Bonner and they will forever guide me in my life and career.

I would also like to thank my committee members Dr. Robert Smart, Dr. Jun Ninomiya-Tsuji, and Dr. Philip Sannes for their guidance and support. I recognize and am greatly appreciate the time and effort they have put into helping my graduate career develop over the past four years to help me be successful in the program.

I would also like to thank current, honorary, and previous laboratory members, Lexie Taylor-Just, Dr. Kelly Shipkowski, Mark Ihrie, Dr. Gina Hilton, Dr. Erinn Dandley-Needham, Dorothy You, and Dr. Elizabeth Thompson for their guidance and assistance throughout this journey. As constant sources of guidance and support they have been the key source of a happy lab environment as well as making my time here at NCSU enjoyable.

The Toxicology program has been a wonderful experience and would not be the same without key support from all members involved. A special thank you is reserved for Janet Roe and Jeanne Burr who have helped make every step of the process on time and as seamless as possible.

Last but not least, the experience would have been much more intense and stressful without the love and support of my family: my parents, sister, in-laws, brother-in-law, as well as my friends. The journey would not have been the same without my husband, Bobby, who has been there through it all and who has been a bottomless source of support and encouragement for me the whole journey through.

TABLE OF CONTENTS

LIST OF TABLES

LIST OF FIGURES

APPENDIX A: Supplemental Figures and Tables: Chapter II

APPENDIX B: Supplemental Figures and Tables: Chapter III

APPENDIX C: Supplemental Figures and Tables: Chapter IV

LIST OF ABBREVIATIONS

α-sma – α-smooth muscle actin
AAM – alternatively activated macrophage
ALD – atomic layer deposition
Al_2O_3 – aluminum oxide
CAM – classically activated macrophage
CNT – carbon nanotube
CCR7 – chemokine receptor 7
COLI – mesenchymal marker collagen I
COPD – chronic obstructive pulmonary disease
CVD – chemical vapor deposition
ECM – extracellular matrix
EGF – endothelial growth factor
ELT – ectopic lymphoid tissue
EMT – epithelial to mesenchymal transition
ENM – engineered nanomaterial
FSP – fibroblast specific protein
HMGB1 – high-mobility group box 1
IARC – International agency for research on cancer
IL – interleukin
IL-1R – interleukin – 1 receptor
IFN – interferon
IFNAR – transmembrane interferon receptor
iBALT – inducible bronco-associated lymphoid tissue
iNOS – inducible nitric oxide synthase
i.p. – intraperitoneal
IPF – idiopathic pulmonary fibrosis
JAK – Janus kinase
LPS – lipopolysaccharide
MCA – 3- methylcholanthrene
MLD – molecular layer deposition
MMP – matrix metalloproteinase
MPM – malignant pulmonary mesothelioma
MPO – myeloperoxidase
MWCNT – multi-walled carbon nanotube
NAC – N-acetyl cysteine
NADPH – nicotinamide adenine dinucleotide phosphate
NF-κB – nuclear factor kappa B
Nrf2 – nuclear factor (erythroid-derived 2)-like 2
NSCLC – non-small cell lung cancer
OPN – osteopontin

p53 – tumor suppressor p53
PDGF – platelet derived growth factor
PEG – polyethylene glycol
PEI – polyetherimide
PLC – phospholipase C
PPAR – peroxisome proliferator-activated receptor
R-COOH – carboxylated
R-NH_3 – aminated
RA – rheumatoid arthritis
RLE-6TN – epithelial cell specific adhesion molecule
RNS – reactive nitrogen species
ROS – reactive oxygen species
RXR – retinoid x receptor
SARA – Smad anchor for receptor activation
SBPL – static bending persistence length
SCLC – small cell lung cancer
Smad – *Drosophila* protein, mothers against decapentaplegic (MAD), *C. elegans* protein, small body size (SMA)
SNP – single nucleotide polymorphism
SRE – Smad response element
STAT – signal transducer and activator of transcription
SWCNT – single-walled carbon nanotube
TEM – transmission electron microscope
TGF – transforming growth factor
TIMP – tissue inhibitor of metalloproteinases
TIPS – trans tracheal intrapulmonary spraying
TLO – tertiary lymphoid organ
TLR – toll like receptor
TNF – tumor necrosis factor
ZnO – zinc oxide

CHAPTER 1

Introduction

Adapted from WILEYs Nanomedicine and Nanobiotechnology Review: Duke KS and Bonner JC. (2017) Mechanisms of Carbon Nanotube-Induced Pulmonary Fibrosis: A Physicochemical Characteristic Perspective

1.1 Introduction to Carbon Nanotubes

Carbon nanotubes (CNTs) are a class of engineered nanomaterial (ENM) that comprise a major portion of the nanotechnology market. CNT production rates increase each year for incorporation into a variety of consumer products. Of interest, CNTs have unique optical, physical, and conductive properties that enhance the functionality of polymers, batteries, and electronics [1]. Single-walled CNTs (SWCNTs) are a rolled graphene sheet with a diameter similar to that of a DNA double helix (1 to 4 nm), whereas multi-walled CNTs (MWCNTs) are composed of multiple concentric layers of graphene and may have a diameter typically between 10 and 100 nm. Both SWCNTs and MWCNTs may have lengths in the micrometer range. CNTs are synthesized by processes, such as chemical vapor deposition, that require high temperatures and metal catalysts to initiate the reaction process to 'grow' a forest of CNTs. Increased manufacturing of CNTs implicates an increasing risk of occupational exposure and development of pulmonary diseases. Exposure to CNTs occurs primarily at the manufacturing level where they are first synthesized [2]. However, the potential for exposure also occurs during or after incorporation into consumer products, during recycling, or after disposal. Therefore,

potential human exposure to CNTs throughout their life cycle may be of concern particularly because of their striking similarities to a known pulmonary toxicant, asbestos. Of specific interest to the safety and risk assessment community is the potential for CNTs, like asbestos, to result in pulmonary diseases like fibrosis and cancer (e.g. adenocarcinoma and mesothelioma).

Overview of CNT-Induced Pulmonary Fibrosis in Rodents

Experimental evidence in rodents shows that inhalation or aspiration exposure to CNTs causes pulmonary fibrosis, a disease characterized by excessive deposition of collagen and progressive lung tissue scarring [3–5]. Pulmonary fibrosis is defined by the American Thoracic Society as the production and deposition of collagen in the lung resulting in the buildup of scar tissue, thereby reducing the exchange of oxygen and carbon dioxide between the alveolar airspace and pulmonary capillaries [6]. From a historical perspective, it is well-established that inhalation of specific types of particles and fibers such as silica, metals, coal dust, or asbestos leads to the development of pulmonary fibrosis [7–10]. Thus, there is already a fundamental understanding of some of the cellular and molecular mechanisms of pulmonary fibrosis caused by particle or fiber exposure. However, due to the unique physicochemical characteristics of CNTs, including but not limited to their nanoscale dimensions, these ENMs may interact with the intracellular microenvironment or extracellular matrix to mediate fibrotic reactions in the lungs or other tissues through novel mechanisms that remain to be elucidated. As CNTs are relatively new in terms of their emergence into society, there is no comprehensive

epidemiologic data to convincingly support the conclusion that all types of CNTs will cause pulmonary fibrosis, as human exposures thus far have been limited, and the development of pulmonary fibrosis in humans may take decades to manifest respiratory symptoms after the initial exposure due to the long latency period of the disease. Understanding specific CNT physicochemical characteristics that are important for initiating and perpetuating lung injury will be important towards determining the relative risk for pulmonary fibrosis. Deposition of inhaled ENMs in the lung depends on many factors, one of which is size. Particles on the nanomaterial scale are able to be inhaled deep into the lung, reach the alveolar region, and interact directly with alveolar macrophages and epithelial cells [11,12]. Because of their small size, CNTs also have the potential to be transported from the lungs into the systemic circulation or lymphatic system and reach organs such as the liver, kidney, heart, brain, and the thymus [11,13]. With increasing production and use of CNTs, it is imperative that we understand mechanisms of CNT-induced pulmonary fibrosis in order to evaluate a wide spectrum of different CNT types for relative risk in order to prevent a future respiratory disease.

Exposure Methodology as a Determinant of CNT-Induced Pulmonary Fibrosis

Fibrosis has been documented in the lungs of rodents after exposure to CNTs delivered by several methods, including inhalation, instillation, or oropharyngeal aspiration. Inhalation exposure is ideal as it represents a more realistic exposure in terms of deposition patterns in the lung that would occur in occupational settings. The deposition of inhaled CNTs is determined by several factors including size, shape, electrostatic charge, and aggregation state.

Inhalation exposure to well-dispersed MWCNTs results in deposition into the distal regions; i.e., alveolar duct bifurcations and alveolar epithelial surfaces of the lungs of mice or rats [4,14]. Less aggregated or more dispersed nanotubes are more biologically available for macrophage uptake and clearance from the lung. Inhalation of dry or aerosolized CNTs in surfactant-containing media causes diffuse interstitial fibrotic lesions within the alveolar and subpleural regions of the lung. Exposure by instillation or oropharyngeal aspiration, which involves a bolus delivery of CNTs suspended in aqueous media, can also result in deposition at distal sites in the lungs if the nanoparticles are well-dispersed, but typically stimulate focal granuloma formation. Furthermore, experiments conducted in multiple laboratories at different institutions using harmonized methods and identical sources of CNTs have demonstrated interlaboratory reproducibility in deposition patterns and pro-inflammatory responses in the lungs of mice and rats [15]. Many studies have reported granulomas in the lungs of rodents resulting from agglomerated SWCNTs or MWCNTs lodged within small airways, but this is not observed in most inhalation studies probably due to better dispersion of the respirable fraction of inhaled CNTs, which primarily includes singlet CNTs or small agglomerates of CNTs. Methods for dispersing CNTs in an aqueous suspension using surfactant-containing media prior to instillation or aspiration in rats or mice have greatly improved, making this route of exposure generally acceptable [16]. Moreover, long term *in vivo* studies demonstrate that while CNTs clear from the lung to some extent via the mucociliary escalator or pulmonary lymphatics, longer nanotubes remain in the lung tissue of rodents over time due to their

biopersistent nature [13,17,18]. Rodent exposure methods (e.g., inhalation vs aspiration) should be taken into consideration when comparing the relative fibrotic effects of CNTs.

Exposure Methodology as a Determinant of CNT-Induced Carcinogenesis

Interestingly, to date there are few inhalation, instillation or inspiration studies with evidence of CNT inducing tumors, however, surrogate assays deploying intraperitoneal (i.p.) injections of asbestos or MWCNTs into the abdomen, pleural space, or scrotum of mice or rats do show incidences of mesothelioma development [19–24]. Inhalation exposure of CNTs is optimal due to its more relevant exposure; however, this method has not been observed to result in the development of mesothelioma from either CNT or asbestos exposures. Recently, one study of MWCNT (MWCNT-7) inhaled by F344 rats for 104 weeks resulted in instances of epithelial hyperplasia, bronchiole-alveolar carcinoma and adenoma [25]. Another study employing a trans tracheal intrapulmonary spraying (TIPS) technique to deliver MWCNTs in male F344/Crj rats resulted in large agglomerates of MWCNTs in the lungs and observed about 50% of the animals develop neoplasms including malignant mesothelioma, adenoma, and adeno-carcinoma [26]. While lung deposition is similar between methodologies, there are differences in the aggregate status of the CNTs. Inhalation exposure results in greater dispersion of singlet CNTs while aspiration results in greater aggregation. Exposure method is an important consideration when determining carcinogenic potential of CNTs.

1.2 Physicochemical Properties of CNTs as Determinants of Disease Severity

Physicochemical properties of CNTs are key in determining their reactive potential. Size, charge, length, rigidity, residual metal catalyst content, and surface functionalization can each greatly impact the toxicity and fibrogenic and carcinogenic potential of these materials.

Residual Metal Catalyst Content

A variety of metals are used as catalysts in the manufacturing of CNTs by chemical vapor deposition (CVD). For instance, cobalt is used as a catalyst in the synthesis of MW- and SW-CNTs, while nickel or iron have been used as catalysts in the synthesis of MWCNTs. These same metals are known to mediate pulmonary fibrosis in humans in occupational settings [27]. For example, nickel is known to cause occupational asthma and contact dermatitis, whereas iron and cobalt cause interstitial pulmonary fibrosis in occupations related to mining and metallurgy. Metal catalysts used in the CVD manufacturing process become integrated into the carbon structure of nanotubes and mediate at least some of the proinflammatory effects seen after exposure to MWCNTs in rodents. For example, activation of macrophage inflammasomes and subsequent interleukin- (IL-) 1β production induced by MWCNT-exposure is due at least in part to residual nickel contamination [28]. Acid washing of MWCNTs removes some, but not all, of residual nickel and interlaboratory comparisons of the pro-inflammatory effects of acid-washed MWCNTs versus pristine MWCNTs show that neutrophilic inflammation in the lungs of mice is reduced by partial removal of nickel [29,30]. The biological availability of trace metals on or in CNTs limits their interactions in the lung and resulting pathology *in vivo*. Residual

metal content has the potential to drive CNT pulmonary toxicity and should be a consideration in the design of CNTs.

Length

CNTs can have a length that greatly exceeds their nanoscale diameter (10-100 nM) and this high length to width aspect ratio is an important determinant of their toxic potential. Only a few studies have addressed variations in length as a determinant of fibrosis. One study comparing two MWCNTs, a long (5-15 μm) and a short (350-700 nm) MWCNT, found pulmonary fibrosis to be length-dependent. In this study, mice treated with long MWCNTs via instillation resulted in a significant increase in expression of the profibrotic mediator transforming growth factor (TGF) -β1 and collagen deposition in the lungs compared to those treated with the shorter MWCNTs [31]. Another study examined the effects of a long (~12 μm) and a short (~1 μm) SWCNT on fibroblasts *in vitro* and found the longer SWCNTs to induce greater reactive oxygen species, collagen, and TGF-β [17]. These data were also validated *in vivo* by oropharyngeal aspiration exposure of mice to the long or short SWCNTs; while both treatments resulted in collagen deposition in the lungs of these mice, greater fibrosis was measured in the lungs from the mice treated with the longer SWCNTs [17]. Furthermore, instillation of long (20-50 μm) MWCNTs in rat lungs resulted in macrophage activation and profibrotic mediator (TGF-β1) production as well as greater fibroblast proliferation, collagen production, and granuloma formations compared to rats treated with short (0.5-2μm) MWCNTs [32]. Interestingly, direct instillation of two types of long or two types of short CNTs

into the parietal pleura resulted in greater inflammation and fibrogenesis from both the long CNTs and greater clearance of the shorter CNTs [24]. Length is also a key property of these nanomaterials that determines their clearance from the lung where longer MWCNTs are retained in the lung and unable to exit through stomata in the lung lymph system and persist in the lung and pleural space [24]. Length is clearly a property of CNTs that plays a key role in determining the exposure risk of CNT pulmonary fibrogenesis and toxicity.

Rigidity

Toxicity and fibrogenic potential of CNTs can also be derived from how long, rigid or tortuous they are versus how short, flexible and pliable they are. MWCNTs from different manufacturing sources possess different degrees of rigidity even though they may have similar width and length; some are 'curly' whereas others are straight. This comparison is reminiscent of the comparison between asbestos fiber types; chrysotile asbestos is a curly fiber whereas crocidolite asbestos is a more toxic straight rigid fiber. A useful metric for assessing rigidity that has been adopted by the International Standards Organization is the static bending persistence length (SBPL) and bending ratio, which are derived by measuring convolutions within the nanotube structure from transmission electron microscope (TEM) images [33]. Thick straight MWCNTs delivered to the lungs of female mice via intratracheal instillation cause similar inflammatory responses yet result in more severe pulmonary fibrosis and interstitial pneumonia compared to thinner, more curled MWCNTs [34]. Long, rod-like MWCNTs disrupt macrophage function because their length makes them more resistant to compaction within the

cell resulting in CNT protrusion from the macrophage causing frustrated phagocytosis, disruption of cell membranes, and cell death [35,36]. Cell membrane disruption also causes leakage of cellular constituents (e.g., reactive oxygen species, enzymes, cytokines) that can cause injury to surrounding cells and tissues. Rod-like MWCNTs also result in mucous cell metaplasia while tangled MWCNTs do not [37–39]. While CNT length is an important determinant of clearance rate from the lungs, length alone does not necessarily determine CNT persistence [32,40]. For example, long SWCNTs or tangled MWCNTs can be compacted and contained within phagolysosomes after uptake by macrophages without causing frustrated phagocytosis (Fig. 1.1). Rigid, rod-like, MWCNTs disrupt macrophage function if the nanotube length exceeds the width of the engulfing phagocyte, however short, rigid MWCNTs are capable of being taken up and cleared by macrophages without causing frustrated phagocytosis. Therefore, both rigidity and length are important determinants when considering the fibrogenic potential of these ENMs.

Surface Functionalization

Functionalization refers to surface modification (e.g. coatings or side-chain additions) of CNTs and is important in enhancing specific properties of CNTs. These modified nanomaterials can be useful as polymer composites, sensors, and for biomedical applications. Functionalization of CNTs can be accomplished via two predominant methods; atomic layer deposition (ALD) or molecular layer deposition (MLD), however others are being developed or optimized [41]. CNTs have been functionalized with carboxyl (R-COOH), amine ($R\text{-}NH_3$), polysaccharide

hyaluronic acid groups, metal oxides (aluminum oxide, zinc oxide, titanium dioxide) and silver (summarized in Table 1.1). The nature of the coating can influence the biocorona, which refers to proteins, lipids, and other biomolecules that adsorb to the nanomaterial [42]. CNT coatings alter profibrotic mediators released from THP-1 monocytes (IL-1β) and epithelial BEAS-2B cells (TGF-β1, platelet derived growth factor (PDGF)-AA) *in vitro*, suggesting that these coatings will similarly modify cytokine release and pulmonary fibrosis *in vivo* [43]. Nearly all the published work on CNTs have used 'pristine' or unmodified CNTs. These studies are relevant to human occupational exposures where individuals will be exposed to CNTs directly after synthesis. However, most CNTs will likely undergo some sort of post-synthesis functionalization to modify or enhance their unique properties. This means that most consumer and environmental exposures will be related to some type of functionalized CNTs. Surface functionalization can also influence agglomeration status of CNTs. For example, agglomeration of CNTs due to electrostatic forces presents a problem for the purposes of many engineering designs and a variety of dispersal agents (e.g., surfactants) have been employed to improve dispersion by reducing electrostatic attraction [16,44]. More dispersed CNTs delivered to mice cause a more severe chronic interstitial fibrosis in the lungs along with elevated levels of growth factors (PDGF and TGF-β1) that play important roles in the promotion of fibrogenesis [45]. However, some functionalizations can reduce the fibrogenic response of CNTs, even though they remain dispersed. For example, R-COOH CNTs cause similar rat lung inflammation and fibrosis [46,47], but reduced mouse neutrophilic lung inflammation as compared to unmodified CNTs [48], and cause less pulmonary fibrosis [43,49]. Likewise, aluminum oxide

(Al_2O_3) ALD coating of MWCNTs results in decreased fibrosis compared to uncoated MWCNTs *in vivo* [50]. MWCNT coating with polyethylene glycol (PEG) also results in decreased fibrotic mediators IL-1β, TGF-β1, and PDGF-AA compared to pristine exposure [43] furthermore, hyaluronic acid coating results in decreased airway fibrosis and inflammation [51]. In contrast, polyetherimide (PEI) functionalized CNTs result in increased collagen deposition and fibrosis in the lungs of mice [43]. Zinc oxide (ZnO) ALD coating of MWCNTs also results in acute systemic inflammation in mouse lungs *in vivo* and proinflammatory cytokine (e.g., IL-6) production in THP-1 monocytes *in vitro*. However, ZnO-MWCNT exposure in the lung *in vivo* does not result in an altered fibrotic response compared to uncoated MWCNTs [52]. Therefore, some functionalization processes reduce CNT-induced toxicity and lung injury while others increase toxicity and the potential for fibrogenesis. A comparison of different types of functionalized MWCNTs and their relative fibrotic potential is shown in Table 1.1. Thus, to best assess human health effects, consideration should be given to both acute and chronic effects of functionalized CNTs. Consumer exposure to specific types of functionalized CNTs in products is largely unknown based on this information being classified 'proprietary' by CNT manufacturers and their clients. An increasing variety of functionalization's are employed to modify specific characteristics of CNTs, which makes assessing the toxicity each type of functionalized CNTs in rodents impractical. In response to this growing challenge, high through-put *in vitro* screening techniques will be necessary to test the vast majority of engineered nanomaterials for toxic signatures [53].

Table 1.1. Summary of fibrogenic effects of CNT surface functionalizations in rodent models.

MWCNT Functionalization	Pathological or Biochemical Outcome	Rodent/Strain	Dose	Exposure Time	Exposure Method	Reference
-COOH	Reduced neutrophilia compared to pristine	Mouse:C57BL/6 Rat:F344, Sprague-Dawley	Mouse: 10, 20, 40 µg Rat: 10, 50, 200 µg	21 days	Mouse: oropharyngeal aspiration Rat: intratracheal instillation	Bonner *et al* 2013 [15]
	Decreased TGF-β1 and PDGF-AA compared to pristine	Mouse: C57BL/6	50 µg	21 days	Oropharyngeal aspiration	Wang *et al* 2014 [43]
	Significant increase in TGF-β1 and IL-6 compared to control	Rat: Sprague-Dawley	1 mg/kg	16 days	Intratracheal instillation	Roda *et al* 2011 [41]
	Similar IL-6, TGF-β1, and collagen as pristine	Rat: Sprague-Dawley	1 mg/kg	16 days	Intratracheal instillation	Coccini *et al* 2013 [42]
	Decreased profibrotic mediators and collagen	Mouse:C57BL/6	2 mg/kg	21 days	Oropharyngeal instillation	Li *et al* 2013 [38]
$-NH_3$	Increased IL-6 compared to pristine	Rat: Sprague-Dawley	1 mg/kg	16 days	Intratracheal instillation	Roda *et al* 2011 [41]
	Increase in IL-6 and TGF-β1 compared to pristine	Rat: Sprague-Dawley	1 mg/kg	16 days	Intratracheal instillation	Coccini *et al* 2013 [42]
	Significantly increased TGF-β1, but similar IL-1β and PDGF-AA as pristine CNTs	Mouse:C57BL/6	2 mg/kg	21 days	Oropharyngeal instillation	Li *et al* 2013 [38]
-PEG	Decreased profibrotic mediators	Mouse:C57BL/6	2 mg/kg	21 days	Oropharyngeal instillation	Li *et al* 2013 [38]
-PEI	Increased fibrotic mediators and collagen	Mouse:C57BL/6	2 mg/kg	21 days	Oropharyngeal instillation	Li *et al* 2013 [38]
-Hyaluronic acid	Decrease airway fibrosis and inflammation compared to pristine	Mouse:C57BL/6J	1.5 mg/kg	21 days	Oropharyngeal aspriation	Hussain *et al* 2016 [45]
$-Al_2O_3$	Reduced fibrosis compared to pristine	Mouse:C57BL/6	4 mg/kg	28 days	Oropharyngeal aspiration	Taylor *et al* 2015 [44]
-ZnO	Similar lung fibrosis to pristine	Mouse:C57BL/6	10 mg/kg	28 days	Oropharyngeal aspiration	Dandley *et al* 2016 [46]

1.3 Mechanisms of CNT-Induced Fibrosis

It is well established that rodents exposed to CNTs via inhalation, instillation, or aspiration develop pulmonary fibrosis [12,44,54–56]. CNTs initiate an early inflammatory response in the lung characterized by increased cytokine and chemokine production by resident lung cells (e.g., macrophages, epithelial cells) followed by neutrophil recruitment and infiltration. The persistence of CNTs in the lung leads to chronic activation of pulmonary cells to produce pro-fibrogenic growth factors (e.g., TGF-β1, PDGF) and increased production of extracellular matrix (ECM) proteins (e.g., collagens, fibronectin) that lead to progressive fibrogenesis. The mechanism of CNT-induced fibrogenesis is driven largely by the production of reactive oxygen species (ROS) which serve to activate intracellular signaling pathways that favor the increased production of pro-fibrogenic growth factors (Fig. 1.1). The resultant increase in pro-fibrogenic cytokines also expands the resident fibroblast population by recruiting circulating fibrocytes which differentiate into myofibroblasts in the lung, and by stimulating the differentiation of resident lung epithelial cells or fibroblasts into myofibroblasts.

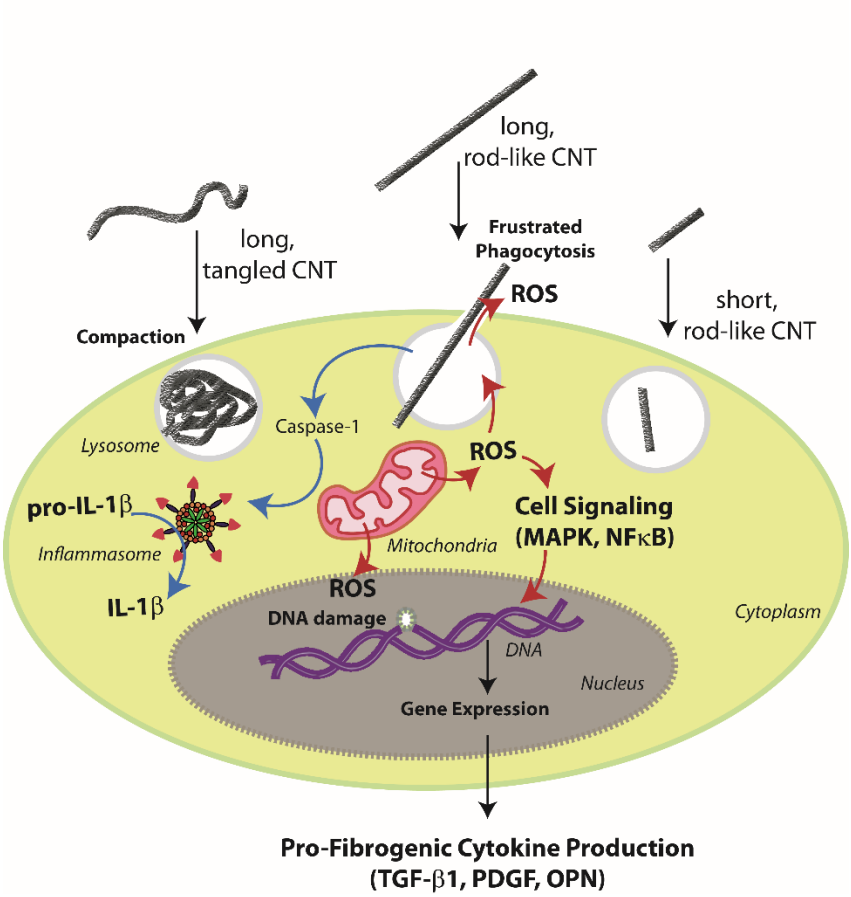

Figure 1.1. Macrophage host responses to carbon nanotubes (CNTs) differs based on selected physicochemical properties. Longer, tangled or short, rod-like CNTs are able to be engulfed and contained within a phagolysosome while long, rod-like CNTs result in frustrated phagocytosis, ROS production, and activation of signaling pathways resulting in the production of profibrogenic cytokines.

Oxidative Stress as an Initiator of CNT-Induced Fibrosis

Oxidative stress is a major driver of inflammation and fibrosis. CNTs have the potential to generate ROS directly in the absence of cells, possibly due the presence of residual metal catalysts (e.g., Fe, Co, Ni). Alternatively, ROS can be generated by lung cells stimulated with CNTs via activation of nicotinamide adenine dinucleotide phosphate (NADPH) oxidases, as shown *in vitro* with macrophages, fibroblasts, and alveolar epithelial cells [57–60]. Treatment of RAW264.7 macrophages with SWCNTs results in the induction of inflammatory cytokine production (tumor necrosis factor (TNF)-α, IL-1β, IL-6), NADPH oxidase activation, and nuclear factor (NF)-κB activation [57]. Interestingly, when comparing SW- versus MW- CNTs, ROS production *in vitro* activates the same pathways, however, SWCNTs are more acutely toxic compared to MWCNTs due to enhanced ROS generation [57]. Alveolar macrophages in particular are notorious for releasing a 'respiratory burst' of ROS after activation with particles, fibers, or bacterial products. Generated ROS can then activate the inflammasome and induce the release of the pro-inflammatory IL-1β, a leukocyte pyrogen that is secreted after pro-IL-1β is cleaved by caspase [61]. Elevated ROS also causes the release of profibrotic cytokines like PDGF and TGF-β1 [62]. Systemic oxidative markers of stress are increased after MWCNT treatment of mouse lungs showing an increase in DNA 8-hydroxy-2'-deoxyguanosine adducts in the urine as well as increased lactate dehydrogenase, tumor necrosis factor-α, IL-1β, mucin, and surfactant protein -D in the lavage fluid after one-day of exposure; all levels decrease after a week except mucin and surfactant protein-D [63]. The initial burst of CNT-induced oxidative stress causes cellular damage and is pivotal in perturbing inflammation and the fibrogenic

potential of these materials. A decrease in ROS, achieved via antioxidant N-acetyl cysteine (NAC) treatment, results in suppressed fibrosis in the lungs of MWCNT-treated mice [61]. NADPH oxidase, a membrane associated enzyme which produces ROS when internal metabolism of CNTs occurs, adds to intracellular oxidative stress. The removal of a critical subunit of NADPH oxidase via induced knockout reduced ROS generation and resulted in decreased bleomycin-induced fibrosis as measured by a hydroxyproline assay for collagen deposition in mouse lungs compared to wild type counterparts [64]. Suppression of ROS by nuclear factor erythroid 2-related factor (Nrf2) reduced inflammation, and fibrosis in the lungs of mice treated with MWCNTs as Nrf2 knockout mice exhibit increased basal collagen deposition and immune cell infiltration in the lung [65]. Oropharyngeal aspiration of MWCNTs into mouse lungs resulted in increased Nrf2 expression [65]. ROS can also be generated by macrophages as a result of frustrated phagocytosis, where excess ROS from the phagolysosome is released into the lumen and surrounding tissue causing inflammation and promotion of fibrosis (Fig. 1.1) [66]. Elevated levels of ROS can trigger redox sensitive switches within a cell to activate redox responsive cellular signaling (i.e. NF-κB, ERK). Initial ROS generation from CNT-cell interactions initiates the inflammatory response and drives the beginning steps of fibrosis.

Inflammasome Activation

Increasing evidence demonstrates that CNTs and other fiber-like materials (e.g., asbestos, silica), cause an inflammatory response via activation of the macrophage inflammasome.

Inflammasomes are intracellular protein scaffolds that incorporate activated caspase-1 to cleave pro-IL-1β to a mature, secreted form of IL-1β. IL-1β has a variety of key functions in inflammation, including the recruitment of neutrophils to sites of lung injury. CNTs have been reported to stimulate inflammasome activation in macrophages [61,67,68]. Inflammasomes likely play an important role in host defense to pathogens and inhaled nanomaterials (including CNTs), but have also been implicated in a variety of disease states [69]. Inflammasome activation is a two-step process where step 1 involves induction of pro-IL-1β by stimulation of toll-like receptors (e.g., TLR4 activated by LPS). It has also been suggested that high-mobility group box 1 (HMGB1) can serve to initiate step 1 of the inflammasome mechanism [70]. Step 2 involves organization of the inflammasome scaffold and cleavage of pro-IL-1β to mature IL-1β and is initiated by fiber-like agents such as asbestos, silica, and CNTs. MWCNTs stimulate inflammasome activation (i.e., step 2) through lysosomal disruption and ROS production [61]. Activation of the inflammasome has been proposed as a mechanism of CNT-induced pulmonary fibrosis. Inflammasome activation and IL-1β release is clearly important for recruiting neutrophils to the lung to participate in microbial killing [71]. Moreover, inflammasome activation occurs primarily in classically activated macrophages (CAMs) that function in microbial killing. In contrast, "alternatively activated macrophages" (AAMs) are the predominate phenotype in fibrosis and are polarized by Th2 cytokines, such as IL-4 and IL-13 [72]. Interestingly, inflammasome activation and IL-1β production is suppressed by IL-4 and IL-13 in human THP-1 macrophages *in vitro* and in the lungs of mice sensitized with house dust mite allergen prior to MWCNT exposure by oropharyngeal aspiration [73]. The mechanism

of inflammasome suppression by these Th2 cytokines is through a STAT6-dependent decrease in pro-caspase-1, the precursor to caspase-1 which serves as the key inflammasome component to cleave pro-IL-1β to mature IL-1β [73]. This study also showed that MWCNT exposure exacerbated allergen-induced airway fibrosis and yet reduced IL-1β and neutrophils in the lung, suggesting that inflammasome activation was not a mechanism of airway fibrosis in this model system. Neutrophilia is a common response to MWCNT exposure in the lung. An important study showed that IL-1 receptor knockout (IL-1R KO) mice do not display neutrophilia and yet develop pulmonary fibrosis to a greater degree than wild type mice [74]. Recently, inflammasome activation by MWCNTs in human airway epithelial cells *in vitro* was reported as a possible mechanism of driving pro-fibrogenic responses in fibroblasts [75]. The role of inflammasomes and IL-1β in CNT-induced fibrosis remains controversial and whether IL-1β is pro-fibrogenic or anti-fibrogenic may depend on temporal expression in the lung, which in turn could determine the duration of neutrophilic inflammation.

Canonical TGF-β1 Pathway

A major mechanism of collagen deposition in the lung involves production, activation and cell signaling via TGF-β1. CNTs stimulate pulmonary cells (e.g., epithelial, macrophage, or fibroblast) to produce latent TGF-β1 which can be sequestered in the ECM by thrombospondin 1 or can be cleaved to an active form via proteolysis [76–79]. Active TGF-β1 then binds to a transmembrane tetramer receptor consisting of two type I and two type II receptors on mesenchymal cells such as fibroblast or myofibroblasts. These TGF-β1 receptors activate the

Smad anchor for receptor activation (SARA) to recruit transcription factors Smad2 and/or Smad3. The type I receptor is a serine/threonine kinase which phosphorylates and activates Smad2/3. A trimer of two phosphorylated Smad2/3 molecules and co-activator Smad4 then translocate into the nucleus where they recognize the Smad response element (SRE) and activate transcription of ECM mRNAs (col1a1, col1a2) which eventually become translated collagen proteins that can be secreted by the cell. Negative feedback occurs as the SRE also activates transcription and expression of Smad7, a repressor of Smad2/3 signaling. The activity of the phosphorylated Smad complex is primarily abolished by phosphatase activity or to a lesser extent ubiquitination of the complex [80]. TGF-β1 signaling inhibits proliferation of most cell types, while also functioning to initiate the differentiation of fibroblasts into myofibroblasts [81]. While TGF-β1 is pro-fibrogenic, it also has beneficial immunoregulatory properties by suppressing excessive inflammation; TGF-β1 knockout mice have a short survival time and ultimately succumb to systemic inflammation [82]. TGF-β1 is increased in the lung lavage fluid of mice and rats *in vivo* several weeks after exposure to SWCNTs or MWCNTs by aspiration [56,83–85]. Both SWCNTs and MWCNTs also induce TGF-β1 production by RAW264.7 macrophages and BEAS-2B lung epithelial cells *in vitro* [32,58,83,85,86]. Physicochemical characteristics of CNTs, like length, can determine the degree of TGF-β1 induction. For instance, long but not short MWCNTs enhance TGF-β1 and phospho-Smad2 as measured by immunohistochemistry of the lungs of mice exposed via intratracheal instillation [31]. It has also been demonstrated that the TGF-β1/Smad pathway is necessary for collagen production in mice *in vivo* and in fibroblasts *in vitro* after exposure to CNTs [32,56,87]. The

mechanism for initiating increased TGF-β1 is not yet elucidated but is most likely a response to cellular oxidative damage and stress. While TGF-β1 appears to play a central role in fibrosis, it is unclear whether it will be a useful biomarker of exposure in humans. For example, workers exposed occupationally to MWCNTs express similar levels of TGF-β1 in sputum or serum as compared to unexposed control individuals, while sputum levels of other pro-inflammatory or pro-fibrotic cytokines (e.g., IL-1β, IL-4, IL-5, IL-6, TNF-α) were significantly increased compared to unexposed workers [88]. Other epidemiology studies observe increased C-C motif ligand 20, basic fibroblast growth factor and IL-1 receptor II [89].Taken together, there is strong evidence to support a role for TGF-β1 driven collagen synthesis as a key mechanism of CNT-induced fibrogenesis, yet it is unclear whether TGF-β1 will be a useful early biomarker of fibrosis to monitor occupational exposure to CNTs.

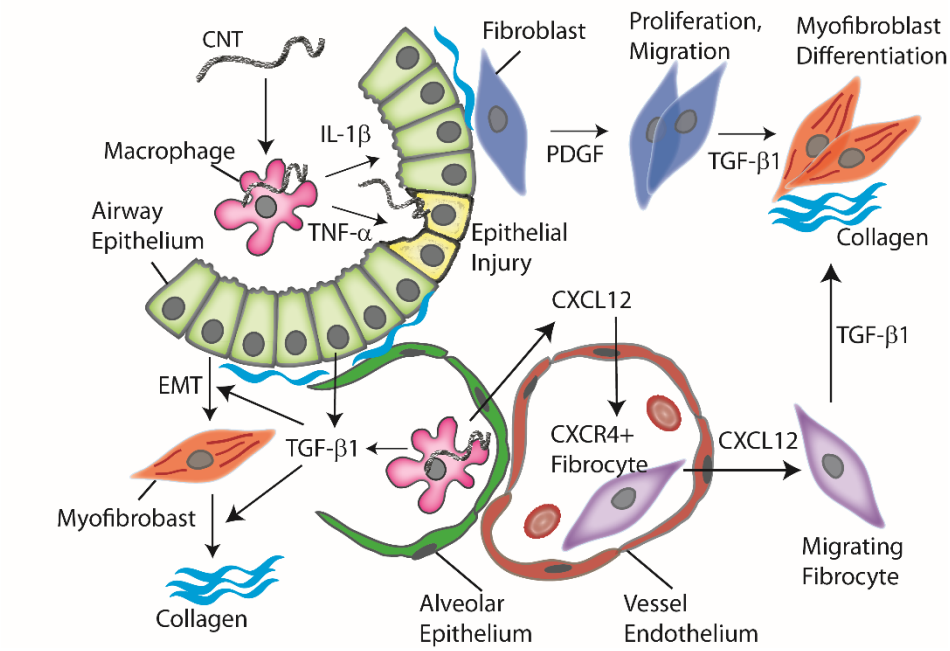

Figure 1.2. Cell signaling in the lung after carbon nanotube (CNT) exposure resulting in expansion of the myofibroblast population through three possible mechanisms: fibroblast-to-myofibroblast differentiation, epithelial-to-mesenchymal transition (EMT), and recruitment and differentiation of circulating fibrocytes.

Epithelial to Mesenchymal Cell Transition

Pulmonary fibrosis is the result of a disruption in the homeostatic balance of epithelial and mesenchymal cell survival in the lung [90]. The process of epithelial to mesenchymal cell transition (EMT) occurs when epithelial cells are stimulated to undergo differentiation to a myofibroblast phenotype (Fig. 1.2) [91]. During this process, epithelial cells lose their adhesion strength and polarity while gaining invasive and migratory properties [92]. EMT induced by MWCNTs can be mediated via TGF-β1 stimulation and the resultant immediate but transient

activation of Smad2 [31,93]. Activation of Smad2 by long, but not short, MWCNTs results in an increase of collagen I and III 30 days after intratracheal instillation exposure in rats [32]. Wang *et al*. also demonstrates that long MWCNTs interact directly with epithelial cells *in vivo* and *in vitro* to activate the TGF-β/Smad2 signaling pathway, resulting in alveolar type II epithelial cell (RLE-6TN) loss of E-cadherin, an epithelial cell specific adhesion molecule, and a gain of fibronectin expression thereby inducing EMT [93]. Likewise, these MWCNTs are shown to directly interact with fibroblasts *in vivo* and *in vitro* and enhance expression of fibroblast-to-myofibroblast specific marker expression (i.e. fibroblast specific protein (FSP-1), α-smooth muscle actin (α-SMA), and collagen III) in 3T3-L1 fibroblasts [93]. Alternatively, human bronchial epithelial cells under TGF-β1-induced EMT are initiated by rod-like MWCNTs through Smad-independent activation of the AKT/GSK-3β/SNAIL signaling pathway [94]. The GSK/SNAIL pathway is an established pathway that regulates the process of EMT [95]. In other studies these same rod-like MWCNTs have been observed to directly promote EMT [32]. In C57BL6 female mice, SWCNT exposure results in epithelial-derived fibroblasts composing almost half of the fibroblast population in the lung, demonstrating that epithelial-derived fibroblasts contribute significantly to CNT-induced pulmonary fibrosis [55]. *In vitro* studies of human epithelial cells treated with low doses of MWCNTs demonstrate an altered morphology of epithelial cells towards a mesenchymal cell phenotype [96]. Examining protein expression of epithelial or mesenchymal specific markers like E-cadherin, vimentin, α-SMA, and fibronectin can clarify the extent of differentiation of the epithelial-derived fibroblasts in EMT in human bronchoalveolar cells [96]. CNT-induced pulmonary fibrosis is driven by an increase in the

myofibroblast population, some of which can be derived from epithelial cells through the process of EMT.

Expansion of the Resident Lung Myofibroblast Population

In addition to EMT, the resident lung fibroblast population can be amplified via growth factor-induced proliferation (i.e., hyperplasia) by stimulation of fibroblasts to differentiate into myofibroblasts (Fig. 1.2). This can occur in fibroblasts *in vitro* directly in the presence of TGF-β1 [32]. PDGFs are an important family of growth factors that also drive fibroblast proliferation [97]. This family of glycoproteins is composed of two chains of PDGF-AA, -BB, -AB, -CC, and -DD. PDGFs act as both mitogens and chemoattractants for fibroblasts. Transgenic overexpression of the PDGF-B gene in rat lungs causes increased fibroblast proliferation and collagen deposition [98]. Exposure of rats or mice to MWCNTs by intratracheal instillation or oropharyngeal aspiration, respectively, increases PDGF-AA in the bronchoalveolar lavage fluid as well as in bronchiolar epithelial cells and macrophages as determined by immunohistochemical staining [5,56,99]. Priming of fibroblasts *in vitro* with low doses of growth factors TGF-β1, PDGF, or epithelial growth factor (EGF) and subsequent treatment of the fibroblasts with MWCNTs promotes proliferation through prolonged ERK1/2 signaling [62]. Additionally, this study also showed that the ability of several different types of MWCNTs to stimulate proliferation was correlated with prolonged ERK1/2 signaling specifically in fibroblasts [62]. Furthermore, rat pleural mesothelial cells treated *in vitro* with MWCNTs or nickel nanoparticles, a residual catalyst present in some MWCNTs, caused prolonged PDGF-

induced ERK1/2 signaling and synergistically enhanced PDGF-induced chemokine production [100]. Mesothelial cell signaling of fibroblasts via chemokines or growth factors could be a mechanism of subpleural fibrosis observed in mice exposed to MWCNTs by inhalation [5]. Treatment of mouse RAW264.7 macrophages with MWCNTs results in the production of ROS, inflammatory cytokines (IL-1β, IL-10, IL-6), and profibrogenic growth factors (PDGF and TGF-β1) that collectively promote the proliferation and transformation of lung fibroblasts-to-myofibroblasts through paracrine signaling [58]. Taken together, these data indicate that MWCNTs increase growth factor production (TGF-β1 and PDGF) and enhance growth factor-induced cell signaling via ROS generation, resulting in expansion of the resident lung myofibroblast population.

Circulating Fibrocyte Recruitment

Fibrocytes are mesenchymal progenitor cells derived from the bone marrow that migrate towards sites of fibrosis and can play an active role in the development of fibrosis (Fig. 1.2). Fibrocytes express cell-surface markers related to leukocyte progenitor cells, and fibrocytes can differentiate into fibroblasts, myofibroblasts, or adipocytes. They have been demonstrated in both mouse and rat models to migrate from the bone marrow to sites of lung injury following bleomycin exposure through a mechanism involving the CXCR4 receptor and the release of its chemokine ligand CXCL12, as well as release of PDGF from the lung [101,102]. Fibrocytes are identified by unique cell surface markers like hematopoietic stem cell marker CD34, leukocyte marker CD45, mesenchymal marker collagen I (COLI), and chemokine receptor (CCR7) [103].

Regulation of the CCR7 signaling pathway decreases differentiation and migration of human circulating fibrocytes [104]. The number of circulating fibrocytes is positively correlated with pulmonary inflammation, collagen content, and severity of fibrosis [105]. Furthermore, patients with interstitial lung diseases have higher levels of circulating fibrocytes, decreased lung function, and interstitial pneumonitis associated with collagen vascular disease compared to patients who do not experience these diseases [106]. It is clear that circulating fibrocytes contribute to pulmonary fibrosis, but currently there is no research on their migration and differentiation after MWCNT exposure. The current state of research suggests circulating fibrocytes contribute to pulmonary fibrosis due to induction of lung PDGF production, and it is known that MWCNTs induce PDGF in the lung. However, further studies need to be conducted to better understand the role of fibrocytes in the development of pulmonary fibrosis from CNT exposures.

Alternative Macrophage Activation

Pulmonary exposure to CNTs can result in a Th1 or a Th2 driven immune microenvironment. A Th1 driven response conventionally is stimulated by a viral or bacterial infection polarizing macrophages towards a classically activated M1 function, compared to an alternatively activated M2 macrophage which is polarized under the influence of a Th2 microenvironment. A Th1 driven M1 macrophage drives the inflammatory response by producing interferon (IFN)-γ, IL-12, IL-6, and other pro-inflammatory cytokines. MWCNTs that are more flexible or tangled promote a Th1 response in the lungs of mice exposed via oropharyngeal aspiration

marked by neutrophilia [39]. MWCNTs that have been functionalized with a carboxyl group have the ability to activate phospholipase C (PLC) and recruit macrophages through the PLC/IP3/Calcium release-activate calcium channel signaling pathway [107]. M2 macrophages are classically driven by helminth infection and TGF-β1 stimulation. M2 macrophages also produce more TGF-β1 in response to stimuli. Interestingly, a rod-like MWCNT treatment via oropharyngeal aspiration results in a more Th2 response as indicated via mucous cell metaplasia and/or eosinophilia [38]. M2 macrophages produce Th2 cytokines, like IL-4, IL-5, and IL-13 which drive the adaptive immune response and are upregulated in bleomycin-induced fibrosis [108]. IL-17 is also upregulated in bleomycin treated lungs which can down-regulate the Th1 response and drive production of growth factors, like TGF-β1, and result in excess collagen deposition into the ECM and decreased collagen metabolism thereby disrupting homeostasis [108]. Therefore, the microenvironment cultivated by CNT exposure can drive differential immune responses based on the physicochemical properties of the CNTs.

1.4 Genetic Susceptibility to Pulmonary Fibrosis

There are multiple genes that determine susceptibility to pulmonary fibrosis. Variability in rodent genetic strain and sex differences are two very important susceptibility factors to consider when first designing a study. In addition, studies with transgenic "knockout" mice have provided evidence for specific genes in lung fibrosis caused by CNT exposure. A loss or deficiency of genes coding for key factors involved in the process of the immune response, cell to cell adhesion, and wound healing pathways can determine the susceptibility and severity

of CNT-induced fibrogenesis. Though the literature provides a plethora of these deficiencies with regard to pulmonary fibrosis in general, only a handful have been investigated specifically with CNT exposures in experimental animals and are discussed in Fig. 1.3.

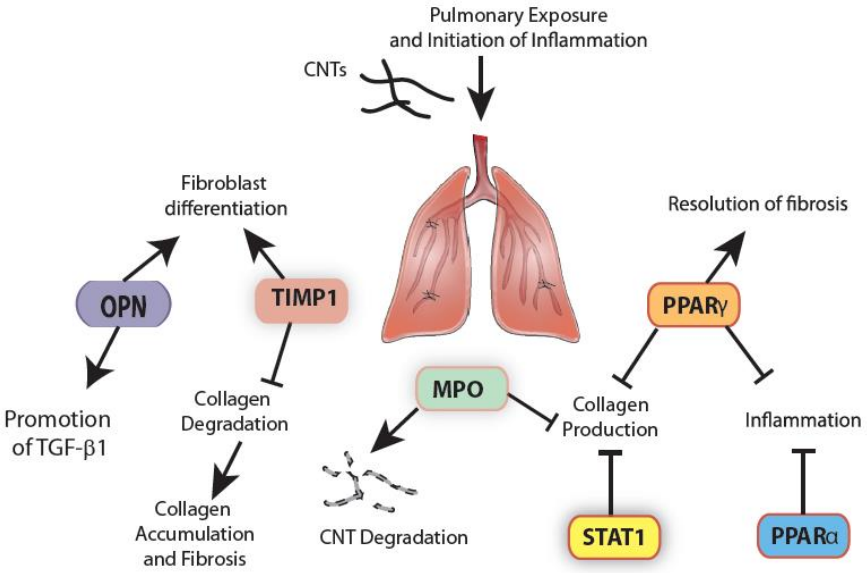

Figure 1.3. Protein modulators of carbon nanotube (CNT)-induced pulmonary fibrosis identified from transgenic mouse studies and how they regulate inflammation and fibrosis.

Rodent Strain Variation

Inherent variability between genomes of mouse or rat species is an important determinant in fibrogenesis after pulmonary injury by a variety of agents. Walkin *et al*. reviewed strain differences of mice in the development of fibrosis and concludes that strain variation is a determinant for organ specific fibrosis severity [109]. A study examining pulmonary inflammation and fibrosis following intratracheal instillation of an alkylating agent, like

melphalan or mustard gas, in six strains of rats (DA, PVG, PVG.1AV1, WF, F344, LEW) exemplifies the genetic component of the severity and response timing of inflammation and fibrosis following lung injury [110]. Interestingly, 90 days post exposure, F344 rats have little to no increase in collagen content compared to controls, while all five other strains do [110]. Likewise, studies of bleomycin-induced pulmonary fibrosis in multiple strains of mice finds the severity of fibrosis and collagen deposition in the lungs to be strain dependent as well [111]. Specifically, the C57BL/6 strain responds greater than DBA/2, Swiss, and BALB/c mice with the least response observed in BALB/c mice [111]. Another study examining the fibrotic outcome of pulmonary exposure to vanadium pentoxide in two mouse strains found increased inflammatory and collagen content in DBA/2J mice compared to C57BL/6J mice [112]. Therefore, strain susceptibility to pulmonary fibrosis may depend on the agent used to induce fibrosis. Of interest, the sex of mice has also been linked to the inflammatory response experienced by mice following MWCNT aspiration exposure where female mice, especially those with reduced glutathione levels, have reduced neutrophilia and MWCNT clearance from their lungs [113]. Currently, there is a lack of information on sex differences in response to pulmonary exposure to CNTs. The strain of the rodent model used for CNT exposures is an important consideration when analyzing the effects of CNTs in the lung, and when evaluating for fibrotic endpoints the study design should utilize susceptible mouse strains to truly assess the fibrogenic potential of these nanomaterials.

Specific Mediators Determining Susceptibility

Signal Transducer and Activator of Transcription-1 (STAT1): The signal transducer and activator of transcription-1 (STAT1) plays a key regulatory role in suppressing the development and progression of CNT-induced fibrogenesis. STAT1 is a transcription factor that is responsive to IFN -α, -β, and -γ stimulation. IFN-γ activates the transmembrane interferon receptor (IFNAR) -1 and -2 which have an internal Janus kinase (JAK) activity to recruit and activate STAT1. Activation and dimerization of STAT1 leads to translocation of the dimerized transcription factors and expression of genes that are involved in growth inhibition. Individuals with idiopathic fibrosis and systemic sclerosis have decreased STAT1 transcription and expression as well as fibroblast hyper-proliferation and apoptotic resistance [114]. STAT1 knockout mice exhibit an increased susceptibility to bleomycin induced fibrosis [115]. Furthermore, these STAT1 knockout mice experience MWCNT-induced exacerbation of fibrosis and asthma demonstrating STAT1 as protective against fibrosis [39]. STAT1 knockout fibroblasts isolated from mouse lungs are hyper-responsive to TGF-β1 treatment, transcribing significantly more collagen mRNA and producing more soluble collagen than wild type primary mouse lung fibroblasts [39]. STAT1 antagonizes the activity of other STAT family members (STAT3 and STAT6) that have been shown to play roles in promoting fibrogenesis. Therefore, a reduction or loss of STAT1 may also result in less restriction of STAT3 or STAT6. STAT3 is implicated in cell growth and carcinogenesis, while STAT6 is responsible for promoting a more allergic phenotype. TGF-β1 treatment of lung myofibroblasts has been shown to activate STAT3 and promote proliferation adjacent of epithelial damage [116]. Either

STAT dysregulation would result in an abnormal phenotype and could result in increased proliferation or exacerbation of fibrosis or asthma [39].

Peroxisome Proliferator-Activated Receptor (PPAR): Peroxisome proliferator-activated receptors (PPAR) are nuclear receptor proteins that heterodimerize to retinoid X receptor (RXR) and function as transcription factors to regulate processes of fibrogenic inflammation, cellular differentiation, and wound healing [117]. There are three isoforms of PPARs -α, -γ, and -β/δ. Each of these have been found to play a role in fibrogenesis. PPARα is found to be highly expressed in the heart, muscle, kidney, and liver while PPARβ/δ and γ are ubiquitously expressed [118,119]. In cases of idiopathic pulmonary fibrosis there is an incidence of down-regulated peroxisomal biogenesis and metabolism [120]. A reduction in peroxisomes from decreased biogenesis results in more severe inflammation and dysregulation of the wound healing process and exacerbation of fibrogenesis. PPARα knockout mice develop greater inflammation and fibrosis from bleomycin treatment than wild type mice, while PPARα agonist treatment paired with bleomycin resulted in decreased scaring of mouse lungs [121]. Treatment of fibroblasts with a PPARα agonist results in a reduction of TGF-β1 induction of myofibroblast differentiation and collagen production [120]. PPARβ/δ mainly plays a role in regulating the timing of inflammation to wound healing, however little is known about its role in pulmonary fibrosis [122]. The most influential PPAR in fibrogenesis appears to be PPARγ. PPARγ is a negative regulator of inflammatory cytokines and knockout mouse models exhibit increased inflammation and inflammatory cytokine expression compared to controls [123].

Activation of PPARγ following pulmonary injury from bleomycin has been observed to promote the resolution of both inflammation and fibrosis by suppressing tumor necrosis factor α, procollagen I and connective tissue growth factor expression and was mainly found to be localized to alveolar macrophages and some parenchymal cells [124,125]. Treatment of hypertrophic scar fibroblasts with a PPARγ agonist resulted in decreased expression of Smad3 and Collagen 1 mRNA through induction of miR-145 [126]. Furthermore, PPARγ ligands inhibit TGF-β-induced myofibroblast differentiation in a dose-dependent manner through the PI3K/AKT pathway [127,128]. PPARγ knockout mice have higher expression of Twist1, a transcription factor responsive to M1 but not M2 macrophage stimulation [129]. Alveolar macrophages from mice 60 days post-MWCNT exposure exhibit a decrease in PPARγ expression and knockout mice exposed this way experience increased inflammation and larger granuloma formation [129]. Furthermore, PPARγ knockout mouse skin fibroblasts experience an enhanced rate of dermal wound closure, and increased activation of Smad3, AKT, and ERK suggesting that PPAR functions to control fibroblast activation and function following injury [130]. As prominent regulators of inflammation, differentiation, fibrogenesis and wound healing, any PPAR deficiency combined with a fiber insult like CNT exposure could result in a more severe fibrosis.

Osteopontin (OPN): Commonly used as a biomarker of lung diseases (i.e. idiopathic pulmonary fibrosis and non-small cell lung cancer), osteopontin (OPN) plays a pivotal role in inflammation, fibrosis and cancer and may be a good biomarker of particle-induce lung injury

as well [131,132]. OPN, a glycoprotein also known as SPP1, regulates inflammatory infiltration, tissue and bone remodeling and metastasis. OPN is highly produced immediately following a titanium dioxide particle exposure during inflammation and OPN levels are maintained at high levels in BALF well into fibrogenesis [133]. Only recently have studies elucidated the role of OPN in CNT-induced fibrosis. OPN knockout studies have elucidated it's regulatory role in the transition from inflammation to fibrogenesis where OPN knockout mice on a C57BL/6J background had decreased fibrosis, as well as reduced TGF-β1 levels and TGF-β1 signaling after exposure to rMWCNT via pharyngeal aspiration [134]. Furthermore, OPN was shown to promote MWCNT-induced fibrosis through the activation of TGF-β1 signaling and thereby promote myofibroblast differentiation [134]. The requirement of OPN to stimulate TGF-β1 and thereby activate TGF-β1 signaling is critical in the development and severity of MWCNT-induced pulmonary fibrosis.

Myeloperoxidase (MPO): Myeloperoxidase (MPO) is a lysosomal peroxidase enzyme produced and stored in neutrophil granulocytes which is released with the purpose of quickly producing hypochlorous acid during the neutrophil-mediated respiratory burst to kill pathogens. Peroxidases have also been implicated in the biodegradation of CNTs [135]. Bronchoalveolar lavage fluid from B6 mice following a 24-hour exposure to uncoated or aluminum oxide coated MWCNTs experienced a significant increase in MPO, indicating that it is involved in the CNT host immune response [136]. Changes to CNTs, like adding a metal oxide coating, may alter the biodegradation process and should be studied further. Degradation

of CNTs by neutrophilic MPO can decrease inflammation, as modeled from *in vitro* testing; a loss or reduction of MPO could then result in increased inflammation and fibrosis from a CNT insult [137]. MPO knockout mice exhibit a 2.5-fold increase in lung collagen content compared to wild type counterparts treated with SWCNTs [138]. MPO knockout mouse lungs also exhibit decreased clearance of SWCNTs compared to wild type exposed mice [138]. Epidemiologic studies have identified a MPO polymorphism in women with hepatitis C that causes increased severity of hepatic fibrosis [139]. MPO is key in the mechanism of CNT degradation which decreases tube length, thereby rendering CNTs more manageable for macrophage phagocytosis and clearance. A decrease or absence of MPO has the potential to extend the biopersistence of CNTs and prolong the inflammatory and fibrogenic effects of these materials in the lung. As a potentially important mechanism involved in the biodegradation of CNTs, the presence and function of MPO is likely important for the extent of inflammation and the severity of fibrosis.

Tissue Inhibitor of Metalloproteinase (TIMP): Tissue inhibitor of metalloproteinases (TIMP) are a group of four proteinase inhibitors (TIMP-1, -2, -3, and -4) functioning to inhibit metalloproteinase degradation of ECM proteins. The regulatory balance of ECM production and deconstruction following injury is extremely important in the wound healing and resolution process. Lungs from patients with idiopathic pulmonary fibrosis have overexpression of all four TIMP proteins and result in the accumulation of ECM and enhanced fibrogenesis [140]. However, in a mouse model with bleomycin-induced pulmonary fibrosis, only TIMP1 was found to be significantly increased at both the mRNA and protein levels [141].

Similarly, TIMP1 mRNA and protein levels are rapidly induced in a time- and dose- responsive manner from MWCNT exposure in a mouse model; TIMP1 knockout mice display significantly less fibrotic foci, collagen, fibroblast recruitment and differentiation indicating it has a key role in pulmonary fibrosis caused by MWCNT exposure [142]. Fibroblast expression of TIMP1 can be activated by epithelial cell inflammasome activation and production of IL-1β and IL-18 thereby promoting a profibrogenic environment *in vitro* [75]. TIMP1 complexes with CD63 and integrin β1 on the surface of lung fibroblasts consequently activating ERK1/2 and promoting fibroblast activation and proliferation [142]. An imbalance in the ratio of TIMP to matrix metalloproteinases (MMP) can be utilized as a measure of fibrosis. For example, bleomycin-treatment of rats results in a reduction in MMP-9/TIMP1 ratio; or a reduction in MMP-9 and increase in TIMP1 during the promotion of fibrosis [143]. Unfortunately, while the studies referenced here did look at specific matrix metalloproteinases, they did not examine the ratio of TIMPs to MMPs to examine how these vary between controls and CNT-exposed lungs. The increased expression of TIMP proteins, specifically TIMP1, is associated with CNT injury and without it, tissue metalloproteinases continue to degrade the ECM subsequently dysregulating the balance of ECM production and deconstruction in favor of continued inflammation.

1.5 Immune Response to CNT Pulmonary Exposure

The innate and adaptive immune responses play a dynamic and complex role in the development of the pulmonary response to CNT exposure, and the type and severity of these

responses varies drastically depending on the physicochemical characteristics of the CNT. The immediate pulmonary immune response to CNTs is well characterized based on data from numerous acute studies observing initial inflammation and neutrophilia with most MWCNTs. However, the adaptive immune response to CNTs differs widely dependent on CNT and is poorly understood.

Immediately following CNT or asbestos inhalation, instillation, or inspiration exposure rodent models experience neutrophilia and have instances of increased protein in the lung indicating physical damage to cellular components [37,56,83,144–146]. Within three days post exposure to MWCNTs, there is a significant increase in acute phase cytokines (i.e. tumor necrosis factor (TNF)-α, CCL2, IL-1β, IL-6, and Il-1α) and growth factors (i.e. PDGF -A, -B, and -C) mRNA and/or protein levels in the lungs of mice and rats [56,145,147]. Dependent on the residual metal content of the CNT, there have been instances of weight loss, lethargy, shivering, hypothermia, and death within hours following nickel but not iron containing-CNT exposure in mice [148]. Generally, following seven days post exposure, the inflammatory profile changes either towards resolution of inflammation, profibrogenic, or chronic inflammation. Interestingly, the rigidity of the CNT can determine the predominant type of inflammation. A rod-like MWCNT has been shown to result in T helper cell type 2-driven allergic airway inflammation while a tangled MWCNT resulted in neutrophilia [38,149]. Further investigation into this phenomenon resulted in the identification of an initial neutrophilic response accompanied with increased inflammatory cytokines (i.e. CXCL1, CXCL9 mRNA and protein) to both asbestos and rod-

like MWCNT after 16 hours This inflammation switched predominantly to eosinophilia after 7 days, and finally resulted in goblet cell hyperplasia and acidophilic macrophages containing Charcot-Leyden like crystals and increased proinflammatory cytokines (i.e. TGF-β1, TNF, and IL-1β mRNA) [38]. The initial neutrophilic recruitment response was found to be dependent on the IL-1β-receptor [150]. The tangled MWCNT experienced significantly decreased neutrophilia and proinflammatory cytokine production after 16 hours, however, the macrophages in mice exposed to the higher dose also contained comparable levels of Charcot-Leyden like crystals [150]. The rod-like MWCNT resulted in a significantly larger percent of lung occupied by granulomas [150]. Differences in CNT properties have a significant effect on the acute and chronic inflammatory effects in the lung and determine if the lung progresses towards a disease state or resolves inflammation and recovers from the CNT insult.

During times of chronic pulmonary inflammation or infection, tertiary lymphoid organs (TLOs) are induced and form functional B cell germinal follicles surrounded by T cell areas (Figure 4). The development of these TLOs is not pre-programmed during neonatal development and they form in addition to primary lymphatic tissues (i.e. bone marrow and thymus) and secondary lymphoid organs (i.e. spleen, Payers patch, lymph nodes, tonsils, mucosa associated-lymphoid tissue). These TLOs are thought to develop in order to aid the local immune response to what is inflicting the infection or inflammation. TLOs are termed based on their location within the lung. When adjacent to a bronchus or vessel these tissues are termed inducible bronchus-associated lymphoid tissue (iBALT), however when TLOs form in

the lung parenchyma independent of airways or vessels, they are termed ectopic lymphoid tissue (ELT). Healthy lung tissue in both mice and humans rarely develop TLOs. The presence of TLOs in the lung are tied to many disease states including Sjogren's syndrome, idiopathic pulmonary fibrosis (IPF), rheumatoid arthritis (RA), autoimmunity, asthma, chronic obstructive pulmonary disease (COPD), respiratory infections, and lung cancer [151–153].

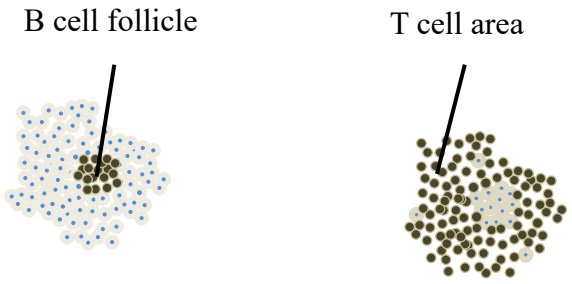

Figure 1.4. Tertiary Lymphoid Structure.

Interestingly, the development of these tissues is not well understood. TLOs are known to develop in mice within eight days of infection [154], and are known to be persistent for at least 2-4 months in the absence of inflammation [155,156]. There appears to be a developmental window in younger mice, where exposure to an inflammogenic source causes a robust development of TLO compared to older mice [155]. Increased neutrophil inflammation is directly associated with increased TLO neogenesis and is suppressed by regulatory T cells [157]. B cell knockout mice do not develop the B cell germinal center, and thus do not develop TLOs [158]. Mice lacking primary or secondary lymphoid organs are capable of a robust response to respiratory viral infections where they survive higher doses of infection and clear the infection faster than normal

counterparts suggesting that TLOs provide a protective, less pathogenic response than systemic immune responses [159]. In areas of TLOs there is enhanced protective immunity where T cells are primed and B cell education occurs to clear infectious agents. Dendritic cells are key in the organization and persistence of TLOs and in priming T cells at these locations [151,154]. IL-17 expression and activation of CXCL13 and CCL21 expression within TLOs, is required for development of the TLOs [155,159]. Also, increased iBALT is associated with increased disease severity in COPD [158]. Pulmonary exposure of rodents to particulate matter has resulted in increased incidences of formation. Cigarette smoke exposure resulted in increased iBALT and associated macrophages in models of COPD and emphysema which was shown to be a result of B cell derived IL-10 and MMP12 driving macrophage activation and continued inflammatory status in the lung [158]. The chronic inflammatory response in the lung perpetuated by TLO neogenesis is one theory of how these are tied to autoimmunity. MWCNT exposure of Fisher 344 rats via intratracheal instillation resulted in a gradual increase of MWCNT in iBALT over time [160]. The presence of MWCNTs within the TLOs is indicative of either macrophage or dendritic cell transfer of the materials to the lymphatic tissue. The lymphatic system is capable of clearing foreign material from the lung, however it is drastically slower than the intrinsic mucociliary escalator [160].

1.6 Neoplastic Potential of Fiber-Like Exposures

Due to the similarities CNTs have with asbestos they are a concern for the development of pulmonary tumors, such as carcinomas and mesothelioma. Though CNTs are similar to

asbestos, studies have a difficult time correlating the carcinogenic effects of asbestos observed in humans to those of CNTs in experimental models. To date there are some key studies focused on teasing out these effects in the lung and are summarized in Table 1.2 and Table 1.3. Combined *in vivo* and *in vitro* experimental data point in the direction of some CNTs being more of a risk than others.

An increased number of cells in an organ, termed hyperplasia, occurs at times of cellular replacement during tissue repair. Hyperplasia is also the first step cells undergo on their way to dysplasia and cancer development. However, hyperplastic and dysplastic cells may or may not become cancer, and may simply be proliferating at a faster rate than normal. Mice exposed to SWCNTs and MWCNTs experience epithelial hyperplasia, alveolar hyperplasia and dysplastic characteristics (mitotic figures, anisokaryosis and anisocytosis) [37,44,161–163]. Persistent hyperplasia is a characteristic of cancer development. Interestingly, oropharyngeal aspiration of crocidolite asbestos into male Non-swiss Albino CF-1 mice results in predominantly bronchoalveolar hyperplasia and the same exposure set-up of MWCNTs results in mostly alveolar hyperplasia of type II pneumocytes [161]. Intratracheal instillation of SWCNT into C57BL/6 female mice also resulted in epithelial hyperplasia accompanied by an increase in fibroblast expansion and epithelial to mesenchymal transition [55]. Aspiration of MWCNTs or asbestos in mice was observed to result in goblet cell hyperplasia after only 28 days [150].

Table 1.2. Summarization of carcinogenic potential of CNTs in mice.

Lesions Resulting from Fiber Exposure	Fibers Used	Dose	Mouse Sex/Strain	Duration	Exposure Method	Study
granuloma, weight loss, lethargy, inactivity	RNT (SWCNT, Rice product), CNT (SWCNT CarboLex nanotubes), quartz	0.1 mg/head 0.5 mg/head	B6C3F1	7 and 90 days	Intratracheal instillation	Lam *et al.* 2004
pleural mononuclear aggragates, subpleural fibrosis	MWCNT (Helix Material Solutions)	1 mg/m^3 or 30 mg/m^3	male C57BL/6J	1 day, 2, 6, and 14 weeks	Nose-Only Inhalation (6 h)	Ryman-Rasmussen *et al*. 2009
interstitial fibrosis, granuloma	MWCNT-7	10, 20, 40, 80 µg/head	male C57BL/6J	1, 7, 28, and 56 days	Pharyngeal aspiration	Mercer *et al*. 2011
acute pleural inflammation, parietal pleural fibrosis and mesothelial proliferation from long fibers	Amosite, NT_{short} (Nanostructured & amorphous Materials), NT_{tang1} (NanoLab), NT_{tang2} (NanoLab), NT_{long1} (MWCNT-7), NT_{long2} (University of Manchester), $NiNW_{short}$ (CRANN-Trinity College Dublin), $NiNW_{long}$ (CRANN-Trinity College Dublin)	5 µg/head	female C57BL/6J	1 and 7 days 4, 12 and 24 weeks	Intrapleural injection	Murphy *et al*. 2011
extrapulmonary transport	MWCNT-7	5 mg/m^3	male C57BL/6J	1 and 336 days	Whole body inhalation (5h/d for 12 d)	Mercer *et al*. 2013
granuloma, fibrosis, inflammation	MWCNT-7	5, 20, 40 µg/head	male C57BL/6J	1, 3, 7, and 14 days	Pharyngeal aspiration	Dong *et al*. 2014
bronchiolo-alveolar adenoma, bronchiolo-alveolar adenocarcinoma, malignant sarcomatous mesotheliomas	MWCNT-7 + MCA	5 mg/m^3	male B6C3F1	17 months	Whole body inhalation (5h/d 5d/wk for 15 d)	Sargent *et al*. 2014
eosinophilia, mucous hypersecretion and increase in goblet cells with rCNT	tCNT (Cheap Tubes), rCNT (MWCNT-7)	6.2-8.2 mg/m^3 (rCNT) 17.5-18.5.51 mg/m^3 (tCNT)	female BALB/c, C57BL Kit^{W-sh}/HNihrJaeBsmJ	4 days	Whole body inhalation (4h/d 4 d)	Rydman *et al*. 2014
broncho-alveolar hyperplasia and lympho-histiocytic infiltration near hyperplasia with just MWCNT1, granuloma, fibrosis and inflammation resulting from both fibers	MWCNT1 (MWCNT-7), MWCNT2 (NM-400 Nanocyl)	2 mg/kg	female C57B16/J	8 weeks	Pharyngeal aspiration	von Belro *et al* 2014

Table 1.3. Summarization of carcinogenic potential of CNTs in rats.

Lesions Resulting from Fiber Exposure	Fibers Used	Dose	Rat Sex/Strain	Duration	Exposure Method	Study
pleural macrophage recruitment and activation	crocidolite, chrysotile	7.55 mg/m^3 (crocidolite) 8.51 mg/m^3 (chrysotile)	male Fischer 344	6 weeks	Full body inhalation (6h/d 5d/wk for 2 wk)	Choe *et al*. 1997
granuloma, fibrosis	MWCNT (Facultes Universitarires Notre Dame de la Paix Namur), Chrysotile	0.5 or 2 mg/head	female Sprague-Dawley	1, 3, 15, 28, and 60 days	Intratracheal administration	Muller *et al*. 2005
extrapulmonary transport of fibers into pleural space, granuloma, hyperplastic visceral mesothelial proliferation and inflammation	crocidolite, MWCNT-N (Nikkiso), MWCNT-M (MWCNT-7)	1.25 mg/head	male F344	9 days	intrapulmonary spray (every other day for 9 days)	Xu J *et al*. 2012
granuloma, extrapulmonary transport of fibers, adenoma, adeno-carcinoma, bronchiolo-alveolar carcinoma, malignant mesothelioma	MWCNT-N (Nikkiso)	1 mg/head	male F344/Crj	109 weeks	Trans-tracheal intrapulmonary spraying (8 times over 2 wk)	Suzui *et al*. 2016
carcinoma, epithelial hyperplasia, bronchiolo-alveolar carcinoma, adenoma, granuloma, focal fibrosis	MWCNT-7	0.02, 0.2, or 2 mg/m^3	male and female F344/DuCrlCrlj	104 week	Whole body inhalation (6h/d 5d/wk for 104 wk)	Kasai *et al*. 2016

Intrapulmonary spraying of MWCNTs or crocidolite in F344 rats five times over nine days was seen to result in hyperplastic proliferative lesions of the visceral mesothelium, and these lesions were associated with inflammatory cell infiltrate and fibrosis in pleural tissues [164,165]. Of interest, the hyperplastic lesions on the pleural lining did not contain any foreign material [164]. Furthermore, pharyngeal aspiration of other nanomaterials, like carbon nanofibers and graphene nanoplates in rats and mice also results in hypertrophy and hyperplasia of the epithelium [166,167]. ENMs, especially CNTs, have the ability to cause epithelial hyperplasia and may be a potential risk for transition from hyperplasia to dysplasia in the lung.

Abnormal cellular growth marks the transition from hyperplasia to neoplasia. CNTs may be able to initiate this transition. MWCNTs have been shown to promote pulmonary tumor growth. In mice pretreated with a known tumor initiator and promoter 3-methylcholanthrene (MCA) followed by exposure to MWCNTs, an increase in the incidences of broncho-alveolar adenocarcinomas and sarcomatous mesotheliomas was observed, demonstrating the role of MWCNT as a tumor promoter [168]. Other chronic studies exposing mice just to CNTs have observed incidences of interstitial fibrosis [56,169], parietal pleural fibrosis and inflammation [24], subpleural fibrosis and mononuclear aggregates at the pleura [12], and broncho-alveolar hyperplasia coupled with lympho-histiocytic infiltration [170]. Exposure of rats to MWCNTs via TIPS resulted in about half of the exposed rats developing tumors (i.e. malignant mesothelioma, adenoma, adeno-carcinoma) [26]. A more recent study exposing rats to MWCNT observed carcinoma, adenoma and epithelial hyperplasia [25]. The sensitivity and susceptibility

of tumorigenesis and mesothelioma development is very different between mouse and rat models. However, the current literature is suggestive of the capability of CNTs to induce carcinogenesis in the lung.

The induction of malignant mesothelioma has been studied *in vivo* in rodent lungs and by extrapulmonary exposures methods (summarized in Table 1.4). To date, only pulmonary CNT exposure of rats has resulted in MWCNT-induced lung tumors, and only two studies have observed mesothelial hyperplasia or malignant mesothelioma [26,164]. Intrapleural injection of CNTs into rats and mice has resulted in mesothelial proliferation [24]. Multiple studies have shown extrapulmonary transport of CNTs from the rodent lung into the pleura and lymphatic system [13,26,164]. The translocation of these CNTs within 24 hours suggests that CNTs are able to reach the pleura and persist for long periods of time. Surrogate assays employing the mesothelial lining of the abdomen inject the CNTs or asbestos interperitoneally into rodents and observed malignant mesothelioma development. Of greatest significance are two studies utilizing mice deficient in one allele of the tumor suppressor p53. These studies i.p. injected a rod-like MWCNT and crocidolite asbestos into p53 deficient mice and observed that mesothelioma developed at a faster pace from MWCNTs compared to asbestos [19,20]. A follow up study administered intrascrotal injections of rod-like MWCNTs and crocidolite into rats and observed mesothelioma and mesothelial hypertrophy and hyperplasia from the MWCNTs but not crocidolite [22]. Further studies administrating CNTs via i.p. injections have also observed mesothelioma development [23,171,172]. Interestingly, several studies using different

manufactured CNTs did not observe mesothelioma development, but did observe adenocarcinoma or granulomatous inflammation [173,174]. What has been consistent between studies is the fact that MWCNT induce faster tumor development than asbestos in these extrapulmonary exposure models [19,20,22,171]. It is based on these facts that has led the International Agency for Research on Cancer (IARC) to classify the MWCNT-7, a rod-like MWCNT, as group 2B or a possible human carcinogen. Interestingly, to date pulmonary exposure of mice to MWCNT or asbestos alone has not resulted in mesothelioma development.

Table 1.4. Extrapulmonary MWCNT exposures and mesothelioma development.

Lesion	Fibers Used	Dose	Duration	Species	Exposure Method	Study
granuloma, inflammation	NanoLab (NT_{tang1}, NT_{tang2}), MWCNT-7 (NT_{long1}), Univeristy of Manchester (NT_{long2}), Asbestos (Amosite)	50 µg/head	1, 7 day	female C57BL/6J mice	Intraperitoneal instillation	Poland *et al*. 2008
mesothelioma	MWCNT-7, crocidolite, fullerene C_{60}	3 mg/head	10, 180 day	male $p53^{-/+}$ C57BL/6 mice	Intraperitoneal injection	Takagi *et al*. 2008
peritoneal mesothelioma and fibrosis, mesothelial hyperplasia, granuloma formation, mononuclear lymphocyte inflammation	MWCNT-7	300, 30 and 3 µg/head	1 year	male $p53^{-/+}$ C57BL/6 mice	Intraperitoneal injection	Takagi *et al*. 2012
mesothelioma, mesothelial hypertrophy and hyperplasia, granuloma, ascites	MWCNT-7	1 mg/kg or 0.24 mg/head	52 weeks	male Fischer 344 DuCrlCrlj rats	Intrascrotal administration	Sakamoto *et al*. 2009
granuloma,	crocidolite	2 mg/kg or 0.47 mg/head				
Granuloma	SWCNT, MWCNT (Shenzhen Nanotech Port Co LTD) *No control group	10mg/head	1 year	F344 rats	Intraperitoneal implantation of pharmaceuticle hard gelatine capsule	Vagara and Szendi 2010
fibrosis	MWCNT-7 (NT50a)	1, 5 mg/head	1 month	male and female rats	Intraperitoneal injection	Nagai *et al*. 2011
malignant mesothelioma	MWCNT-7 (NT50a), Showa Denko (NT50b, NT145, NTtngl)	1, 10 mg/head	12 months			
granuloma, rare adenocarcinoma, fibroadenomas	Showa Denko (NTtngl), MWCNT-7 (NT50a)	10 mg/head	lifetime (<3 years)	male and female Fischer 344/brown Norway F1 hybrid rats	Intraperitoneal administration	Nagai *et al*. 2013
malignant mesothelioma, granuloma, mesothelial hyperplasia with multifocal papillary projections	Amosite, WHO MWCNT (A, B, C, D)	1, 5 x 10^9 fibers/head	2 years	Wistar Rats	Intraperitoneal injection	Rittinghausen *et al.* 2014
peritoneal mesothelioma	MWCNT-7, Muller (MWCNT-M), MWCNT-T (tangled Nagoya Univeristy, Japan), crocidolite asbestos	6 mg/head MWCNT, 2 mg/head asbestos	12 months	male Wistar rats C57BL/6 mice	Intraperitoneal injection	Huaux *et al.* 2016

1.7 Mechanisms of CNT-Induced Neoplasms

MWCNTs are a concern for cancer development due to their similarities to asbestos and resulting potential development of asbestos-related tumors like malignant pulmonary

mesothelioma (MPM), non-small cell lung cancer (NSCLC) and small-cell lung cancer (SCLC) [175]. MWCNT exposures *in vivo* have indicated that rod-like MWCNTs pose a higher risk of carcinogenic development than tangled MWCNTs or SWCNTs. Studies completed *in vitro* indicate potential mechanisms of MWCNT-induced tumorigenesis from both MWCNTs and SWCNTs, however, these mechanisms are not fully understood in respect to how CNTs directly cause lung cancers. MWCNT-induced tumorigenesis is thought to develop through oxidative and non-oxidative stress resulting in cytotoxic and genotoxic effects. Mechanisms of cancer development have been studied extensively and point towards multiple events that must culminate in enough random events to result in cancer or tumor development. Studies comparing asbestos to CNTs show that even these two fiber-like toxicants result in different signatures of genotoxicity and that they could likely result in cellular transformation and cancer development through different mechanisms of action [176]. The similarities between MWCNTs and asbestos have directed studies to look for similar signatures of oxidative stress, however the mechanisms of CNT-induced carcinogenesis are not fully understood and therefore more research is needed.

Oxidative Stress

An increase in radical generation results in a greater chance of adducts forming on DNA, lipids or proteins. Genotoxic effects of oxidative radicals can either be repaired or cause irreversible damage requiring tolerance or apoptosis. In instances of high oxidative stress levels, DNA damage can be excessive or irreparable and result in mutations or chromosomal aberrations. If

not forced to undergo apoptosis the cells containing these genotoxic signatures may progress through somatic proliferation, accumulate damage, become transformed, and develop as a tumor or malignancy. Oxidative radicals are highly reactive and may form DNA adducts resulting in large biological effects, where the regulation or gene product of the adduct results in changes in cellular homeostasis. Both ROS adducts like 8-oxo-guanine or reactive nitrogen species (RNS) adducts like 8-Nitroguanine have the potential to be mutagenic and result in a guanine to thymidine transversion and if the DNA is replicated this could result in a mutation. Loss of function mutations in tumor suppressors, or gain of function in proto-oncogenes from such mutations increase the chance of tumor development. ROS and RNS are produced during inflammation; CNTs generate oxidative radicals and contain an intrinsic potential to generate ROS and RNS over the entire course of exposure [177–181]. Experimentation *in vitro* has shown a noticeable difference in oxidative stress production in professional phagocytic cells versus non-phagocytic cells, where the phagocytic cells experience greater oxidative stress from internalized material and from NADPH oxidase-induced oxidative burst [182]. Human lung alveolar epithelial cells (A549) exposed to two MWCNTs of differing diameters exhibit a significant increase in inducible nitric oxide synthase (iNOS) and 8-nitroguanine formations equally from both MWCNTs [181]. RNS production within the alveolar cells results from MWCNT-induced inflammation and the resultant DNA nitrative damage can contribute to carcinogenesis [181]. Specifically, TLR9, which is located in endosomes and lysosomes, has been heavily implicated in the mechanism of CNT-induced carcinogenesis. Knock down of TLR9 greatly reduced endocytosis of MWCNTs and 8-nitroguanine adducts in lung epithelial cells

[183]. Combined *in vivo* and *in vitro* experiments exposing straight and tangled MWCNT to epithelial BEAS-2B cells and C57Bl/6 mice resulted in DNA strand breaks, however only *in vivo* exposure resulted in micronucleated alveolar type II cells after 4 days [184]. Furthermore, *in vitro* experiments demonstrate MWCNTs cause BEAS-2B epithelial cells to produce increased intracellular ROS and chromosomal breakage after three weeks exposure [185]. Experiments completed *in vitro* have shown a nanomaterial-specific protection of ROS-mediated cell death through upregulation of the anti-oxidant enzyme microsomal glutathione transferase 1 by silica nanoparticles which protects MCF-7 cells from lipid peroxidation [186]. However no protection from ZnO nanoparticles was observed [186]. Both SWCNTs and MWCNT treatment of RAW 264.7 macrophages cause increased ROS and chromosomal damage (i.e. Micronuclei) as well as oxidization of purines as measured by the comet assay [182]. The potential these materials have to produce ROS and their ability penetrate deep into and translocate to other organs increases the chance of both intra- and extra-pulmonary cellular and genotoxic oxidative damage. For instance, large needle-like MWCNTs translocate to the pleural cavity resulting in fibrosis, parietal mesothelial proliferative lesions and inflammation whereas a smaller cotton candy-like MWCNTs result in greater inflammation and 8-hydroxydeoxyguanosine levels in the lung [165]. Increased genotoxic events prior to somatic proliferation with little DNA repair is concerning because any mutation is then permanently passed along. Chronic oxidative stress can result in many genotoxic events and ultimately culminate in metaplasia or neoplasia. Oxidative stress can drive both inflammation and genotoxicity and may contribute to CNT-induced carcinogenesis.

Non-Oxidative Stress

Direct interaction of CNTs with cellular constituents has also been hypothesized to be a mechanism of CNT-induced cancer development where a prolonged low grade inflammogenic and fibrotic environment has been implicated in the etiology of particle-induced lung cancers [187]. However, the mechanisms of these processes in the development of lung cancer in rodents is not well understood. A 90 day exposure assessment of rod-like MWCNTs in Muta^{TM}mice, a mouse model with 40 copies of the bacterial *LacZ* gene incorporated to easily detect mutations, observed upregulation of cancer genes involved in cell death, cell proliferation, and free radical scavenging in the lung following SWCNT or MWCNT exposure [187,188]. This study did not find any DNA damage in the lungs of exposed mice, but found a high rate of apoptosis and proliferation suggesting that CNT-induced genotoxic effects occur slowly [187]. Studies have even shown CNTs can result in chromosomal aberrations not related to oxidative stress. Studies focused on cytotoxicity of CNT exposure *in vitro* have found the physical similarity of both SWCNTs and MWCNTs to mitotic spindles to result in mitotic spindle aberrations including chromosome disruption, abnormal mitotic spindles, monopolar mitosis, and aneuploid chromosomes in primary and immortal human epithelial cells after only 24 hours [168,189]. These SWCNTs were shown to be directly incorporated into the centrosome structure where they induced DNA damage [189]. Interestingly, oxidative stress has been shown to cause genotoxicity and similar chromosomal aberrations [190]. The potential for MWCNT to cause cancer as whole is relatively poorly understood, where only one rod-like MWCNT has

been classified in Group 2B by IARC, and the mechanism of cancer development of even this one variant of MWCNT is largely unknown and currently being investigated.

1.8 Genetic Susceptibility to Pulmonary Neoplasms

Tumor susceptibility, like any disease development, depends greatly on exposure dose and genetic background. Studies thus far have shown there to be a difference in susceptibility between rodent species as well as rodent strains. Beyond species and strain, genetic susceptibility within specific genes has been identified in disease states of mesothelioma and other lung tumors. For example, deficiencies in the p53 tumor suppressor result in greater frequency of tumor development, and have been seen to develop mesothelioma with MWCNT i.p. exposure.

Rodent and Strain Variation

Susceptibility to the development of cancers is as much based on environmental exposure as it is genetic background of the individual or rodent being investigated. In studies of the hyperplastic potential of MWCNT in rodents there has been a clear divide in rodent models where rats have been shown to develop mesothelioma following pulmonary exposure of CNTs, whereas mice exposed to these same CNTs have not been observed to develop these malignancies [24–26,161,169,171,191,192]. Interestingly, a study investigating the carcinogenic potential of these materials in different murine strains found increased susceptibility of C57Bl/6 mice to epithelial type II hyperplasia and DBA/2 mice to be the most resistant but with increased

sensitivity to pulmonary leukocyte infiltration with C3H/He and BALB/c mice indicating intermediate hyperplasia comparatively [191]. These studies highlight the importance of rodent and strain selection when analyzing these ENMs for carcinogenic potential and occupational exposure safety.

Loss of p53

Tumor suppressor p53 is a 53 kDa transcription factor which is often called the guardian of the genome due to its cell cycle control and DNA repair functions. Levels of p53 increase drastically with certain types of physiological stress, and it is activated by phosphorylation of one of its many phosphorylation sites. p53 functions as a homotetrameric transcription factor to regulate cell cycle arrest, inhibit metastasis, and promote apoptosis and DNA repair (Fig. 1.5). Interestingly, rats homozygous or heterozygous for p53 exhibit loss of heterozygosity and higher frequencies of carcinoma development compared to wild type rats [193]. It is because of this high susceptibility of the heterozygous model to cancer development that they are used frequently to study the tumorigenic potential of toxicants. Furthermore, alveolar cell DNA damage in a p53 dominant negative mouse strain results in greater inflammation and scarring compared to wild type mice [194]. These studies suggest that p53 is involved in regulating development of fibrosis and cancers. Mice heterozygous for p53 have been utilized previously in a mesothelioma surrogate assay where MWCNTs or asbestos were intraperitoneally injected and were observed to develop mesothelioma faster from MWCNT exposure compared to asbestos [19,20]. However, neither study compared the heterozygous p53 mice to wild type [19,20].

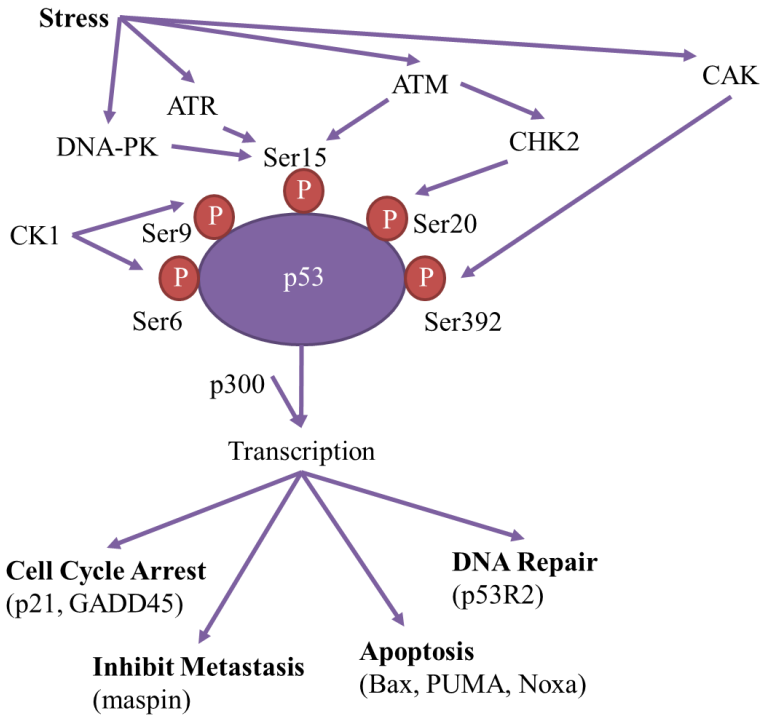

Figure 1.5. General overview of the activation and function of tumor suppressor p53. Physiological stress can activate selective pathways of p53 activation. The activation of specific serine (Ser) residues results in differing transcriptional responses (in bold) and transcripts (in parenthesis).

Mutations found in p53 leading to cancerous development include point mutations and frameshift mutations. If left unrepaired a point mutation results in a single base pair substitution can result in a missense or nonsense mutation resulting in the incorrect amino acid or stop codon incorporation, respectively. These mutations can result in the loss of wild type function, create dominant negative activity or promote oncogenic function through increased cellular growth through dysregulated cell cycle function. Mutations found in tumors are commonly

missense mutations within the DNA binding domain of p53 [195]. The loss of p53 function would leave DNA repair and cell growth unchecked and promote abnormal cell growth. Interestingly, neither asbestos nor MWCNTs have been tested in the lungs of p53 heterozygous mice to follow up these studies. Mutations in p53 are known to be a good prognosis factor in NSCLC [196]. Individuals who were exposed to asbestos and developed MPM (n=34) or NSCLC (n=50) had frequent polymorphisms occurring in p53 intron 7 compared to non-asbestos exposed patients (n=50), which identifies two polymorphisms at this specific location to be genetic susceptibility factors for asbestos-induced thoracic cancers [175]. Interestingly, the majority of the single nucleotide polymorphisms (SNPs) observed were not characteristic of ROS induced transversions of G:C to T:A, suggesting that these SNPs occurred independently of ROS [175]. Lung epithelial cells cultured with SWCNT *in vitro* for six months became transformed by increased AKT activation, p53 destabilization, and overexpression of an anti-apoptotic signaling molecule, Bcl2 [197]. The loss of one or both p53 alleles is a susceptibility factor for tumor development, and epidemiological data demonstrates that the loss of p53 is associated with lung cancer development.

1.9 Epidemiology of CNT Exposure

Products of the emerging nanotechnology industry are relatively new and therefore epidemiologic information related to human health outcomes from CNT-exposure is relatively scarce. CNT manufacturing began early in the 2000's and only a handful of epidemiological studies have been published on CNT-exposure and health risks. Diverse and different types of

ENMs may produce different pathological outcomes based on their physicochemical properties. Often employees manufacture products that contain more than one type of ENM (e.g., CNT plus nanometal catalyst) resulting in exposure to a mixture of ENMs. Currently, published epidemiologic studies have relatively low numbers of participants, lack of data on duration of worker employment/exposure, and only collect data from companies who give permission [198–200]. Epidemiology studies fail to tease out the physicochemical differences between ENMs. The similarities to asbestos make CNTs a concern for human health. Epidemiology studies have tested individuals currently working at a CNT factory but have not followed individuals who have changed occupations. Most importantly, asbestos related lung diseases have a latent period of 30-40 years, suggesting that CNT-induced pulmonary diseases could take decades before we begin to see symptom presentation [201]. A few studies have been successful in identification of potential biomarkers of human lung inflammation and fibrosis; these offer important opportunities to follow up on in the future [88,89].

1.10 General Conclusions

Physicochemical characteristics of CNTs determine the severity of pulmonary disease in rodent models. However, there is still a gap in our knowledge as to which specific characteristics are important towards predicting the human health risks of CNTs. Better characterization of newly synthesized or functionalized nanomaterials may aid in determination of safety or risk of inhalation exposure to such materials. Currently, the state of science in the field of nanotoxicology emphasizes the need to consider physicochemical

characteristics in the safe design of CNTs. However, this approach is only effective if consumer products use the 'safer' CNTs. Metal catalyst content, length, rigidity, agglomeration status and surface functionalization coatings modify fibrogenic responses in the lungs of rodents and therefore should be considered in the design of CNTs. Using rodent models is useful to determine toxicity of these materials, however most studies utilize a single bolus CNT- exposure; to best assess occupational exposure there is a need for more studies comparing different types of CNTs administrated over several doses or via inhalation to best represent occupational settings and exposures. Variations in exposure methodology make comparisons between studies difficult. However, as the body of literature keeps growing on this topic we may be able to more effectively elucidate the appropriate physicochemical properties that are of concern.

CNTs promote fibrogenesis and carcinogenesis through proximal oxidative stress mechanisms which trigger the activation of intracellular signaling pathways including activation of kinases, transcription factors, enzymes and the inflammasome. In the case of fibrogenesis, these signaling events within cells stimulate the production and release of growth factors like TGF-β1 and PDGF which then drive the recruitment, differentiation, and proliferation of myofibroblasts. Interestingly, some CNTs promote an alternative macrophage phenotype and alter the immune response towards a Th2 response while others activate a more classical macrophage population and resulting Th1 immune response. Carcinogenesis stems from genetic aberrations directly or indirectly from CNT-induced mechanisms of ROS production and DNA damage accumulated through multiple rounds of somatic replication can result in

tumor generation. Studies with transgenic mice have elucidated specific genetic determinants of susceptibility. Future directions of CNT research focused on issues of susceptibility and comparison of CNTs with differing physicochemical properties could improve our mechanistic understanding of CNT-induced pulmonary disease. Overall, the fibrogenic and carcinogenic responses to different types of CNTs is due to both the physicochemical characteristics of the nanomaterial and genetic susceptibility of the host.

1.11 General Hypothesis

Considering the inherent physicochemical differences in nanomaterials, it is conceivable that not any two are the same. For my work I have focused on two very different MWCNTs, one that is more tangled and another that is more rod-like. I hypothesized that exposure of mouse lungs to either MWCNT will result in differing pathological outcomes of inflammation, fibrosis and neoplasia. Furthermore, exposure of susceptible mouse models deficient in STAT1 or heterozygous for p53 should result in greater fibrosis or neoplastic events, respectively.

1.12 References:

1. Cha, C.; Shin, S. R.; Annabi, N.; Dokmeci, M. R.; Khademhosseini, A. Carbon-Based Nanomaterials: Multifunctional Materials for Biomedical Engineering. ACS 2013, 7, 2891–2897.

2. NIOSH. CURRENT INTELLIGENCE BULLETIN 65: Occupational Exposure to Carbon Nanotubes and Nanofibers; 2013.

3. Mishra, A.; Stueckle, T. A.; Mercer, R. R.; Derk, R.; Rojanasakul, Y.; Castranova, V.; Wang, L. Identification of TGF- β Receptor-1 as a Key Regulator of Carbon Nanotube-Induced Fibrogenesis. Am J Physiol Lung Cell Mol Physiol 2015, 309, 821–833.

4. Pauluhn, J. Subchronic 13-Week Inhalation Exposure of Rats to Multiwalled Carbon Nanotubes: Toxic Effects Are Determined by Density of Agglomerate Structures, Not Fibrillar Structures. Toxicol. Sci. 2010, 113, 226–242.

5. Ryman-Rasmussen, J. P.; Tewksbury, E. W.; Moss, O. R.; Cesta, M. F.; Wong, B. A.; Bonner, J. C. Inhaled Multiwalled Carbon Nanotubes Potentiate Airway Fibrosis in Murine Allergic Asthma. Am. J. Respir. Cell Mol. Biol. 2009, 40, 349–358.

6. (ATS), A. T. S. Patient Information Series: Idiopathic Pulmonary Fibrosis (IPF). Am J Respir Crit Care Med 2015, 183, 2.

7. Arakawa, H.; Kishimoto, T.; Ashizawa, K.; Kato, K.; Okamoto, K.; Honma, K.; Hayashi, S.; Akira, M. Asbestosis and Other Pulmonary Fibrosis in Asbestos-Exposed Workers: High-Resolution CT Features with Pathological Correlations. Eur. Radiol. 2016, 26, 1485–1492.

8. Blackley, D. J.; Crum, J. B.; Halldin, C. N.; Storey, E.; Laney, A. S. Resurgence of Progressive Massive Fibrosis in Coal Miners — Eastern Kentucky, 2016. MMWR. Morb. Mortal. Wkly. Rep. 2016, 65, 1385–1389.

9. Nemery, B. Metal Toxicity and the Respiratory Tract. Eur. Respir. J. 1990, 3, 202–219.

10. Vitums, V. C.; Edwards, M. J.; Niles, N. R.; Borman, J. O.; Lowry, R. D. Pulmonary Fibrosis from Amorphous Silica Dust, a Product of Silica Vapor. Arch. Environ. Health 1977, 32, 62–68.

11. Nemmar, A.; Holme, J. A.; Rosas, I.; Schwarze, P. E.; Alfaro-Moreno, E. Recent Advances in Particulate Matter and Nanoparticle Toxicology: A Review of the in Vivo and in Vitro Studies. Biomed Res. Int. 2013, 2013, 22.

12. Ryman-rasmussen, J. P.; Cesta, M. F.; Brody, A. R.; Shipley, J. K.; Everitt, J.; Tewksbury, E. W.; Moss, O. R.; Wong, B. a; Darol, E.; Andersen, M. E.; et al. Inhaled Carbon Nanotubes Reach the Sub-Pleural Tissue in Mice. Nat. Nanotechnol. 2009, 4, 747–751.

13. Mercer, R. R.; Scabilloni, J. F.; Hubbs, A. F.; Wang, L.; Battelli, L. a; McKinney, W.; Castranova, V.; Porter, D. W. Extrapulmonary Transport of MWCNT Following Inhalation Exposure. Part. Fibre Toxicol. 2013, 10, 13.

14. Ma-Hock, L.; Treumann, S.; Strauss, V.; Brill, S.; Luizi, F.; Mertler, M.; Wiench, K.; Gamer, A. O.; van Ravenzwaay, B.; Landsiedel, R. Inhalation Toxicity of Multiwall Carbon Nanotubes in Rats Exposed for 3 Months. Toxicol. Sci. 2009, 112, 468–481.

15. Bonner, J. C. Progress Towards Understanding the Health Effects of Carbon Nanotubes. 2013.

16. Mercer, R. R.; Scabilloni, J.; Wang, L.; Kisin, E.; Murray, A. R.; Schwegler-Berry, D.; Shvedova, A. A.; Castranova, V. Alteration of Deposition Pattern and Pulmonary Response as a Result of Improved Dispersion of Aspirated Single-Walled Carbon Nanotubes in a Mouse Model. Am. J. Physiol. Lung Cell. Mol. Physiol. 2008, 294, L87-97.

17. Manke, A.; Luanpitpong, S.; Dong, C.; Wang, L.; He, X.; Battelli, L.; Derk, R.; Stueckle, T.; Porter, D.; Sager, T.; et al. Effect of Fiber Length on Carbon Nanotube-Induced Fibrogenesis. Int. J. Mol. Sci. 2014, 15, 7444–7461.

18. Shinohara, N.; Nakazato, T.; Ohkawa, K. Long-Term Retention of Pristine Multi-Walled Carbon Nanotubes in Rat Lungs after Intratracheal Instillation. J. Appl. Toxicol. 2016, 36, 501–509.

19. Takagi, A.; Hirose, A.; Nishimura, T.; Fukumori, N.; Ogata, A.; Ohashi, N.; Kitajima, S.; Kanno, J. Induction of Mesothelioma in p53+/- Mouse by Intraperitoneal Application of Multi-Wall Carbon Nanotube. J. Toxicol. Sci. 2008, 33, 105–116.

20. Takagi, A.; Hirose, A.; Futakuchi, M.; Tsuda, H.; Kanno, J. Dose-Dependent Mesothelioma Induction by Intraperitoneal Administration of Multi-Wall Carbon Nanotubes in p53 Heterozygous Mice. Cancer Sci. 2012, 103, 1440–1444.

21. Poland, C. a; Duffin, R.; Kinloch, I.; Maynard, A.; Wallace, W. a H.; Seaton, A.; Stone, V.; Brown, S.; Macnee, W.; Donaldson, K. Carbon Nanotubes Introduced into the Abdominal Cavity of Mice Show Asbestos-like Pathogenicity in a Pilot Study. Nat. Nanotechnol. 2008, 3, 423–428.

22. Sakamoto, Y.; Nakae, D.; Fukumori, N.; Tayama, K.; Maekawa, A.; Imai, K.; Hirose, A.; Nishimura, T.; Ohashi, N.; Ogata, A. Induction of Mesothelioma by a Single Intrascrotal Administration of Multi-Wall Carbon Nanotube in Intact Male Fischer 344 Rats. J. Toxicol. Sci. 2009, 34, 65–76.

23. Huaux, F.; d'Ursel de Bousies, V.; Parent, M.A.; Orsi, M.; Uwambayinema, F.; Devosse, R.; Ibouraadaten, S.; Yakoub, Y.; Panin, N.; Palmai-Pallag, M.; et al. Mesothelioma Response to Carbon Nanotubes Is Associated with an Early and Selective Accumulation of Immunosuppressive Monocytic Cells. Part. Fibre Toxicol. 2015, 13, 46.

24. Murphy, F. a.; Poland, C. a.; Duffin, R.; Al-Jamal, K. T.; Ali-Boucetta, H.; Nunes, A.; Byrne, F.; Prina-Mello, A.; Volkov, Y.; Li, S.; et al. Length-Dependent Retention of Carbon

Nanotubes in the Pleural Space of Mice Initiates Sustained Inflammation and Progressive Fibrosis on the Parietal Pleura. Am. J. Pathol. 2011, 178, 2587–2600.

25. Kasai, T.; Umeda, Y.; Ohnishi, M.; Mine, T.; Kondo, H.; Takeuchi, T. Lung Carcinogenicity of Inhaled Multi- Walled Carbon Nanotube in Rats. Part. Fibre Toxicol. 2016, 1–19.

26. Suzui, M.; Futakuchi, M.; Fukamachi, K.; Numano, T.; Abdelgied, M.; Takahashi, S.; Ohnishi, M.; Omori, T.; Tsuruoka, S.; Hirose, A.; et al. Multiwalled Carbon Nanotubes Intratracheally Instilled into the Rat Lung Induce Development of Pleural Malignant Mesothelioma and Lung Tumors. Cancer Sci. 2016, 107, 924–935.

27. Kelleher, P.; Pacheco, K.; Newman, L. S. Inorganic Dust Pneumonias: The Metal-Related Parenchymal Disorders. Environ. Health Perspect. 2000, 108, 685–696.

28. Hamilton, R. F.; Buford, M.; Xiang, C.; Wu, N.; Holian, A. NLRP3 Inflammasome Activation in Murine Alveolar Macrophages and Related Lung Pathology Is Associated with MWCNT Nickel Contamination. Inhal. Toxicol. 2012, 24, 995–1008.

29. Silva, R. M.; Doudrick, K.; Franzi, L. M.; TeeSy, C.; Anderson, D. S.; Wu, Z.; Mitra, S.; Vu, V.; Dutrow, G.; Evans, J. E.; et al. Instillation versus Inhalation of Multiwalled Carbon Nanotubes: Exposure-Related Health Effects, Clearance, and the Role of Particle Characteristics. ACS Nano 2014, 8, 8911–8931.

30. Xia, T.; Hamilton, R. F.; Bonner, J. C.; Crandall, E. D.; Elder, A.; Fazlollahi, F.; Girtsman, T. A.; Kim, K.; Mitra, S.; Ntim, S. A.; et al. Interlaboratory Evaluation of in Vitro Cytotoxicity and Inflammatory Responses to Engineered Nanomaterials: The NIEHS Nano GO Consortium. Environ. Health Perspect. 2013, 121, 683–690.

31. Chen, T.; Nie, H.; Gao, X.; Yang, J.; Pu, J.; Chen, Z.; Cui, X.; Wang, Y.; Wang, H.; Jia, G. Epithelial–mesenchymal Transition Involved in Pulmonary Fibrosis Induced by Multi-Walled Carbon Nanotubes via TGF-beta/Smad Signaling Pathway. Toxicol. Lett. 2014, 226, 150–162.

32. Wang, P.; Nie, X.; Wang, Y.; Li, Y.; Ge, C.; Zhang, L.; Wang, L.; Bai, R.; Chen, Z.; Zhao, Y.; et al. Multiwall Carbon Nanotubes Mediate Macrophage Activation and Promote Pulmonary Fibrosis through TGF-B/smad Signaling Pathway. Small 2013, 9, 3799–3811.

33. ISO/TS. Nanotechnologies — Characterization of Multiwall Carbon Nanotubes - Mesoscopic Shape Factors. Tech. Specif. 2011, 2011.

34. Poulsen, S. S.; Saber, A. T.; Williams, A.; Andersen, O.; Købler, C.; Atluri, R.; Pozzebon, M. E.; Mucelli, S. P.; Simion, M.; Rickerby, D.; et al. MWCNTs of Different Physicochemical Properties Cause Similar Inflammatory Responses, but Differences in Transcriptional and Histological Markers of Fibrosis in Mouse Lungs. Toxicol. Appl. Pharmacol. 2015, 284, 16–32.

35. Donaldson, K.; Murphy, F. a; Duffin, R.; Poland, C. a. Asbestos, Carbon Nanotubes and the Pleural Mesothelium: A Review of the Hypothesis Regarding the Role of Long Fibre Retention in the Parietal Pleura, Inflammation and Mesothelioma. Part. Fibre Toxicol. 2010, 7, 5.

36. Murphy, F. a; Schinwald, A.; Poland, C. a; Donaldson, K. The Mechanism of Pleural Inflammation by Long Carbon Nanotubes: Interaction of Long Fibres with Macrophages Stimulates Them to Amplify pro-Inflammatory Responses in Mesothelial Cells. Part. Fibre Toxicol. 2012, 9, 8.

37. Porter, D. W.; Hubbs, A. F.; Mercer, R. R.; Wu, N.; Wolfarth, M. G.; Sriram, K.; Leonard, S.; Battelli, L.; Schwegler-Berry, D.; Friend, S.; et al. Mouse Pulmonary Dose- and Time Course-Responses Induced by Exposure to Multi-Walled Carbon Nanotubes. Toxicology 2010, 269, 136–147.

38. Rydman, E. M.; Ilves, M.; Koivisto, A. J.; Kinaret, P. A. S.; Fortino, V.; Savinko, T. S.; Lehto, M. T.; Pulkkinen, V.; Vippola, M.; Hämeri, K. J.; et al. Inhalation of Rod-like Carbon Nanotubes Causes Unconventional Allergic Airway Inflammation. Part. Fibre Toxicol. 2014, 11, 17.

39. Thompson, E. A.; Sayers, B. C.; Glista-Baker, E. E.; Shipkowski, K. A.; Ihrie, M. D.; Duke, K. S.; Taylor, A. J.; Bonner, J. C. Role of Signal Transducer and Activator of Transcription 1 in Murine Allergen-Induced Airway Remodeling and Exacerbation by Carbon Nanotubes. Am. J. Respir. Cell Mol. Biol. 2015, 53, 625–636.

40. Vietti, G.; Ibouraadaten, S.; Palmai-Pallag, M.; Yakoub, Y.; Bailly, C.; Fenoglio, I.; Marbaix, E.; Lison, D.; van den Brule, S. Towards Predicting the Lung Fibrogenic Activity of Nanomaterials: Experimental Validation of an in Vitro Fibroblast Proliferation Assay. Part. Fibre Toxicol. 2013, 10, 52.

41. Jaggernauth, A.; Silva, R. M.; Neto, M. A.; Hortiguela, M. J.; Gonçalves, G.; Singh, M. K.; Oliveira, F. J.; Silva, R. F. e; Vila, M. Nano-Graphene Oxide Functionalization with Organic and Hybrid Organic-Inorganic Polymers by Molecular Layer Deposition. J. Phys. Chem. C 2016, 24175–24186.

42. Bhattacharya, K.; Mukherjee, S. P.; Gallud, A.; Burkert, S. C.; Bistarelli, S.; Bellucci, S.; Bottini, M.; Star, A.; Fadeel, B. Biological Interactions of Carbon-Based Nanomaterials: From Coronation to Degradation. Nanomedicine Nanotechnology, Biol. Med. 2016, 12, 333–351.

43. Li, R.; Wang, X.; Ji, Z.; Sun, B.; Zhang, H.; Chang, C. H.; Lin, S.; Meng, H.; Liao, Y.P.; Wang, M.; et al. Surface Charge and Cellular Processing of Covalently Functionalized Multiwall Carbon Nanotubes Determine Pulmonary Toxicity. ACS Nano 2013, 7, 2352–2368.

44. Shvedova, A. A.; Kisin, E.; Murray, A. R.; Johnson, V. J.; Gorelik, O.; Arepalli, S.; Hubbs, A. F.; Mercer, R. R.; Keohavong, P.; Sussman, N.; et al. Inhalation vs. Aspiration of Single-Walled Carbon Nanotubes in C57BL/6 Mice: Inflammation, Fibrosis, Oxidative Stress, and Mutagenesis. Am. J. Physiol. Lung Cell. Mol. Physiol. 2008, 295, L552-65.

45. Jiao, S.; Meng, F.; Zhang, J.; Yang, X.; Zheng, X.; Wang, L. STAT1 Mediates Cellular Senescence Induced by Angiotensin II and H2O2 in Human Glomerular Mesangial Cells. Mol. Cell. Biochem. 2012, 365, 9–17.

46. Coccini, T.; Manzo, L.; Roda, E. Safety Evaluation of Engineered Nanomaterials for Health Risk Assessment: An Experimental Tiered Testing Approach Using Pristine and Functionalized Carbon Nanotubes. ISRN Toxicol. 2013, 2013, 825427.

47. Roda, E.; Coccini, T.; Acerbi, D.; Barni, S.; Vaccarone, R.; Manzo, L. Comparative Pulmonary Toxicity Assessment of Pristine and Functionalized Multi-Walled Carbon Nanotubes Intratracheally Instilled in Rats: Morphohistochemical Evaluations. Histol. Histopathol. 2011, 26, 357–367.

48. Bonner, J. C.; Silva, R. M.; Taylor, A. J.; Brown, J. M.; Hilderbrand, S. C.; Castranova, V.; Porter, D.; Elder, A.; Oberdörster, G.; Harkema, J. R.; et al. Interlaboratory Evaluation of Rodent Pulmonary Responses to Engineered Nanomaterials: The NIEHS Nano GO Consortium. Environ. Health Perspect. 2013, 121, 676–682.

49. Wang, X.; Xia, T.; Addo Ntim, S.; Ji, Z.; Lin, S.; Meng, H.; Chung, C.-H.; George, S.; Zhang, H.; Wang, M.; et al. Dispersal State of Multiwalled Carbon Nanotubes Elicits Profibrogenic Cellular Responses That Correlate with Fibrogenesis Biomarkers and Fibrosis in the Murine Lung. ACS Nano 2011, 5, 9772–9787.

50. Taylor, A. J.; McClure, C. D.; Shipkowski, K. A.; Thompson, E. A.; Hussain, S.; Garantziotis, S.; Parsons, G. N.; Bonner, J. C. Atomic Layer Deposition Coating of Carbon Nanotubes with Aluminum Oxide Alters pro-Fibrogenic Cytokine Expression by Human

Mononuclear Phagocytes in Vitro and Reduces Lung Fibrosis in Mice in Vivo. PLoS One 2014, 9, e106870.

51. Hussain, S.; Ji, Z.; Taylor, A. J.; Degraff, L. M.; George, M.; Tucker, C. J.; Chang, C. H.; Li, R.; Bonner, J. C.; Garantziotis, S. Multiwalled Carbon Nanotube Functionalization with High Molecular Weight Hyaluronan Significantly Reduces Pulmonary Injury. ACS Nano 2016, 10, 7675–7688.

52. Dandley, E. C.; Taylor, A. J.; Duke, K. S.; Ihrie, M. D.; Shipkowski, K. A.; Parsons, G. N.; Bonner, J. C. Atomic Layer Deposition Coating of Carbon Nanotubes with Zinc Oxide Causes Acute Phase Immune Responses in Human Monocytes in Vitro and in Mice after Pulmonary Exposure. Part. Fibre Toxicol. 2016, 13, 29.

53. Nel, A.; Xia, T.; Meng, H.; Wang, X.; Lin, S.; Ji, Z.; Zhang, H. Nanomaterial Toxicity Testing in the 21st Century: Use of a Predictive Toxicological Approach and High-Throughput Screening. Acc. Chem. Res. 2013, 46, 607–621.

54. Bonner, J. C. Mesenchymal Cell Survival in Airway and Interstitial Pulmonary Fibrosis. Fibrogenesis Tissue Repair 2010, 3, 15.

55. Chang, C.C.; Tsai, M.L.; Huang, H.C.; Chen, C.Y.; Dai, S.X. Epithelial-Mesenchymal Transition Contributes to SWCNT-Induced Pulmonary Fibrosis. Nanotoxicology 2012, 6, 600–610.

56. Dong, J.; Porter, D. W.; Batteli, L. A.; Wolfarth, M. G.; Richardson, D. L.; Ma, Q. Pathologic and Molecular Profiling of Rapid - Onset Fibrosis and Inflammation Induced by Multi - Walled Carbon Nanotubes. Arch. Toxicol. 2014, 89, 621–633.

57. He, X.; Young, S.-H.; Fernback, J. E.; Ma, Q. Single-Walled Carbon Nanotubes Induce Fibrogenic Effect by Disturbing Mitochondrial Oxidative Stress and Activating NF-κB Signaling. J. Clin. Toxicol. 2012, S5:005, 19.

58. He, X.; Young, S.-H.; Schwegler-Berry, D.; Chisholm, W. P.; Fernback, J. E.; Ma, Q. Multiwalled Carbon Nanotubes Induce a Fibrogenic Response by Stimulating Reactive Oxygen Species Production, Activating NF-κB Signaling, and Promoting Fibroblast-to-Myofibroblast Transformation. Chem. Res. Toxicol. 2011, 24, 2237–2248.

59. Rothen-Rutishauser, B.; Brown, D. M.; Piallier-Boyles, M.; Kinloch, I. A.; Windle, A. H.; Gehr, P.; Stone, V. Relating the Physicochemical Characteristics and Dispersion of Multiwalled Carbon Nanotubes in Different Suspension Media to Their Oxidative Reactivity in Vitro and Inflammation in Vivo. Nanotoxicology 2010, 4, 331–342.

60. Thurnherr, T.; Brandenberger, C.; Fischer, K.; Diener, L.; Manser, P.; Maeder-Althaus, X.; Kaiser, J.-P.; Krug, H. F.; Rothen-Rutishauser, B.; Wick, P. A Comparison of Acute and Long-Term Effects of Industrial Multiwalled Carbon Nanotubes on Human Lung and Immune Cells in Vitro. Toxicol. Lett. 2011, 200, 176–186.

61. Sun, B.; Wang, X.; Ji, Z.; Wang, M.; Liao, Y.-P.; Chang, C. H.; Li, R.; Zhang, H.; Nel, A. E.; Xia, T. NADPH Oxidase-Dependent NLRP3 Inflammasome Activation and Its Important Role in Lung Fibrosis by Multiwalled Carbon Nanotubes. Small 2015, 11, 2087–2097.

62. Vietti, G.; Lison, D.; van den Brule, S. Mechanisms of Lung Fibrosis Induced by Carbon Nanotubes: Towards an Adverse Outcome Pathway (AOP). Part. Fibre Toxicol. 2016, 13, 11.

63. Han, S. G.; Andrews, R.; Gairola, C. G. Acute Pulmonary Response of Mice to Multi-Wall Carbon Nanotubes. Inhal. Toxicol. 2010, 22, 340–347.

64. Manoury, B.; Nenan, S.; Leclerc, O.; Guenon, I.; Boichot, E.; Planquois, J.-M.; Bertrand, C. P.; Lagente, V.; Crouch, E.; Selman, M.; et al. The Absence of Reactive Oxygen Species Production Protects Mice against Bleomycin-Induced Pulmonary Fibrosis. Respir. Res. 2005, 6, 11.

65. Dong, J.; Ma, Q. Suppression of Basal and Carbon Nanotube-Induced Oxidative Stress, Inflammation and Fibrosis in Mouse Lungs by Nrf2. Nanotoxicology 2016, 10, 699–709.

66. Boyles, M. S. P.; Young, L.; Brown, D. M.; MacCalman, L.; Cowie, H.; Moisala, A.; Smail, F.; Smith, P. J. W.; Proudfoot, L.; Windle, A. H.; et al. Multi-Walled Carbon Nanotube Induced Frustrated Phagocytosis, Cytotoxicity and pro-Inflammatory Conditions in Macrophages Are Length Dependent and Greater than that of Asbestos. Toxicol. Vitr. 2015, 29, 1513–1528.

67. Meunier, E.; Coste, A.; Olagnier, D.; Authier, H.; Lefèvre, L.; Dardenne, C.; Bernad, J.; Béraud, M.; Flahaut, E.; Pipy, B. Double-Walled Carbon Nanotubes Trigger IL-1β Release in Human Monocytes through Nlrp3 Inflammasome Activation. Nanomedicine Nanotechnology, Biol. Med. 2012, 8, 987–995.

68. Palomäki, J.; Välimäki, E.; Sund, J.; Vippola, M.; Clausen, P. A.; Jensen, K. A.; Savolainen, K.; Matikainen, S.; Alenius, H. Long, Needle-like Carbon Nanotubes and Asbestos Activate the NLRP3 Inflammasome through a Similar Mechanism. ACS Nano 2011, 5, 6861–6870.

69. Strowig, T.; Henao-Mejia, J.; Elinav, E.; Flavell, R. Inflammasomes in Health and Disease. Nature 2012, 481, 278–286.

70. Jessop, F.; Holian, A. Extracellular HMGB1 Regulates Multi-Walled Carbon Nanotube-Induced Inflammation in Vivo. Nanotoxicology 2015, 9, 365–372.

71. Martinon, F.; Mayor, A.; Tschopp, J. The Inflammasomes: Guardians of the Body. Annu. Rev. Immunol. 2009, 27, 229–265.

72. Gordon, S.; Martinez, F. O. Alternative Activation of Macrophages: Mechanism and Functions. Immunity 2010, 32, 593–604.

73. Shipkowski, K. A.; Taylor, A. J.; Thompson, E. A.; Glista-Baker, E. E.; Sayers, B. C.; Messenger, Z. J.; Bauer, R. N.; Jaspers, I.; Bonner, J. C. An Allergic Lung Microenvironment Suppresses Carbon Nanotube-Induced Inflammasome Activation via STAT6-Dependent Inhibition of Caspase-1. PLoS One 2015, 10, e0128888.

74. Girtsman, T. A.; Beamer, C. A.; Wu, N.; Buford, M.; Holian, A. IL-1R Signaling Is Critical for Regulation of Multi-Walled Carbon Nanotubes-Induced Acute Lung Inflammation in C57Bl/6 Mice. Nanotoxicology 2014, 8, 17–27.

75. Hussain, S.; Sangtian, S.; Anderson, S. M.; Snyder, R. J.; Marshburn, J. D.; Rice, A. B.; Bonner, J. C.; Garantziotis, S. Inflammasome Activation in Airway Epithelial Cells after Multi-Walled Carbon Nanotube Exposure Mediates a Profibrotic Response in Lung Fibroblasts. Part. Fibre Toxicol. 2014, 11, 28.

76. Jenkins, G. The Role of Proteases in Transforming Growth Factor-β Activation. Int. J. Biochem. Cell Biol. 2008, 40, 1068–1078.

77. Mu, D.; Cambier, S.; Fjellbirkeland, L.; Baron, J. L.; Munger, J. S.; Kawakatsu, H.; Sheppard, D.; Broaddus, V. C.; Nishimura, S. L. The Integrin αvβ8 Mediates Epithelial Homeostasis through MT1-MMP–dependent Activation of TGF-β1. J. Cell Biol. 2002, 157, 493–507.

78. Munger, J. S.; Huang, X.; Kawakatsu, H.; Griffiths, M. J.; Dalton, S. L.; Wu, J.; Pittet, J.F.; Kaminski, N.; Garat, C.; Matthay, M. A.; et al. A Mechanism for Regulating Pulmonary Inflammation and Fibrosis: The Integrin αvβ6 Binds and Activates Latent TGF β1. Cell 1999, 96, 319–328.

79. Murphy-Ullrich, J. E.; Poczatek, M. Activation of Latent TGF-β by Thrombospondin-1: Mechanisms and Physiology. Cytokine Growth Factor Rev. 2000, 11, 59–69.

80. Wrighton, K. H.; Lin, X.; Feng, X. H. Phospho-Control of TGF-Beta Superfamily Signaling. Cell Res. 2009, 19, 8–20.

81. Leask, A.; Abraham, D. J. TGF-Beta Signaling and the Fibrotic Response. FASEB J. 2004, 18, 816–827.

82. Kulkarni, A. B.; Karlsson, S. Transforming Growth Factor-Beta 1 Knockout Mice. A Mutation in One Cytokine Gene Causes a Dramatic Inflammatory Disease. Am. J. Pathol. 1993, 143, 3–9.

83. Shvedova, A. A.; Kisin, E. R.; Mercer, R.; Murray, A. R.; Johnson, V. J.; Potapovich, A. I.; Tyurina, Y. Y.; Gorelik, O.; Arepalli, S.; Schwegler-Berry, D.; et al. Unusual Inflammatory and Fibrogenic Pulmonary Responses to Single-Walled Carbon Nanotubes in Mice. AJP Lung Cell. Mol. Physiol. 2005, 289, L698–L708.

84. Wang, X.; Xia, T.; Doch, M. C.; Ji, Z.; Zhang, H.; Li, R.; Sun, B.; Lin, S.; Meng, H.; Liao, Y.-P.; et al. Pluronic F108 Coating Decreases the Lung Fibrosis Potential of Multiwall Carbon Nanotubes by Reducing Lysosomal Injury. Nano Lett. 2012, 12, 3050–3061.

85. Wang, X.; Duch, M. C.; Mansukhani, N.; Ji, Z.; Liao, Y.-P.; Wang, M.; Zhang, H.; Sun, B.; Chang, C. H.; Li, R.; et al. Use of a pro-Fibrogenic Mechanism-Based Predictive Toxicological Approach for Tiered Testing and Decision Analysis of Carbonaceous Nanomaterials. ACS Nano 2015, 9, 3032–3043.

86. Zhang, Y.; Yan, B. Cell Cycle Regulation by Carboxylated Multiwalled Carbon Nanotubes through p53-Independent Induction of p21 under the Control of the BMP Signaling Pathway. Chem. Res. Toxicol. 2012, 25, 1212–1221.

87. Dong, J.; Ma, Q. Myofibroblasts and Lung Fibrosis Induced by Carbon Nanotube Exposure. Part. Fibre Toxicol. 2016, 13, 22.

88. Fatkhutdinova, L. M.; Khaliullin, T. O.; Vasil'yeva, O. L.; Zalyalov, R. R.; Mustafin, I. G.; Kisin, E. R.; Birch, M. E.; Yanamala, N.; Shvedova, A. A. Fibrosis Biomarkers in Workers Exposed to MWCNTs. Toxicol. Appl. Pharmacol. 2016, 299, 125–131.

89. Vlaandderen, J.; Pronk, A.; Rothman, N.; Hildesheim, A.; Silverman, D.; Hosgood, D.; Suzanne, S.; Kuijpers, E.; Godderis, L.; Hoet, P. A Cross-Sectional Study of Changes in Markers of Immunological Effects and Lung Health due to Exposure to Multi-Walled Carbon Nanotubes. Nanotoxicology 2017, 11, 395–404.

90. Bonner, J. C. Nanoparticles as a Potential Cause of Pleural and Interstitial Lung Disease. Proc. Am. Thorac. Soc. 2010, 7, 138–141.

91. Chen, T.; You, Y.; Jiang, H.; Wang, Z. Z. Epithelial-Mesenchymal Transition (EMT): A Biological Process in the Development, Stem Cell Differentiation and Tumorigenesis. J. Cell. Physiol. 2014, 226, 150–162.

92. Li, Y.; Gao, A.; Yu, L. Monitoring of TGF-β 1-Induced Human Lung Adenocarcinoma A549 Cells Epithelial-Mesenchymal Transformation Process by Measuring Cell Adhesion Force with a Microfluidic Device. Appl. Biochem. Biotechnol. 2016, 178, 114–125.

93. Wang, P.; Wang, Y.; Nie, X.; Braïni, C.; Bai, R.; Chen, C. Multiwall Carbon Nanotubes Directly Promote Fibroblast-Myofibroblast and Epithelial-Mesenchymal Transitions through the Activation of the TGF-β/Smad Signaling Pathway. Small 2015, 11, 446–455.

94. Polimeni, M.; Gulino, G. R.; Gazzano, E.; Kopecka, J.; Marucco, A.; Fenoglio, I.; Cesano, F.; Campagnolo, L.; Magrini, A.; Pietroiusti, A.; et al. Multi-Walled Carbon Nanotubes Directly Induce Epithelial-Mesenchymal Transition in Human Bronchial Epithelial Cells via the TGF- β -Mediated Akt / GSK-3 β / SNAIL-1 Signaling Pathway. Part. Fibre Toxicol. 2016, 1–19.

95. Lan, A.; Qi, Y.; Du, J. Akt2 Mediates TGF-β1-Induced Epithelial to Mesenchymal Transition by Deactivating GSK3β/snail Signaling Pathway in Renal Tubular Epithelial Cells. Cell. Physiol. Biochem. 2014, 34, 368–382.

96. Snyder, R. J.; Hussain, S.; Rice, A.; Garantziotis, S. Multiwalled Carbon Nanotubes Induce Altered Morphology and Loss of Barrier Function in Human Bronchial Epithelium at Noncytotoxic Doses. Int. J. Nanomedicine 2014, 9, 4093–4105.

97. Bonner, J. C. Regulation of PDGF and Its Receptors in Fibrotic Diseases. Cytokine Growth Factor Rev. 2004, 15, 255–273.

98. Yoshida, M.; Sakuma, J.; Hayashi, S.; Abe, K.; Saito, I.; Harada, S.; Sakatani, M.; Yamamoto, S.; Matsumoto, N.; Kaneda, Y.; et al. A Histologically Distinctive Interstitial Pneumonia Induced by Overexpression of the Interleukin 6, Transforming Growth Factor Beta 1, or Platelet-Derived Growth Factor B Gene. Proc. Natl. Acad. Sci. U. S. A. 1995, 92, 9570–9574.

99. Cesta, M. F.; Ryman-Rasmussen, J. P.; Wallace, D. G.; Masinde, T.; Hurlburt, G.; Taylor, A. J.; Bonner, J. C. Bacterial Lipopolysaccharide Enhances PDGF Signaling and Pulmonary Fibrosis in Rats Exposed to Carbon Nanotubes. Am. J. Respir. Cell Mol. Biol. 2010, 43, 142–151.

100. Glista-baker, E. E.; Taylor, A. J.; Sayers, B. C.; Thompson, E. A.; Bonner, J. C. Nickel Nanoparticles Cause Exaggerated Lung and Airway Remodeling in Mice Lacking the T-Box

Transcription Factor, TBX21 (T-Bet) Nickel Nanoparticles Cause Exaggerated Lung and Airway Remodeling in Mice Lacking the T-Box Transcription Factor , TBX21. Part. Fibre Toxicol. 2014, 11, 1–16.

101. Aono, Y.; Kishi, M.; Yokota, Y.; Azuma, M.; Kinoshita, K.; Takezaki, A.; Sato, S.; Kawano, H.; Kishi, J.; Goto, H.; et al. Role of Platelet-Derived Growth Factor/Platelet-Derived Growth Factor Receptor Axis in the Trafficking of Circulating Fibrocytes in Pulmonary Fibrosis. Am. J. Respir. Cell Mol. Biol. 2014, 51, 793–801.

102. Phillips, R. J.; Burdick, M. D.; Hong, K.; Lutz, M. A.; Murray, L. A.; Xue, Y. Y.; Belperio, J. A.; Keane, M. P.; Strieter, R. M. Circulating Fibrocytes Traffic to the Lungs in Response to CXCL12 and Mediate Fibrosis. J Clin Invest 2004, 114, 438–446.

103. Quan, T. E.; Cowper, S. E.; Bucala, R. The Role of Circulating Fibrocytes in Fibrosis. Curr. Rheumatol. Rep. 2006, 8, 145–150.

104. Fu, X.; Zhang, D.; Li, Y.; Zhao, P.; Tang, Y.; Niu, J.; Li, Y. Curcumin Treatment Suppresses CCR7 Expression and the Differentiation and Migration of Human Circulating Fibrocytes. Cell. Physiol. Biochem. 2015, 35, 489–498.

105. Fu, Y.; Rong, M.; Zhu, P.; Chen, L.; Fan, C.; Wang, Y.; Li, J.; Fu, X. [The Circulating Fibrocytes Are Associated with the Lung Inflammation and Fibrosis of Mice with Interstitial Lung Disease]. Xi Bao Yu Fen Zi Mian Yi Xue Za Zhi 2014, 30, 814–818.

106. Fujiwara, A.; Kobayashi, H.; Masuya, M.; Maruyama, M.; Nakamura, S.; Ibata, H.; Fujimoto, H.; Ohnishi, M.; Urawa, M.; Naito, M.; et al. Correlation between Circulating Fibrocytes, and Activity and Progression of Interstitial Lung Diseases. Respirology 2012, 17, 693–698.

107. Li, H.; Tan, X.-Q.; Yan, L.; Zeng, B.; Meng, J.; Xu, H.-Y.; Cao, J.-M. Multi-Walled Carbon Nanotubes Act as a Chemokine and Recruit Macrophages by Activating the PLC/IP3/CRAC Channel Signaling Pathway. Sci. Rep. 2017, 7, 12.

108. Labib, S.; Williams, A.; Yauk, C. L.; Nikota, J. K.; Wallin, H.; Vogel, U.; Halappanavar, S. Nano-Risk Science: Application of Toxicogenomics in an Adverse Outcome Pathway Framework for Risk Assessment of Multi-Walled Carbon Nanotubes. Part. Fibre Toxicol. 2015, 13, 15.

109. Walkin, L.; Herrick, S. E.; Summers, A.; Brenchley, P. E.; Hoff, C. M.; Korstanje, R.; Margetts, P. J. The Role of Mouse Strain Differences in the Susceptibility to Fibrosis: A Systematic Review. Fibrogenesis Tissue Repair 2013, 6, 18.

110. Gustafsson, Å.; Svensson-Elfsmark, L.; Lorentzen, J. C.; Bucht, A. Strain Differences Influence Timing and Magnitude of Both Acute and Late Inflammatory Reactions after Intratracheal Instillation of an Alkylating Agent in Rats. J. Appl. Toxicol. 2014, 34, 272–280.

111. Schrier, D. J.; Kunkel, R. G.; Phan, S. H. The Role of Strain Variation in Murine Bleomycin-Lnduced Pulmonary Fibrosis. Am. Rev. Respir. Dis. 1983, 127, 63–66.

112. Walters, D. M.; White, K. M.; Patel, U.; Davis, M. J.; Veluci-Marlow, R. M.; Bhupanapadu Sunkesula, S. R.; Bonner, J. C.; Martin, J. R.; Gladwell, W.; Kleeberger, S. R. Genetic Susceptibility to Interstitial Pulmonary Fibrosis in Mice Induced by Vanadium Pentoxide (V2O5). FASEB J. 2014, 28, 1098–1112.

113. Cartwright, M. M.; Schmuck, S. C.; Corredor, C.; Wang, B.; Scoville, D. K.; Chisholm, C. R.; Wilkerson, H.-W.; Afsharinejad, Z.; Bammler, T. K.; Posner, J. D.; et al. The Pulmonary Inflammatory Response to Multiwalled Carbon Nanotubes Is Influenced by Gender and Glutathione Synthesis. Redox Biol. 2016, 9, 264–275.

114. Lindahl, G. E.; Stock, C. J.; Shi-Wen, X.; Leoni, P.; Sestini, P.; Howat, S. L.; Bou-Gharios, G.; Nicholson, A. G.; Denton, C. P.; Grutters, J. C.; et al. Microarray Profiling Reveals Suppressed Interferon Stimulated Gene Program in Fibroblasts from Scleroderma-Associated Interstitial Lung Disease. Respir. Res. 2013, 14, 14.

115. Walters, D. M.; Antao-Menezes, A.; Ingram, J. L.; Rice, A. B.; Nyska, A.; Tani, Y.; Kleeberger, S. R.; Bonner, J. C. Susceptibility of Signal Transducer and Activator of Transcription-1-Deficient Mice to Pulmonary Fibrogenesis. Am. J. Pathol. 2005, 167, 1221–1229.

116. Pedroza, M.; Le, T. T.; Lewis, K.; Karmouty-Quintana, H.; To, S.; George, A. T.; Blackburn, M. R.; Tweardy, D. J.; Agarwal, S. K. STAT-3 Contributes to Pulmonary Fibrosis through Epithelial Injury and Fibroblast-Myofibroblast Differentiation. FASEB J. 2016, 30, 129–140.

117. Lakatos, H. F.; Thatcher, T. H.; Kottmann, R. M.; Garcia, T. M.; Phipps, R. P.; Sime, P. J. The Role of PPARs in Lung Fibrosis. PPAR Res. 2007, 2007, 10.

118. Braissant, O.; Foufelle, F.; Scotto, C.; Dauça, M.; Wahli, W. Differential Expression of Peroxisome Proliferator-Activated Receptors (PPARs): Tissue Distribution of PPAR-Alpha, -Beta, and -Gamma in the Adult Rat. Endocrinology 1996, 137, 354–366.

119. Issemann, I.; Green, S. Activation of a Member of the Steroid Hormone Receptor Superfamily by Peroxisome Proliferators. Nature 1990, 347, 645–650.

120. Oruqaj, G.; Karnati, S.; Vijayan, V.; Kotarkonda, L. K.; Boateng, E.; Zhang, W.; Ruppert, C.; Günther, A.; Shi, W.; Baumgart-Vogt, E. Compromised Peroxisomes in Idiopathic Pulmonary Fibrosis, a Vicious Cycle Inducing a Higher Fibrotic Response via TGF-β Signaling. Proc. Natl. Acad. Sci. U. S. A. 2015, 112, E2048-57.

121. Genovese, T.; Mazzon, E.; Di Paola, R.; Muià, C.; Crisafulli, C.; Caputi, A. P.; Cuzzocrea, S. ROLE OF ENDOGENOUS AND EXOGENOUS LIGANDS FOR THE PEROXISOME PROLIFERATOR-ACTIVATED RECEPTOR Alpha IN THE DEVELOPMENT OF BLEOMYCIN-INDUCED LUNG INJURY. Shock 2005, 24, 547–555.

122. Ali, F. Y.; Egan, K.; FitzGerald, G. A.; Desvergne, B.; Wahli, W.; Bishop-Bailey, D.; Warner, T. D.; Mitchell, J. A. Role of Prostacyclin versus Peroxisome Proliferator-Activated Receptor Beta Receptors in Prostacyclin Sensing by Lung Fibroblasts. Am. J. Respir. Cell Mol. Biol. 2006, 34, 242–246.

123. Huizar, I.; Malur, A.; Patel, J.; Mcpeek, M.; Dobbs, L.; Wingard, C.; Barna, B. P.; Thomassen, M. J. The Role of PPAR γ in Carbon Nanotube-Elicited Granulomatous Lung Inflammation. Respir. Res. 2013, 14, 1.

124. Aoki, Y.; Maeno, T.; Aoyagi, K.; Ueno, M.; Aoki, F.; Aoki, N.; Nakagawa, J.; Sando, Y.; Shimizu, Y.; Suga, T.; et al. Pioglitazone, a Peroxisome Proliferator-Activated Receptor Gamma Ligand, Suppresses Bleomycin-Induced Acute Lung Injury and Fibrosis. Respiration 2008, 77, 311–319.

125. Yoon, Y.-S.; Kim, S.-Y.; Kim, M.-J.; Lim, J.-H.; Cho, M.-S.; Kang, J. L. PPARγ Activation Following Apoptotic Cell Instillation Promotes Resolution of Lung Inflammation and Fibrosis via Regulation of Efferocytosis and Proresolving Cytokines. Mucosal Immunol. 2015, 8, 1031–1046.

126. Zhu, H.-Y.; Li, C.; Zheng, Z.; Zhou, Q.; Guan, H.; Su, L.-L.; Han, J.-T.; Zhu, X.-X.; Wang, S.; Li, J.; et al. Peroxisome Proliferator-Activated Receptor-γ (PPAR-γ) Agonist Inhibits Collagen Synthesis in Human Hypertrophic Scar Fibroblasts by Targeting Smad3 via miR-145. Biochem. Biophys. Res. Commun. 2015, 459, 49–53.

127. Burgess, H. A.; Daugherty, L. E.; Thatcher, T. H.; Lakatos, H. F.; Ray, D. M.; Redonnet, M.; Phipps, R. P.; Sime, P. J. PPAR Agonists Inhibit TGF- Induced Pulmonary Myofibroblast Differentiation and Collagen Production: Implications for Therapy of Lung Fibrosis. AJP Lung Cell. Mol. Physiol. 2005, 288, L1146–L1153.

128. Kulkarni, A. A.; Thatcher, T. H.; Olsen, K. C.; Maggirwar, S. B.; Phipps, R. P.; Sime, P. J. PPAR-γ Ligands Repress TGFβ-Induced Myofibroblast Differentiation by Targeting the PI3K/Akt Pathway: Implications for Therapy of Fibrosis. PLoS One 2011, 6, e15909.

129. Barna, B. P.; Huizar, I.; Malur, A.; Mcpeek, M.; Marshall, I. Carbon Nanotube-Induced Pulmonary Granulomatous Disease: Twist 1 and Alveolar Macrophage M1 Activation. 2013, 23858–23871.

130. Sha, W.; Thompson, K.; South, J.; Baron, M.; Leask, A. Loss of PPARγ Expression by Fibroblasts Enhances Dermal Wound Closure. Fibrogenesis Tissue Repair 2012, 5, 5.

131. Rud, A. K.; Boye, K.; Oijordsbakken, M.; Lund-Iversen, M.; Halvorsen, A. R.; Solberg, S. K.; Berge, G.; Helland, A.; Brustugun, O. T.; Mælandsmo, G. M. Osteopontin Is a Prognostic Biomarker in Non-Small Cell Lung Cancer. BMC Cancer 2013, 13, 540.

132. Vij, R.; Noth, I. Peripheral Blood Biomarkers in Idiopathic Pulmonary Fibrosis. Transl. Res. 2012, 159, 218–227.

133. Mangum, J. B.; Bermudez, E.; Sar, M.; Everitt, J. I. Osteopontin Expression in Particle-Induced Lung Disease. Exp. Lung Res. 2004, 30, 585–598.

134. Dong, J.; Ma, Q. Osteopontin Enhances Multi-Walled Carbon Nanotube-Triggered Lung Fibrosis by Promoting TGF-β1 Activation and Myofibroblast Differentiation. Part. Fibre Toxicol. 2017, 14, 18.

135. Kotchey, G. P.; Zhao, Y.; Kagan, V. E.; Star, A. Peroxidase-Mediated Biodegradation of Carbon Nanotubes in Vitro and in Vivo. Adv. Drug Deliv. Rev. 2013, 65, 1921–1932.

136. Hilton, G. M.; Taylor, A. J.; McClure, C. D.; Parsons, G. N.; Bonner, J. C.; Bereman, M. S. Toxicoproteomic Analysis of Pulmonary Carbon Nanotube Exposure Using LC-MS/MS. Toxicology 2015, 329, 80–87.

137. Kagan, V. E.; Konduru, N. V.; Feng, W.; Allen, B. L.; Conroy, J.; Volkov, Y.; Vlasova, I. I.; Belikova, N. A.; Yanamala, N.; Kapralov, A.; et al. Carbon Nanotubes Degraded by Neutrophil Myeloperoxidase Induce Less Pulmonary Inflammation. Nat. Nanotechnol. 2010, 5, 354–359.

138. Shvedova, A. A.; Kapralov, A. A.; Feng, W. H.; Kisin, E. R.; Murray, A. R.; Mercer, R. R.; St. Croix, C. M.; Lang, M. A.; Watkins, S. C.; Konduru, N. V.; et al. Impaired Clearance and Enhanced Pulmonary Inflammatory/Fibrotic Response to Carbon Nanotubes in Myeloperoxidase-Deficient Mice. PLoS One 2012, 7, e30923.

139. do Carmo, R. F.; Vasconcelos, L. R. S.; Mendonça, T. F.; de Mendonça Cavalcanti, M. do S.; Pereira, L. M. M. B.; Moura, P. Myeloperoxidase Gene Polymorphism Predicts Fibrosis Severity in Women with Hepatitis C. Hum. Immunol. 2014, 75, 766–770.

140. Selman, M.; Ruiz, V.; Cabrera, S.; Segura, L.; Ramírez, R.; Barrios, R.; Pardo, A. TIMP-1, -2, -3, and -4 in Idiopathic Pulmonary Fibrosis. A Prevailing Nondegradative Lung Microenvironment? Am. J. Physiol. Lung Cell. Mol. Physiol. 2000, 279, L562-74.

141. Madtes, D. K.; Elston, A. L.; Kaback, L. A.; Clark, J. G. Selective Induction of Tissue Inhibitor of Metalloproteinase-1 in Bleomycin-Induced Pulmonary Fibrosis. Am. J. Respir. Cell Mol. Biol. 2001, 24, 599–607.

142. Dong, J.; Ma, Q. TIMP1 Promotes Multi-Walled Carbon Nanotube-Induced Lung Fibrosis by Stimulating Fibroblast Activation and Proliferation. Nanotoxicology 2016, 11, 41–51.

143. Zuo, W.L.; Zhao, J.M.; Huang, J.X.; Zhou, W.; Lei, Z.H.; Huang, Y.M.; Huang, Y.F.; Li, H.G. Effect of Bosentan Is Correlated with MMP-9/TIMP-1 Ratio in Bleomycin-Induced Pulmonary Fibrosis. Biomed. reports 2017, 6, 201–205.

144. Park, E.-J.; Roh, J.; Kim, S.-N.; Kang, M.; Han, Y.-A.; Kim, Y.; Hong, J. T.; Choi, K. A Single Intratracheal Instillation of Single-Walled Carbon Nanotubes Induced Early Lung Fibrosis and Subchronic Tissue Damage in Mice. Arch. Toxicol. 2011, 85, 1121–1131.

145. Muller, J.; Huaux, F.; Moreau, N.; Misson, P.; Heilier, J. F.; Delos, M.; Arras, M.; Fonseca, A.; Nagy, J. B.; Lison, D. Respiratory Toxicity of Multi-Wall Carbon Nanotubes. Toxicol. Appl. Pharmacol. 2005, 207, 221–231.

146. Reddy, A. R. N.; Reddy, Y. N.; Krishna, D. R.; Himabindu, V. Pulmonary Toxicity Assessment of Multiwalled Carbon Nanotubes in Rats Following Intratracheal Instillation. Environ. Toxicol. 2012, 27, 211–219.

147. Mangum, J. B.; Turpin, E. A.; Antao-Menezes, A.; Cesta, M. F.; Bermudez, E.; Bonner, J. C. Single-Walled Carbon Nanotube (SWCNT)-Induced Interstitial Fibrosis in the Lungs of Rats Is Associated with Increased Levels of PDGF mRNA and the Formation of Unique Intercellular Carbon Structures That Bridge Alveolar Macrophages in Situ. Part. Fibre Toxicol. 2006, 3, 15.

148. Lam, C.-W.; James, J. T.; McCluskey, R.; Hunter, R. L. Pulmonary Toxicity of Single-Wall Carbon Nanotubes in Mice 7 and 90 Days After Intratracheal Instillation. Toxicol. Sci. 2003, 77, 126–134.

149. Dong, J.; Ma, Q. In Vivo Activation of a T Helper 2-Driven Innate Immune Response in Lung Fibrosis Induced by Multi-Walled Carbon Nanotubes. 2016, 90, 2231–2248.

150. Rydman, E. M.; Ilves, M.; Vanhala, E.; Vippola, M.; Lehto, M.; Kinaret, P. A. S.; Pylkkänen, L.; Happo, M.; Hirvonen, M.-R.; Greco, D.; et al. A Single Aspiration of Rod-like Carbon Nanotubes Induces Asbestos-like Pulmonary Inflammation Mediated in Part by the IL-1 Receptor. Toxicol. Sci. 2015, 147, 140–155.

151. Foo, S. Y.; Phipps, S. Regulation of Inducible BALT Formation and Contribution to Immunity and Pathology. Mucosal Immunol. 2010, 3, 537–544.

152. Rangel-Moreno, J.; Hartson, L.; Navarro, C.; Gaxiola, M.; Selman, M.; Randall, T. D. Inducible Bronchus-Associated Lymphoid Tissue (iBALT) in Patients with Pulmonary Complications of Rheumatoid Arthritis. J. Clin. Invest. 2006, 116, 3183–3194.

153. Dieu-Nosjean, M.-C.; Antoine, M.; Danel, C.; Heudes, D.; Wislez, M.; Poulot, V.; Rabbe, N.; Laurans, L.; Tartour, E.; de Chaisemartin, L.; et al. Long-Term Survival for Patients with Non-Small-Cell Lung Cancer with Intratumoral Lymphoid Structures. J. Clin. Oncol. 2008, 26, 4410–4417.

154. Halle, S.; Dujardin, H. C.; Bakocevic, N.; Fleige, H.; Danzer, H.; Willenzon, S.; Suezer, Y.; Hämmerling, G.; Garbi, N.; Sutter, G.; et al. Induced Bronchus-Associated Lymphoid Tissue Serves as a General Priming Site for T Cells and Is Maintained by Dendritic Cells. J. Exp. Med. 2009, 206, 2593–2601.

155. Rangel-Moreno, J.; Carragher, D. M.; de la Luz Garcia-Hernandez, M.; Hwang, J. Y.; Kusser, K.; Hartson, L.; Kolls, J. K.; Khader, S. A.; Randall, T. D. The Development of Inducible Bronchus-Associated Lymphoid Tissue Depends on IL-17. Nat. Immunol. 2011, 12, 639–646.

156. Morissette, M. C.; Jobse, B. N.; Thayaparan, D.; Nikota, J. K.; Shen, P.; Labiris, N. R.; Kolbeck, R.; Nair, P.; Humbles, A. A.; Stämpfli, M. R. Persistence of Pulmonary Tertiary Lymphoid Tissues and Anti-Nuclear Antibodies Following Cessation of Cigarette Smoke Exposure. Respir. Res. 2014, 15, 49.

157. Foo, S. Y.; Zhang, V.; Lalwani, A.; Lynch, J. P.; Zhuang, A.; Lam, C. E.; Foster, P. S.; King, C.; Steptoe, R. J.; Mazzone, S. B.; et al. Regulatory T Cells Prevent Inducible BALT Formation by Dampening Neutrophilic Inflammation. J. Immunol. 2015, 194, 4567–4576.

158. John-Schuster, G.; Hager, K.; Conlon, T. M.; Irmler, M.; Beckers, J.; Eickelberg, O.; Yildirim, A. Ö. Cigarette Smoke-Induced iBALT Mediates Macrophage Activation in a B Cell-Dependent Manner in COPD. Am. J. Physiol. Lung Cell. Mol. Physiol. 2014, 692–706.

159. Moyron-Quiroz, J. E.; Rangel-Moreno, J.; Kusser, K.; Hartson, L.; Sprague, F.; Goodrich, S.; Woodland, D. L.; Lund, F. E.; Randall, T. D. Role of Inducible Bronchus Associated Lymphoid Tissue (iBALT) in Respiratory Immunity. Nat. Med. 2004, 10, 927–934.

160. Aiso, S.; Yamazaki, K.; Umeda, Y.; Asakura, M.; Kasai, T.; Takaya, M.; Toya, T.; Koda, S.; Nagano, K.; Arito, H.; et al. Pulmonary Toxicity of Intratracheally Instilled Multiwall Carbon Nanotubes in Male Fischer 344 Rats. Ind. Health 2010, 48, 783–795.

161. Frank, E. A.; Carreira, V. S.; Birch, M. E.; Yadav, J. S. Carbon Nanotube and Asbestos Exposures Induce Overlapping but Distinct Profiles of Lung Pathology in Non-Swiss Albino CF-1 Mice. Toxicol. Pathol. 2016, 44, 211–225.

162. Kim, J.; Lim, H.; Minai-tehrani, A.; Kwon, J.; Woo, C.; Choi, M.; Baek, J.; Jeong, D. H.; Ha, C.; Chae, C.; et al. Toxicity and Clearance of Intratracheally Administered Multiwalled Carbon Nanotubes from Murine Lung. 2010, 7394.

163. Sargent, L. M.; Shvedova, A. A.; Hubbs, A. F.; Salisbury, J. L.; Benkovic, S. A.; Kashon, M. L.; Lowry, D. T.; Murray, A. R.; Kisin, E. R.; Friend, S.; et al. Induction of Aneuploidy by Single-Walled Carbon Nanotubes. Environ. Mol. Mutagen. 2009, 50, 708–717.

164. Xu, J.; Futakuchi, M.; Shimizu, H.; Alexander, D. B.; Yanagihara, K.; Fukamachi, K.; Suzui, M.; Kanno, J.; Hirose, A.; Ogata, A.; et al. Multi-Walled Carbon Nanotubes Translocate into the Pleural Cavity and Induce Visceral Mesothelial Proliferation in Rats. Cancer Sci. 2012, 103, 2045–2050.

165. Xu, J.; Alexander, D. B.; Futakuchi, M.; Numano, T.; Fukamachi, K.; Suzui, M.; Omori, T.; Kanno, J.; Hirose, A.; Tsuda, H. Size- and Shape-Dependent Pleural Translocation, Deposition, Fibrogenesis, and Mesothelial Proliferation by Multiwalled Carbon Nanotubes. Cancer Sci. 2014, 105, 763–769.

166. DeLorme, M. P.; Muro, Y.; Arai, T.; Banas, D. A.; Frame, S. R.; Reed, K. L.; Warheit, D. B. Ninety-Day Inhalation Toxicity Study with A Vapor Grown Carbon Nanofiber in Rats. Toxicol. Sci. 2012, 128, 449–460.

167. Roberts, J. R.; Mercer, R. R.; Stefaniak, A. B.; Seehra, M. S.; Geddam, U. K.; Chaudhuri, I. S.; Kyrlidis, A.; Kodali, V. K.; Sager, T.; Kenyon, A.; et al. Evaluation of Pulmonary and Systemic Toxicity Following Lung Exposure to Graphite Nanoplates: A Member of the Graphene-Based Nanomaterial Family. Part. Fibre Toxicol. 2016, 13, 34.

168. Siegrist, K. J.; Reynolds, S. H.; Kashon, M. L.; Lowry, D. T.; Dong, C.; Hubbs, A. F.; Young, S.-H.; Salisbury, J. L.; Porter, D. W.; Benkovic, S. A.; et al. Genotoxicity of Multi-Walled Carbon Nanotubes at Occupationally Relevant Doses. Part. Fibre Toxicol. 2014, 11.

169. Mercer, R. R.; Hubbs, A. F.; Scabilloni, J. F.; Wang, L.; Battelli, L. a; Friend, S.; Castranova, V.; Porter, D. W. Pulmonary Fibrotic Response to Aspiration of Multi-Walled Carbon Nanotubes. Part. Fibre Toxicol. 2011, 8, 21.

170. Van Berlo, D.; Wilhelmi, V.; Boots, A. W.; Hullmann, M.; Kuhlbusch, T. A. J.; Bast, A.; Schins, R. P. F.; Albrecht, C. Apoptotic, Inflammatory, and Fibrogenic Effects of Two Different Types of Multi-Walled Carbon Nanotubes in Mouse Lung. Arch. Toxicol. 2014, 88, 1725–1737.

171. Rittinghausen, S.; Hackbarth, A.; Creutzenberg, O.; Ernst, H.; Heinrich, U.; Leonhardt, A.; Schaudien, D. The Carcinogenic Effect of Various Multi-Walled Carbon Nanotubes (MWCNTs) after Intraperitoneal Injection in Rats. Part. Fibre Toxicol. 2014, 11, 59.

172. Nagai, H.; Okazaki, Y.; Chew, S.; Misawa, N.; Yamashita, Y.; Akatsuka, S.; Ishihara, T.; Yamashita, K.; Yoshikawa, Y.; Yasui, H.; et al. Diameter and Rigidity of Multiwalled Carbon Nanotubes Are Critical Factors in Mesothelial Injury and Carcinogenesis. 2011.

173. Varga, C.; Szendi, K. Carbon Nanotubes Induce Granulomas but Not Mesotheliomas. In Vivo (Brooklyn). 2010, 24, 153–156.

174. Nagai, H.; Okazaki, Y.; Chew, S. H.; Misawa, N.; Miyata, Y.; Shinohara, H.; Toyokuni, S. Intraperitoneal Administration of Tangled Multiwalled Carbon Nanotubes of 15nm in Diameter Does Not Induce Mesothelial Carcinogenesis in Rats. Pathol. Int. 2013, 63, 457–462.

175. Andujar, P.; Pairon, J.-C.; Renier, A.; Descatha, A.; Hysi, I.; Abd-Alsamad, I.; Billon-Galland, M.A.; Blons, H.; Clin, B.; Danel, C.; et al. Differential Mutation Profiles and Similar Intronic TP53 Polymorphisms in Asbestos-Related Lung Cancer and Pleural Mesothelioma. Mutagenesis 2013, 28, 323–331.

176. Luanpitpong, S.; Wang, L.; Castranova, V.; Rojanasakul, Y. Induction of Stem-like Cells with Malignant Properties by Chronic Exposure of Human Lung Epithelial Cells to Single-Walled Carbon Nanotubes. Part. Fibre Toxicol. 2014, 11, 22.

177. Hsieh, H.S.; Wu, R.; Jafvert, C. T. Light-Independent Reactive Oxygen Species (ROS) Formation through Electron Transfer from Carboxylated Single-Walled Carbon Nanotubes in Water. Environ. Sci. Technol. 2014, 48, 11330–11336.

178. Mihalchik, A. L.; Ding, W.; Porter, D. W.; McLoughlin, C.; Schwegler-Berry, D.; Sisler, J. D.; Stefaniak, A. B.; Snyder-Talkington, B. N.; Cruz-Silva, R.; Terrones, M.; et al. Effects of Nitrogen-Doped Multi-Walled Carbon Nanotubes Compared to Pristine Multi-Walled Carbon Nanotubes on Human Small Airway Epithelial Cells. Toxicology 2015, 333, 25–36.

179. Alarifi, S.; Ali, D.; Verma, A.; Almajhdi, F. N.; Al-Qahtani, A. A. Single-Walled Carbon Nanotubes Induce Cytotoxicity and DNA Damage via Reactive Oxygen Species in Human Hepatocarcinoma Cells. Vitr. Cell. Dev. Biol. Anim. 2014, 50, 714–722.

180. Yu, M.; Chen, R.; Jia, Z.; Chen, J.; Lou, J.; Tang, S.; Zhang, X. MWCNTs Induce ROS Generation, ERK Phosphorylation, and SOD-2 Expression in Human Mesothelial Cells. Int. J. Toxicol. 2016, 35, 17–26.

181. Guo, F.; Ma, N.; Horibe, Y.; Kawanishi, S.; Murata, M.; Hiraku, Y. Nitrative DNA Damage Induced by Multi-Walled Carbon Nanotube via Endocytosis in Human Lung Epithelial Cells. Toxicol. Appl. Pharmacol. 2012, 260, 183–192.

182. Migliore, L.; Saracino, D.; Bonelli, A.; Colognato, R.; D'Errico, M. R.; Magrini, A.; Bergamaschi, A.; Bergamaschi, E. Carbon Nanotubes Induce Oxidative DNA Damage in RAW 264.7 Cells. Environ. Mol. Mutagen. 2010, 51, NA-NA.

183. Hiraku, Y.; Guo, F.; Ma, N.; Yamada, T.; Wang, S.; Kawanishi, S.; Murata, M. Multi-Walled Carbon Nanotube Induces Nitrative DNA Damage in Human Lung Epithelial Cells via HMGB1-RAGE Interaction and Toll-like Receptor 9 Activation. Part. Fibre Toxicol. 2015, 13, 16.

184. Catalán, J.; Siivola, K. M.; Nymark, P.; Lindberg, H.; Suhonen, S.; Järventaus, H.; Koivisto, A. J.; Moreno, C.; Vanhala, E.; Wolff, H.; et al. In Vitro and in Vivo Genotoxic Effects of Straight versus Tangled Multi-Walled Carbon Nanotubes. Nanotoxicology 2016, 10, 794–806.

185. Vales, G.; Rubio, L.; Marcos, R. Genotoxic and Cell-Transformation Effects of Multi-Walled Carbon Nanotubes (MWCNT) Following in Vitro Sub-Chronic Exposures. J. Hazard. Mater. 2016, 306, 193–202.

186. Shi, J.; Karlsson, H. L.; Johansson, K.; Gogvadze, V.; Xiao, L.; Li, J.; Burks, T.; Garcia-Bennett, A.; Uheida, A.; Muhammed, M.; et al. Microsomal Glutathione Transferase 1 Protects against Toxicity Induced by Silica Nanoparticles but Not by Zinc Oxide Nanoparticles. ACS Nano 2012, 6, 1925–1938.

187. Rahman, L.; Jacobsen, N. R.; Aziz, S. A.; Wu, D.; Williams, A.; Yauk, C. L.; White, P.; Willin, H.; Vogel, U.; Halappanavar, S. Multi-Walled Carbon Nanotube-Induced Genotoxic, Inflammatory and pro-Fibrotic Responses in Mice: Investigating the Mechanisms of Pulmonary Carcinogenesis. Mutat. Res. Toxicol. Environ. Mutagen. 2017, 823, 28–44.

188. Myhr, B. C. Validation Studies with Muta Mouse: A Transgenic Mouse Model for Detecting Mutations in Vivo. Environ. Mol. Mutagen. 1991, 18, 308–315.

189. Sargent, L. M.; Hubbs, A. F.; Young, S. H.; Kashon, M. L.; Dinu, C. Z.; Salisbury, J. L.; Benkovic, S. A.; Lowry, D. T.; Murray, A. R.; Kisin, E. R.; et al. Single-Walled Carbon Nanotube-Induced Mitotic Disruption. Mutat. Res. Genet. Toxicol. Environ. Mutagen. 2012, 745, 28–37.

190. Chauhan, L. K. S.; Varshney, M.; Pandey, V.; Sharma, P.; Verma, V. K.; Kumar, P.; Goel, S. K. ROS-Dependent Genotoxicity, Cell Cycle Perturbations and Apoptosis in Mouse Bone Marrow Cells Exposed to Formulated Mixture of Cypermethrin and Chlorpyrifos. Mutagenesis 2016, 31, 635–642.

191. Frank, E. A.; Carreira, V. S.; Shanmukhappa, K.; Medvedovic, M.; Prows, D. R.; Yadav, J. S. Genetic Susceptibility to Toxicologic Lung Responses among Inbred Mouse Strains Following Exposure to Carbon Nanotubes and Profiling of Underlying Gene Networks. Toxicol. Appl. Pharmacol. 2017, 327, 59–70.

192. Sargent, L. M.; Porter, D. W.; Staska, L. M.; Hubbs, A. F.; Lowry, D. T.; Battelli, L.; Siegrist, K. J.; Kashon, M. L.; Mercer, R. R.; Bauer, A. K.; et al. Promotion of Lung Adenocarcinoma Following Inhalation Exposure to Multi-Walled Carbon Nanotubes. Part. Fibre Toxicol. 2014, 11, 3.

193. van Boxtel, R.; Kuiper, R. V.; Toonen, P. W.; van Heesch, S.; Hermsen, R.; de Bruin, A.; Cuppen, E. Homozygous and Heterozygous p53 Knockout Rats Develop Metastasizing Sarcomas with High Frequency. Am. J. Pathol. 2011, 179, 1616–1622.

194. Ghosh, S.; Mendoza, T.; Ortiz, L. A.; Hoyle, G. W.; Fermin, C. D.; Brody, A. R.; Friedman, M.; Morris, G. F. Bleomycin Sensitivity of Mice Expressing Dominant-Negative p53 in the Lung Epithelium. Am. J. Respir. Crit. Care Med. 2002, 166, 890–897.

195. Ahrendt, S. A.; Hu, Y.; Buta, M.; McDermott, M. P.; Benoit, N.; Yang, S. C.; Wu, L.; Sidransky, D. p53 Mutations and Survival in Stage I Non-Small-Cell Lung Cancer: Results of a Prospective Study. JNCI J. Natl. Cancer Inst. 2003, 95, 961–970.

196. Chen, D.; Stueckle, T. A.; Luanpitpong, S.; Rojanasakul, Y.; Lu, Y.; Wang, L. Gene Expression Profile of Human Lung Epithelial Cells Chronically Exposed to Single-Walled Carbon Nanotubes. Nanoscale Res. Lett. 2015, 10, 12.

197. Lee, J. S.; Choi, Y. C.; Shin, J. H.; Lee, J. H.; Lee, Y.; Park, S. Y.; Baek, J. E.; Park, J. D.; Ahn, K.; Yu, I. J. Health Surveillance Study of Workers Who Manufacture Multi-Walled Carbon Nanotubes. Nanotoxicology 2015, 9, 802–811.

198. Liao, H.-Y.; Chung, Y.-T.; Lai, C.-H.; Lin, M.-H.; Liou, S.-H. Sneezing and Allergic Dermatitis Were Increased in Engineered Nanomaterial Handling Workers. Ind. Health 2014, 52, 199–215.

199. Liao, H.-Y.; Chung, Y.-T.; Lai, C.-H.; Wang, S.-L.; Chiang, H.-C.; Li, L.-A.; Tsou, T.-C.; Li, W.-F.; Lee, H.-L.; Wu, W.-T.; et al. Six-Month Follow-up Study of Health Markers of Nanomaterials among Workers Handling Engineered Nanomaterials. Nanotoxicology 2014, 8, 100–110.

200. Kamp, D. W. Asbestos-Induced Lung Diseases: An Update. Transl. Res. 2009, 153, 143–152.

CHAPTER 2

STAT1-Dependent and -Independent Pulmonary Allergic and Fibrogenic Responses in Mice after Exposure to Tangled Versus Rod-Like Multi-Walled Carbon Nanotubes

Adopted from publication: Particle and Fibre Toxicology, Volume 14, 2017

Katherine S. Duke[1], Alexia J. Taylor[1], Mark D. Ihrie[1], Kelly A. Shipkowski[1], Elizabeth A. Thompson[1], Erinn C. Dandley[2], Gregory N. Parsons[2], and James C. Bonner[1*]

[1]Toxicology Program, Department of Biological Sciences, North Carolina State University, Raleigh, NC 27695 USA

[2]Department of Chemical and Biomolecular Engineering, North Carolina State University, Raleigh, North Carolina 27695 USA

***Correspondence:** James C. Bonner, PhD
Department of Biological Sciences
North Carolina State University
Campus Box 7633
Raleigh, NC 27695-7633 USA
Email: jcbonner@ncsu.edu

Abstract

Background: Pulmonary toxicity of multi-walled carbon nanotubes (MWCNTs) is influenced by physicochemical characteristics and genetic susceptibility. We hypothesized that contrasting rigidities of tangled (t-) versus rod-like (r-) MWCNTs would result in differing immunologic or fibrogenic responses in mice and that these responses would be exaggerated in transgenic mice lacking the signal transducer and activator of transcription-1 (STAT1), a susceptible mouse model of pulmonary fibrosis.

Methods: Male wild type (*Stat1*$^{+/+}$) and STAT1-deficient (*Stat1*$^{-/-}$) mice were exposed to 4 mg/kg tMWCNTs, rMWCNTs, or vehicle alone via oropharyngeal aspiration and evaluated for inflammation at one and 21 days post exposure via histopathology, differential cell counts, and cytokine levels in bronchoalveolar lavage fluid (BALF). Granuloma formation, mucous cell metaplasia, and airway fibrosis were evaluated by quantitative morphometry. Airway epithelial cell proliferation was assessed by bromodeoxyuridine (BrdU) incorporation. Cytokine protein levels in BALF and serum IgE levels were measured by ELISA. Lung protein Smad2/3 levels and activation were measured by Western blot. Lung mRNAs were measured by PCR.

Results: There was a 7-fold difference in rigidity between tMWCNTs and rMWCNTs as determined by static bending ratio. Both MWCNT types resulted in acute inflammation (neutrophils in BALF) after one-day post exposure, yet only rMWCNTs resulted in chronic

inflammation at 21 days as indicated by neutrophil influx and larger granulomas. Both MWCNTs induced BrdU uptake in airway epithelial cells, with the greatest proliferative response observed in rMWCNT-exposed mice after one-day. Only rMWCNTs induced mucous cell metaplasia, but this index was not different between genotypes. *Stat1*$^{-/-}$ mice had higher levels of baseline serum IgE than *Stat1*$^{+/+}$ mice. Greater airway fibrosis was observed with rMWCNTs compared to tMWCNTs, and exaggerated airway fibrosis was seen in the *Stat1*$^{-/-}$ mouse lungs with rMWCNTs but not tMWCNTs. Increased fibrosis correlated with elevated levels of TGF-β1 protein levels in the BALF of *Stat1*$^{-/-}$ mice exposed to rMWCNTs and increased lung Smad2/3 phosphorylation.

Conclusions: Rigidity plays a key role in the toxicity of MWCNTs and results in increased inflammatory, immunologic, and fibrogenic effects in the lung. STAT1 is an important protective factor in the fibroproliferative response to rMWCNTs, regulating both induced TGF-β1 production and Smad2/3 phosphorylation status. Therefore, both rigidity and genetic susceptibility should be major considerations for risk assessment of MWCNTs.

Key Words: carbon nanotubes, lung, fibrosis, growth factors, transcription factors

Background

Carbon nanotubes (CNTs) are engineered nanomaterials that have structural similarities to asbestos because of their fiber-like shape and biopersistence [1–3]. While little is known about their adverse human health effects, rodent studies show multi-walled (MW) CNTs, like asbestos fibers, possess carcinogenic activity or cause pulmonary fibrosis after inhalation exposure or oropharyngeal aspiration [4–6]. Also reminiscent of asbestos fibers, MWCNTs reach the lung pleura after inhalation exposure in mice, where they irritate the pleural lining and cause pleural inflammation and subpleural fibrosis [7]. While some MWCNTs delivered to the lungs could translocate to other organs after pulmonary exposure, a significant fraction are biopersistent and remain in the lung and pleura up to a year after exposure in rodents, leading to chronic DNA damage and tissue fibrosis [8].

MWCNTs are a heterogeneous class of materials that can mediate different pathogenic responses in the lung, depending on their physicochemical properties. For instance, lung exposure to rod-like (r-) MWCNTs can lead to allergic airway inflammation and mucous cell metaplasia, while exposure to tangled (t-) MWCNTs causes non-allergic lung inflammation with no mucous cell metaplasia [9–11]. Other properties of MWCNTs have been shown to play a role in their pulmonary toxicity (i.e. length, surface charge, residual metals) yet only a few studies comparing MWCNTs with contrasting rigidity have been conducted [9,12]. However, to our knowledge there are no studies that address genetic susceptibility to allergic or fibrogenic responses to MWCNTs with different rigidities. Examining the differences in allergic or

fibroproliferative responses between tMWCNTs and rMWCNTs in genetically susceptible mouse models may elucidate differences in the fibrotic mechanisms of these MWCNTs.

Signal transducer and activator of transcription-1 (STAT1) is a transcription factor activated primarily by interferons (IFN-α, -β, -γ), growth factors (e.g., epidermal growth factor (EGF), platelet derived growth factor (PDGF)), or by oxidative stress [13–15]. Upon activation, STAT1 is phosphorylated and homodimerizes with another STAT1 molecule, or heterodimerizes with other STAT family members (e.g. STAT2). Homodimers or heterodimers then translocate to the nucleus to bind a DNA consensus sequence; each STAT1 dimer has a high affinity for its specific response element [16]. STAT1 serves as a protective response to injury, and is responsible for activating the transcription of key genes involved in cell viability, growth arrest, apoptosis, and differentiation [17,18]. *Stat1*$^{-/-}$ mice exhibit increased fibrosis following exposure to the chemotherapeutic drug bleomycin compared to wild type (*Stat1*$^{+/+}$) mice, demonstrating that STAT1 is protective against fibrogenesis [19]. Also, ovalbumin sensitized *Stat1*$^{-/-}$ mice that were subsequently challenged with tMWCNTs by oropharyngeal aspiration exhibit greater airway fibrosis than *Stat1*$^{+/+}$ mice, indicating that STAT1 plays a role in the immune response to tMWCNTs and allergens [11]. Moreover, fibroblasts isolated from lungs of *Stat1*$^{-/-}$ mice are more responsive *in vitro* to exogenous transforming growth factor (TGF)-β1, produce more collagen than *Stat1*$^{+/+}$ fibroblasts treated with TGF-β1 and display an increased proliferative response *in vitro* to PDGF or EGF compared to *Stat1*$^{+/+}$ fibroblasts [19].

It is unknown if STAT1 regulates differential fibrogenic or immune responses to tMWCNTs versus rMWCNTs. In the present study, we hypothesized that MWCNTs with different rigidities would produce different pulmonary immunologic and fibroproliferative responses and that these effects would be enhanced in *Stat1*$^{-/-}$ mice. We investigated MWCNT-induced lung inflammation, allergic airway remodeling and fibrosis in *Stat1*$^{+/+}$ or *Stat1*$^{-/-}$ mice *in vivo* for one and 21 days after oropharyngeal aspiration of tMWCNTs or rMWCNTs. We observed that rMWCNTs caused more persistent lung inflammation, as well as airway mucous cell metaplasia and larger granulomas compared to tMWCNT exposure in wild type *Stat1*$^{+/+}$ mice. Interestingly, compared to *Stat1*$^{+/+}$ mice, *Stat1*$^{-/-}$ mice exposed to rMWCNTs but not tMWCNTs exhibited enhanced airway fibrosis, airway epithelial cell proliferation, exaggerated serum IgE and increased levels of lung TGF-β1 and increased activation of the TGF-β1-induced transcription factors, Smad2 and Smad3. The results from this study are important because they reveal an interaction between a physicochemical attribute (rigidity) and a genetic factor (STAT1) to further our understanding of susceptibility to pulmonary fibrogenesis and allergic immune responses. Moreover, we identify a novel mechanism of enhanced lung fibrogenesis in *Stat1*$^{-/-}$ mice induced by rMWCNTs that involves exaggerated TGF-β1 production and Smad2/3 activation.

Results

Characterization of MWCNT Rigidity: Both tMWCNTs and rMWCNTs have been previously characterized for average residual metal content, length, and width and these data

are summarized in Appendix A.1 [7,10]. We further characterized these MWCNTs based on their rigidity using a measure of the bending ratio (D_b) to approximate the static bending persistence length (SBPL) (i.e. the average length between each bend in the tube) (Fig 2.1). TEM images clearly show that tMWCNTs are more tortuous compared to rMWCNTs (Fig. 2.1A). The rMWCNTs, with a D_b of 0.8996 (stdev 0.2743) and a SBPL of 0.860, are about seven-fold more rigid than the tMWCNTs with a D_b of 0.162 (stdev 0.3300) and a SBPL of 0.1191 (Fig 2.1B).

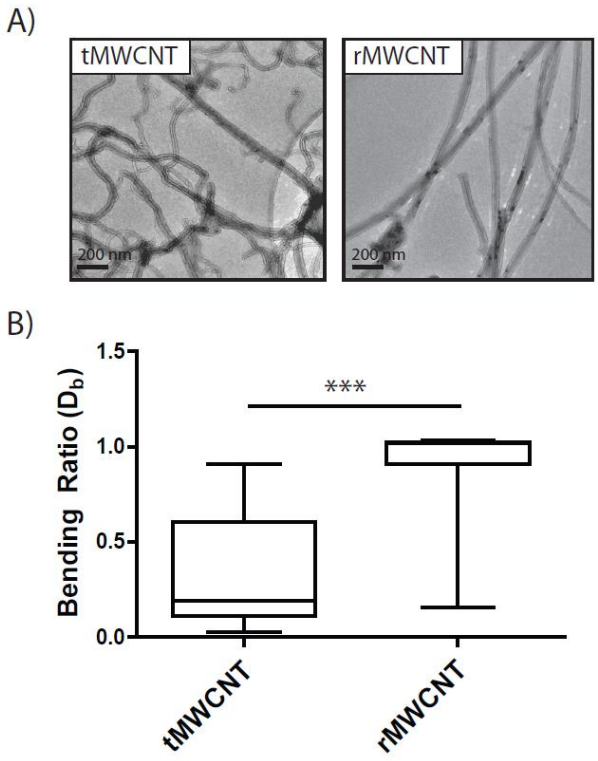

Figure 2.1. Rigidity measurements of multi-walled carbon nanotubes (MWCNTs). **A)** Transmission electron microscope (TEM) images of the tangled (t-) MWCNTs and rod-like (r-) MWCNTs showing the gross differences in rigidity taken at 10000X. **B)** Box and whisker plots of the bending ratios (D_b) of tMWCNTs and rMWCNTs (***$p<0.001$ between means of MWCNT D_b as determined by t-test).

Macrophage Uptake and Inflammation: *Stat1*$^{+/+}$ and *Stat1*$^{-/-}$ mice exposed to tMWCNTs or rMWCNTs by oropharyngeal aspiration (OPA) were evaluated for changes in bronchoalveolar lavage fluid (BALF) inflammatory cells at one and 21 days post-exposure according the protocol illustrated in Fig 2.2A. BALF differential cell counts showed that both *Stat1*$^{+/+}$ and *Stat1*$^{-/-}$ mice exhibited similar increases in infiltrating neutrophils at one-day post exposure (Fig 2.2B). Neutrophilic inflammation in the tMWCNT-treated mouse lungs resolved by 21 days, while neutrophilia in the lungs of rMWCNT-treated mice remained elevated at 21 days in both *Stat1*$^{+/+}$ and *Stat1*$^{-/-}$ mice (Fig 2.2B). The tMWCNTs are flexible and were completely engulfed by alveolar macrophages, while many of the rMWCNTs protruded from macrophages, indicating frustrated phagocytosis (Fig 1.2C).

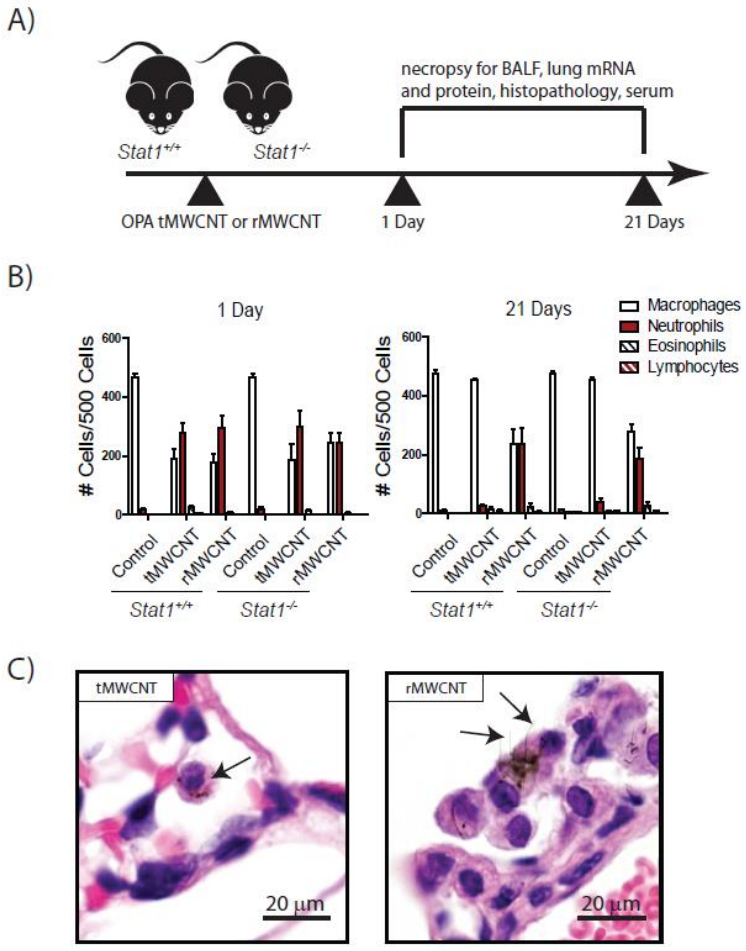

Figure 2.2. Acute pulmonary response after oropharyngeal aspiration (OPA) to tangled t- or r-MWCNTs. **A)** Illustration of experimental design. **B)** Differential cell counts quantified from Cytospins of BALF from *Stat1*$^{+/+}$ and *Stat1*$^{-/-}$ mice exposed to tMWCNTs or rMWCNTs. **C)** Hematoxylin and eosin-stained (H&E) lung sections from mice treated with tMWCNTs or rMWCNTs at one-day post exposure showing uptake of tMWCNTs and rMWCNTs by alveolar macrophages (arrows). Note frustrated phagocytosis of rMWCNTs but not tMWCNTs by macrophages.

MWCNT-Induced Granulomatous Inflammation: To ascertain if the *Stat1*$^{+/+}$ versus *Stat1*$^{-/-}$ genotypes determine differential chronic pulmonary inflammatory responses to each

MWCNT type, the lungs of mice were analyzed for granuloma size and cellularity. Histopathologic analysis of lung tissue from MWCNT-treated mice showed alveolar parenchyma dispersion of MWCNTs and predominantly multifocal granulomatous inflammation and bronchitis (Fig 2.3A). The granulomas observed following rMWCNT treatment contained a high number of neutrophils and eosinophils after 21 days. This is notable bearing in mind that classical granulomas consist of epithelioid, multinucleated giant cells, and a very sparse eosinophil or neutrophil presence (Fig 2.3A insets). Only rMWCNT exposure resulted in bronchial inflammation and airway epithelial growth over the foreign body protrusions of rMWCNTs into the lumen of the airway, similar to some pathologic features of bronchiolitis obliterans. Quantitative analysis of granuloma number showed that at the same dose of 4 mg/kg, both types of MWCNTs induced similar numbers of granulomas at 21 days with no differences between genotypes (Fig 2.3B). While granulomas were observed in both tMWCNT and rMWCNT-treated mice after 21 days, granuloma size was significantly greater in rMWCNT-treated mice compared to tMWCNT-treated mice, although there were not significant differences between *Stat1*$^{+/+}$ and *Stat1*$^{-/-}$ mice (Fig 2.3C). Together, these data demonstrate that rMWCNTs caused a more severe chronic inflammatory state in the lung, resulting in larger granuloma formations and that this inflammatory response was STAT1-independent.

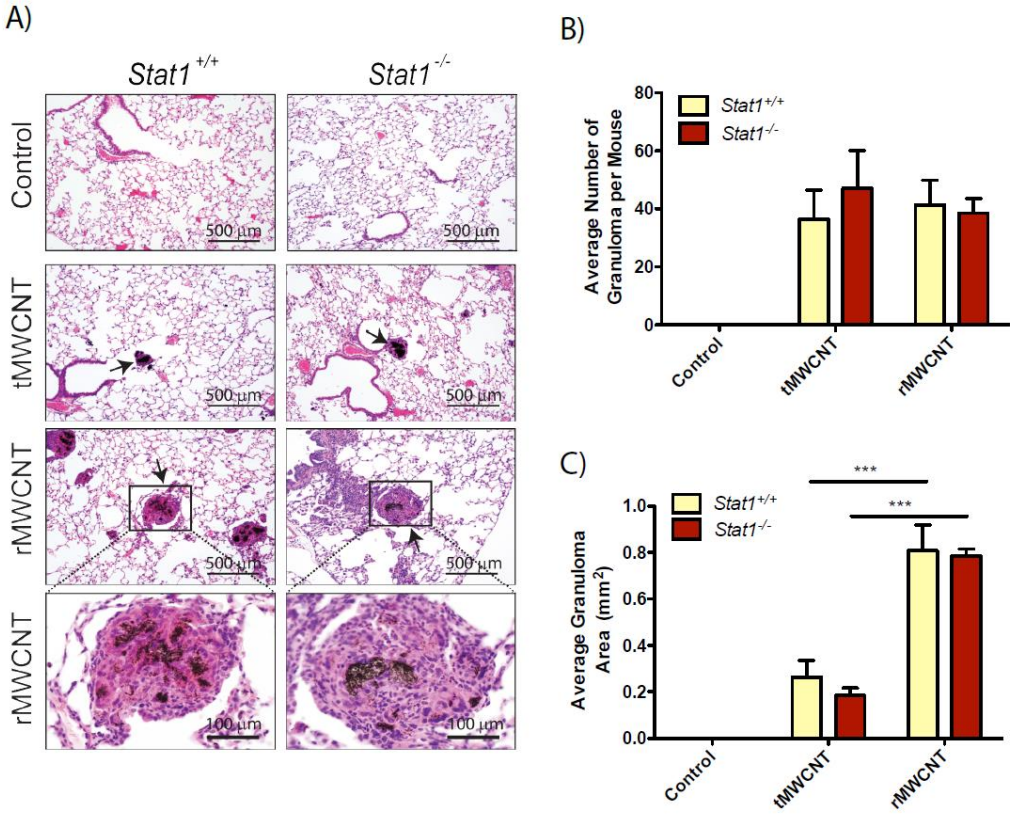

Figure 2.3. Granuloma development at 21 days post-exposure to tMWCNTs or rMWCNTs. **A)** Representative H&E photomicrographs of 21 day control, tMWCNT or rMWCNT exposed mouse airways showing granulomas (arrows) taken at 200X magnification (scale bars equal 500 µm). Insets of rMWCNT granulomas (Scale bars equal 100 µm) taken at 400X magnification. **B)** Average number of granulomas per 3 lung sections per mouse. **C)** Average size of granulomas measured by quantitative morphometry as described in Methods (***p<0.001 between tMWCNTs and rMWCNTs).

Airway Epithelial Cell Proliferation After MWCNT Exposure: To determine if tMWCNTs or rMWCNTs caused lung cell proliferation, mice were injected i.p. with BrdU one-hour prior to euthanasia and incorporation of BrdU into nuclei was visualized by immunohistochemistry (Fig 2.4A). Vehicle treatment did not cause a significant increase in BrdU uptake in *Stat1*$^{+/+}$

or *Stat1*$^{-/-}$ mice at either one or 21 days (<1% BrdU-positive cells in airways). Both tMWCNTs and rMWCNTs caused a modest and similar increase in BrdU uptake in the airway epithelium of *Stat1*$^{+/+}$ mice at one-day post-exposure (5-10% BrdU-positive cells in airways). In contrast, rMWCNTs caused a significant increase in BrdU uptake in the airway epithelium of *Stat1*$^{-/-}$ mice (10-15% BrdU-positive cells in airways) compared to tMWCNT treatment or vehicle at one-day post-exposure in *Stat1*$^{-/-}$ mouse lungs, but there was no significant difference compared to *Stat1*$^{+/+}$ MWCNT exposed mouse lungs (Fig 2.4B). At 21 days post-exposure BrdU uptake in response to MWCNTs had subsided to ~5% BrdU-positive cells or less, although there was a significant increase in proliferation of the airway epithelial cells in the lungs of both *Stat1*$^{+/+}$ and *Stat1*$^{-/-}$ mice treated with rMWCNTs compared to tMWCNTs or vehicle control (Fig 2.4B).

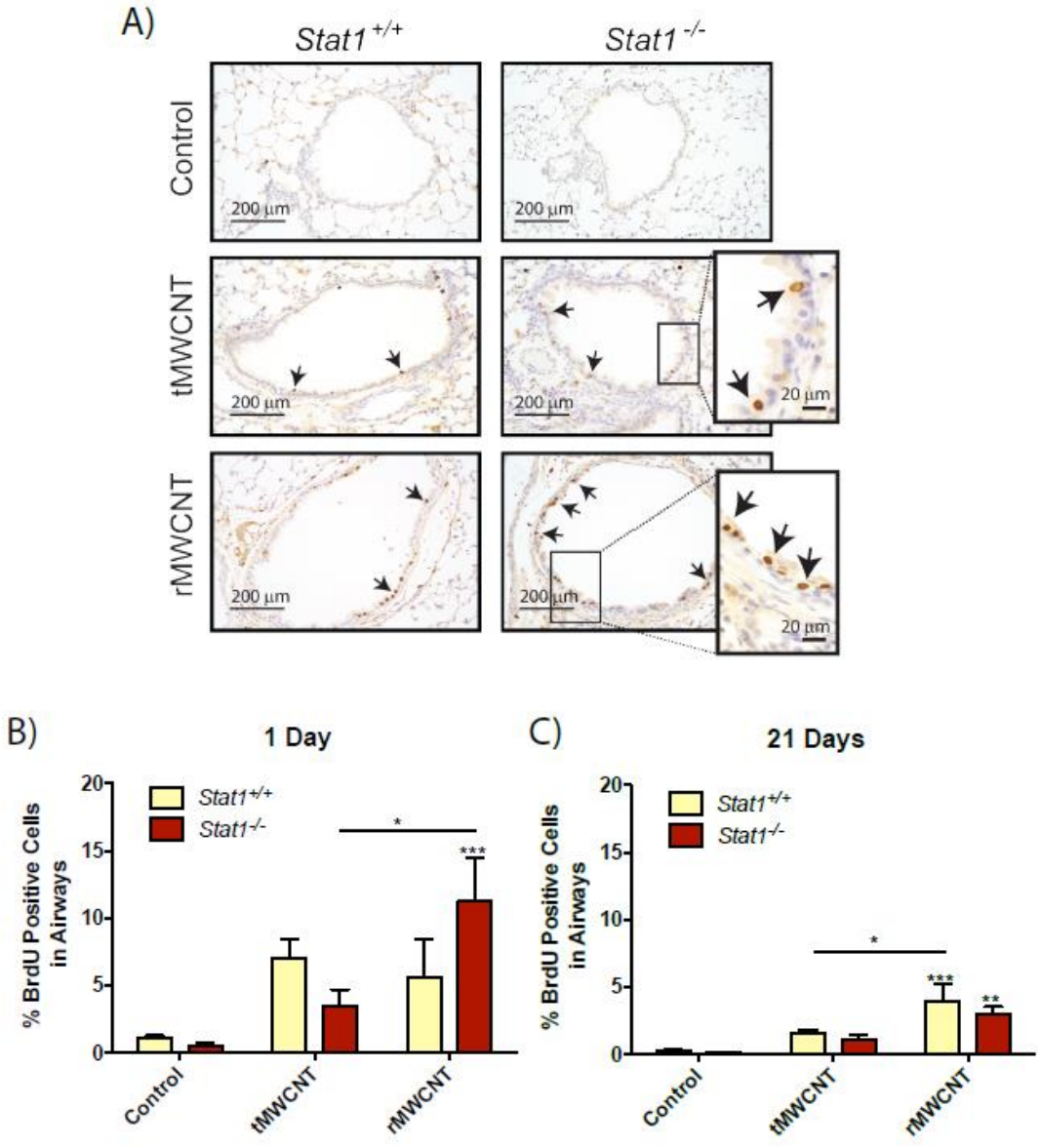

Figure 2.4. Airway epithelial cell proliferation in *Stat1*$^{+/+}$ and *Stat1*$^{-/-}$ mice after one and 21 days exposure to MWCNTs. **A)** Bromodeoxyuridine (BrdU) immunostaining at one-day post-exposure to tMWCNTs or rMWCNTs showing BrdU-positive brown nuclei of proliferating cells (arrows). **B)** Quantitation of BrdU positive cells per airway after one and **C)** 21 days of exposure. (***$p<0.001$ compared to control; *$p<0.05$ between tMWCNTs and rMWCNTs).

MWCNT-Induced Mucous Cell Metaplasia: We observed airway mucous cell metaplasia in the lungs of both *Stat1*$^{+/+}$ and *Stat1*$^{-/-}$ mice exposed to rMWCNTs at 21 days but not in mice treated with tMWCNTs (Fig 2.5A). Mucous cell metaplasia in response to rMWCNTs was evident by the appearance of AB-PAS-positive goblet cells in the airway epithelium. Quantitative morphometry of all airways sectioned from each mouse revealed a similar increase in AB-PAS goblet cells induced by rMWCNTs in both *Stat1*$^{+/+}$ and *Stat1*$^{-/-}$ mice (Fig 2.5B).

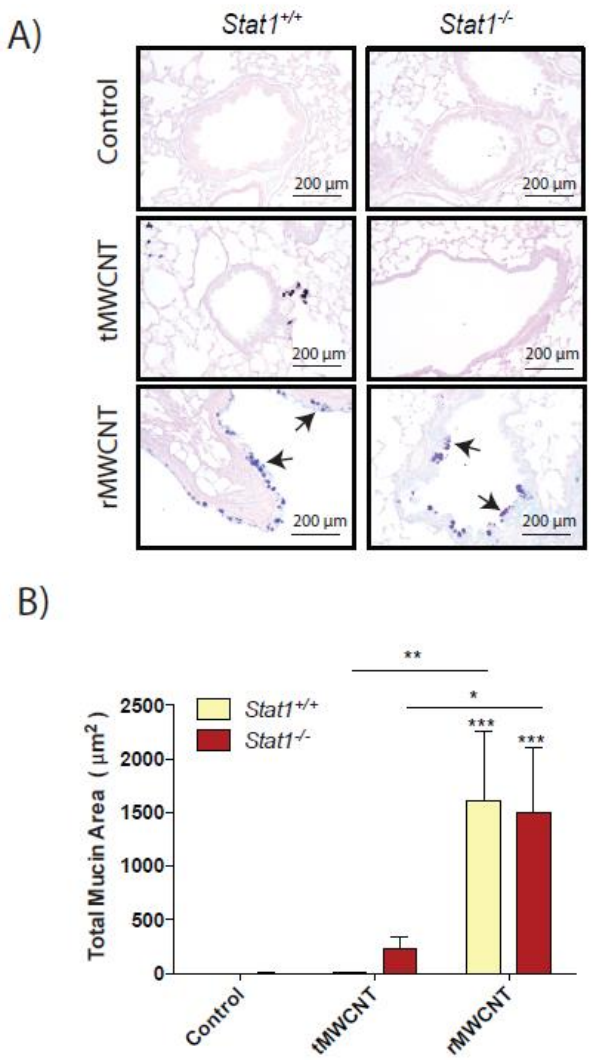

Figure 2.5. Mucous cell metaplasia after exposure to tMWCNTs or rMWCNTs. **A)** Representative photomicrographs of Alcian-blue Periodic Acid-Schiff (AB-PAS)-stained lungs from 21 days post exposure. AB-PAS positive goblet cells are indicated by arrows. **B)** Quantification of mucous cell metaplasia as average mucous stain per total area of airway (***$p<0.001$ compared to controls; **$p<0.01$ or *$p<0.05$ between tMWCNTs and rMWCNTs).

MWCNT-Induced Serum IgE and Allergic Cytokine Pulmonary mRNA Levels: There was an increased amount of basal IgE levels in the serum of *Stat1*$^{-/-}$ mice compared to *Stat1*$^{+/+}$ mice at one and 21 days after exposure to the pluronic vehicle control (Fig 2.6). Exposure to tMWCNTs did not increase serum IgE levels in either *Stat1*$^{+/+}$ or *Stat1*$^{-/-}$ mice at either time point (Fig 2.6). In contrast, rMWCNTs significantly increased levels of serum IgE at 21 days after exposure to rMWCNTs in *Stat1*$^{-/-}$ mice as compared to *Stat1*$^{-/-}$ vehicle control (Fig 2.6B). There was a slight increase in lung IL-4 mRNA expression at one-day post exposure to rMWCNTs in the *Stat1*$^{-/-}$ mice compared to *Stat1*$^{+/+}$ mice (Appendix A.2A). This difference abated by 21 days post-exposure (Appendix A.2B). IL-13 mRNA levels were not significantly changed by exposure to tMWCNTs or rMWCNTs in either genotype at one or 21 days (Appendix A.2C and 2D).

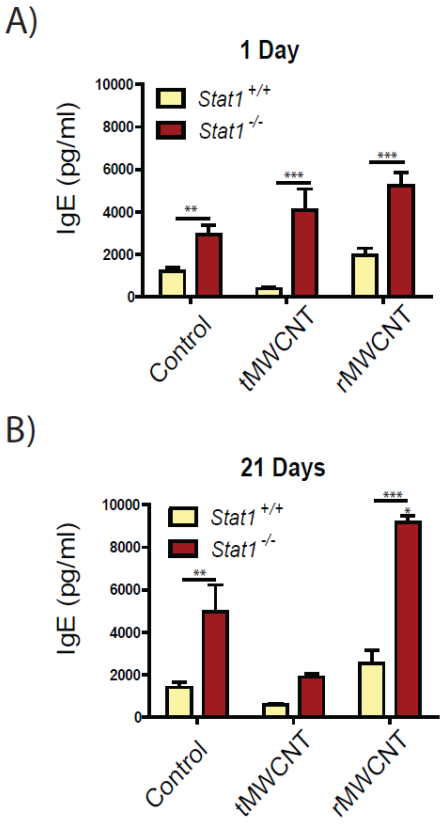

Figure 2.6. Quantification of immunoglobulin E (IgE) by ELISA in the serum from *Stat1*$^{+/+}$ and *Stat1*$^{-/-}$ mice. **A)** Serum IgE concentrations one-day and **B)** 21 days post exposure to tMWCNTs or rMWCNTs (***$p<0.001$ or **$p<0.01$ between genotypes, *$p<0.05$ compared to control).

MWCNT-Induced Pulmonary Fibrosis: Lung and airway fibrosis was quantified by morphometric analysis of Masson's trichrome-stained slides and soluble collagen content from lung protein lysates. Histopathologic evaluation revealed that fibrosis was limited primarily to airways and induced by rMWCNTs but not tMWCNTs. Quantitative morphometry of airway fibrosis to generate area/perimeter ratio measurements indicated significant focal peribronchiolar collagen deposition after exposure to rMWCNTs but not tMWCNTs in the

lungs of *Stat1*$^{+/+}$ and *Stat1*$^{-/-}$ mice (Fig 2.7A-B). Moreover, *Stat1*$^{-/-}$ mice had significantly more airway fibrosis as compared to *Stat1*$^{+/+}$ mice 21 days after exposure to rMWCNTs (Fig. 2.7B). Despite the regional increase in airway fibrosis caused by rMWCNTs, there was not a significant difference in total lung collagen at 21 days post exposure among treatment groups or genotypes as measured by Sircol assay (Appendix A.3) or hydroxyproline assay (data not shown).

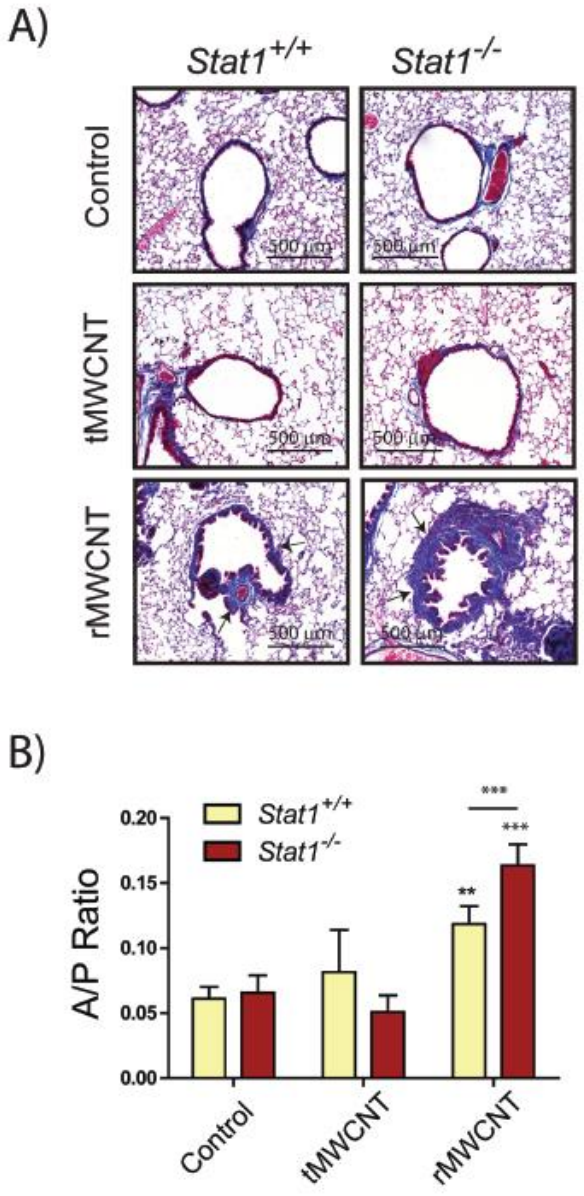

Figure 2.7. Airway fibrosis in *Stat1*$^{+/+}$ and *Stat1*$^{-/-}$ mice exposed to tMWCNTs or rMWCNTs. **A)** Representative photomicrographs taken at 200X magnification of Massons trichrome-stained lung sections showing collagen deposition around airways (arrows) in mouse lungs at 21 days post exposure. Connective tissue (e.g. collagen) stains blue. Scale bars equal 500 μm. **B)** Area to perimeter (A/P) ratios of mouse lung airway thickness at 21 days post exposure (***$p<0.001$ or **$p<0.01$ compared to control; ***$p<0.001$ between tMWCNTs and rMWCNTs).

MWCNT-Induced Expression of TGF-β1 and Other Profibrogenic Cytokines: TGF-β1, a primary mediator of fibrosis, was measured at the protein level by ELISA in the BALF of mice. TGF-β1 was significantly increased by rMWCNT-treatment in *Stat1*$^{+/+}$ mouse BALF at 21 days, and further significantly increased in the BALF of *Stat1*$^{-/-}$ mice that were treated with rMWCNTs (Fig 2.8A). In contrast, TGF-β1 was not increased in the BALF from tMWCNT-treated mice at one or 21 days post exposure (Fig 2.8A). TGF-β1 was not detectable in the BALF from any of the treatment groups or genotypes at one-day post-exposure (data not shown). Several other cytokines implicated in fibrogenesis, including osteopontin (OPN), platelet-derived growth factor (PDGF), and interleukin-1β (IL-1β), were also measured at the protein level in BALF or at the mRNA level in lung tissue. The BALF from rMWCNT-exposed mice contained significantly more OPN protein after the one-day exposure, while the BALF from tMWCNT-treated mice contain significantly more OPN 21 days after exposure (Appendix A.4A-B). Induction of OPN by MWCNTs was not significantly different between *Stat1*$^{+/+}$ and *Stat1*$^{-/-}$ mice. An ELISA was also conducted to measure the IL-1β in BALF. However, no significant differences in secreted IL-1β protein were observed among treatment groups or genotypes (data not shown). The expression of two PDGF isoforms (PDGF-A and PDGF-B) were measured from lung tissue by Taqman qRT-PCR. While there was a trend for higher levels of PDGF-A and PDGF-B mRNA in the lung tissue from *Stat1*$^{-/-}$ mice, these increased levels were not significant (Appendix A.5).

Effect of MWCNTs on TGF-β1 Signaling Molecules. Because changes in TGF-β1 protein levels in BALF closely matched the pathologic changes in airway fibrosis in *Stat1*$^{+/+}$ and *Stat1*$^{-/-}$ mice exposed to rMWCNTs, we sought to investigate components of the TGF-β1 signaling pathway. Total protein lysates were extracted from snap frozen lung tissue and separated by SDS-PAGE followed by Western blot analysis using antibodies specific for TGF-β1 Receptor II (TGF-βRII), phosphorylated Smad2/3 (p-Smad2/3) and total Smad2/3. β-actin was measured as a constitutively expressed protein and used to normalize for densitometry of visualized protein bands (Fig 2.8B). The levels of TGF-βRII remained unchanged in both genotypes following either treatment (data not shown). Overall levels of Smad2/3 were increased with rMWCNT exposure and decreased with tMWCNT exposure, but not significantly different among genotypes (Fig 2.8C). The ratio of p-Smad2/3 to total Smad2/3 levels displays a higher trend of Smad2/3 activation in *Stat1*$^{-/-}$ mouse lungs compared to *Stat1*$^{+/+}$ with no significant difference between exposures (Fig 2.8D). The transcriptional targets of activated p-Smad2/3, Col1a1 and Col1a2, mirror this trend as measured via Taqman qRT-PCR from whole lung mRNA, however the transcription levels of these collagen mRNAs did not change with treatment (Appendix A.6).

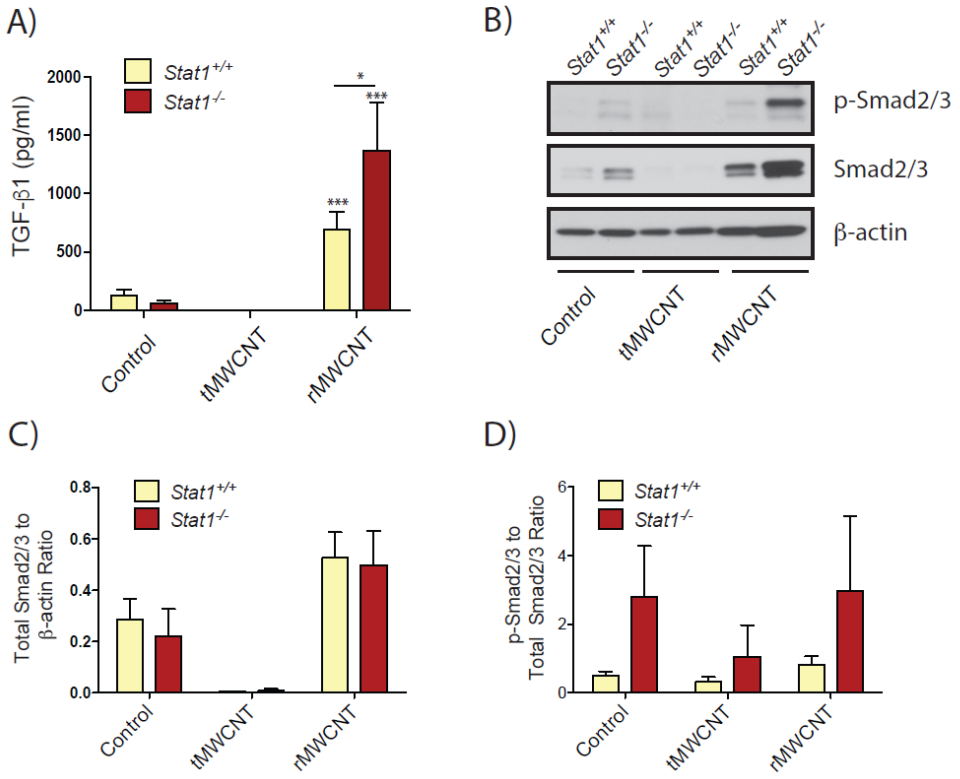

Figure 2.8. TGF-β1 protein levels and p-Smad2/3 levels in lung tissue from *Stat1*$^{+/+}$ and *Stat1*$^{-/-}$ mice after 21 days of exposure to tMWCNTs or rMWCNTs. **A)** TGF-β1 protein in BALF was measured by ELISA (***p<0.001 compared to controls; *p<0.05 between genotypes). **B)** Representative Western blot showing p-Smad2/3 and total Smad2/3 protein levels in lung tissue. **C)** Densitometry of total Smad2/3 levels normalized to β-actin levels. **D)** Quantification of the ratio of p-Smad2/3 to total Smad2/3 densitometry levels relative to β-actin.

Discussion

In this study, we investigated the pulmonary allergic, inflammatory and fibrogenic responses of *Stat1*$^{+/+}$ and *Stat1*$^{-/-}$ mice to rod-like (r-) or tangled (t-) MWCNTs delivered by oropharyngeal aspiration. Since significant differences were observed in airway fibrogenic responses to rMWCNTs between *Stat1*$^{+/+}$ and *Stat1*$^{-/-}$ mice, we further investigated a

mechanism of enhanced fibrosis involving induction of TGF-β1 and Smad2/3 transcription factors that mediate collagen production. Previous studies by other investigators have focused on differential inflammatory, fibrotic, allergic, or carcinogenic effects of r- versus t-MWCNTs in wild type mice [5,9,20-22]. However, to our knowledge this is the first time MWCNT rigidity has been quantified and differential allergic or fibrogenic responses to rMWCNTs versus tMWCNTs have been studied in *Stat1*$^{-/-}$ mice, or any other susceptible transgenic mouse strain.

We previously reported that *Stat1*$^{-/-}$ mice are susceptible to lung fibrosis caused by oropharyngeal aspiration of bleomycin or by co-exposure to MWCNTs and ovalbumin allergen [11,19]. In the latter study, tMWCNTs in the absence of allergen did not cause significant pulmonary fibrosis in *Stat1*$^{-/-}$ or *Stat1*$^{+/+}$ mice, an observation confirmed in the current study. In the present study, we observed that rMWCNTs but not tMWCNTs significantly increased airway fibrosis in the lungs of *Stat1*$^{+/+}$ mice and fibrosis was further increased in *Stat1*$^{-/-}$ mice focally around airways. Similarly, rMWCNTs but not tMWCNTs significantly increased TGF-β1 levels in the BALF of *Stat1*$^{+/+}$ mice and further increased TGF-β1 in *Stat1*$^{-/-}$ mice after 21 days. We also noted that while both MWCNTs resulted in inflammation after one-day exposure, only the rMWCNTs resulted in fibrogenesis while inflammation in the tMWCNT exposed lungs resolved without fibrogenesis. This supports previous literature that indicates inflammation is not necessarily a prerequisite for fibrogenesis [23]. However, the increase in TGF-β1 did not correlate with increased total lung collagen mRNAs (Col1a1 and Col1a2) at one or 21 days post exposure, indicating that a regional increase in airway fibrosis might not

be detectable by assays that measure total lung collagen mRNA or protein levels (i.e., Sircol and hydroxyproline assays). In addition, rMWCNTs but not tMWCNTs induced total lung levels of Smad2/3 and greater Smad2/3 phosphorylation was observed in *Stat1*$^{-/-}$ mouse lungs compared to *Stat1*$^{+/+}$ mouse lungs. Therefore, our findings suggest that STAT1 regulates fibrosis through suppressing TGF-β1 production and decreasing Smad2/3 phosphorylation status. No changes were observed in TGF-βRII protein levels in the lungs of *Stat1*$^{+/+}$ or *Stat1*$^{-/-}$ mice treated with or without MWCNTs. These findings suggest that increased airway fibrosis in the lungs of *Stat1*$^{-/-}$ mice exposed to rMWCNTs is mediated by increased levels of TGF-β1 in the BALF as well as increased Smad2/3 activation in lung tissue. A proposed mechanism illustrating the role of STAT1 in suppressing TGF-β1 and Smad2/3 activation in rMWCNT-induced air way fibrosis is shown in Fig. 2.9.

The susceptibility of *Stat1*$^{-/-}$ mice to pulmonary fibrosis is consistent with the well-established function of STAT1 as a primary growth inhibitory signaling pathway for interferons [17,18]. For example, STAT1 specifically interacts with cyclin D1 and CDK4 to mediate cell cycle arrest in a human fibrosarcoma cell line after treatment with interferon (IFN)-γ [24]. We originally reported that *Stat1*$^{-/-}$ mouse lung fibroblasts (MLFs) have enhanced proliferative responses to PDGF or EGF *in vitro* when co-treated with IFN-γ, whereas the proliferative response to these growth factors was inhibited by IFN-γ in *Stat1*$^{+/+}$ MLFs [19]. The enhanced proliferative response of *Stat1*$^{-/-}$ MLFs was likely due to the fact that IFN-γ activates other pathways independent of STAT1 (e.g., mitogen activated protein kinases (MAPKs) and protein kinase

B (Akt)) [17]. Therefore, in the absence of STAT1, IFN-γ signaling can participate in growth promoting pathways otherwise kept in check by the presence of STAT1.

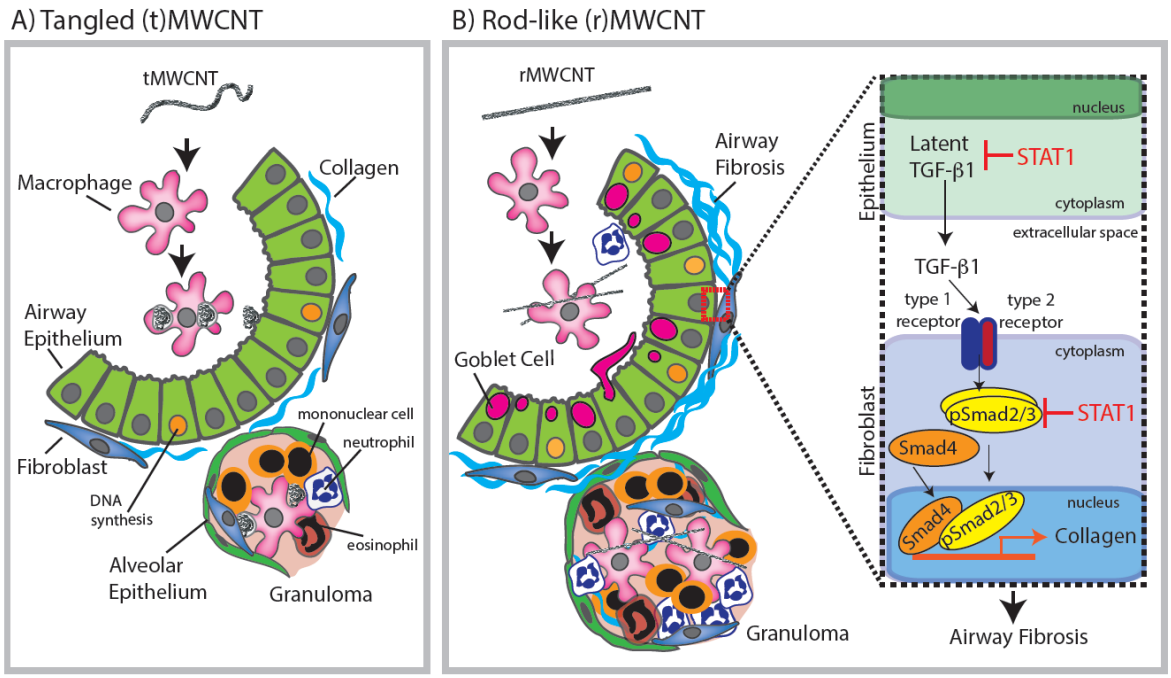

Figure 2.9. Summary illustration depicting differential chronic lung immune and fibrotic responses at 21 days post-exposure to **A)** tangled (t-)MWCNTs or **B)** Rod-like (r-)MWCNTs. The inset in panel B highlights the postulated role of STAT1 in suppressing TGF-β1 production by epithelial cells and Smad2/3 activation levels in fibroblasts.

In addition to suppression of fibroblast growth, another anti-fibrotic mechanism of STAT1 involves inhibition of TGF-β1 signaling. We previously established that *Stat1*$^{-/-}$ MLFs express higher levels of collagen mRNAs and produce more collagen protein than *Stat1*$^{+/+}$ MLFs when stimulated with TGF-β1 [11]. STAT1 has also been shown to be a negative regulator of hepatic fibrosis, where IFN-γ treatment of *Stat1*$^{+/+}$ mice did not result in fibrosis while the same treatment of *Stat1*$^{-/-}$ mice resulted in increased hepatic fibrosis and accelerated TGF-β1/Smad

signaling [25]. Here, we showed for the first time that *Stat1*$^{-/-}$ mice have exaggerated levels of TGF-β1 in the bronchoalveolar lavage fluid relative to *Stat1*$^{+/+}$ mice after exposure to rMWCNTs, demonstrating that STAT1 negatively regulates TGF-β1 production and that rMWCNTs are more potent inducers of TGF-β1 compared to tMWCNTs. We also established that Smad2/3 phosphorylation status was increased in *Stat1*$^{-/-}$ mice compared to *Stat1*$^{+/+}$ mice. Collectively, these data suggest that STAT1 suppresses rMWCNT-induced fibrosis by suppressing TGF-β1 production and intracellular Smad2/3 activation (Fig. 9). The mechanism of enhanced phosphorylation of Smad2/3 in *Stat1*$^{-/-}$ MLFs by rMWCNTs remains to be elucidated. However, others have shown that activated STAT1 homodimers upregulate SOCS1 and Smad7, thereby inhibiting TGF-β1-induced Smad2/3 activation [26,27]. Also, TGF-β1 suppresses IFN-γ-induced STAT1-dependent gene transcription in epithelial cells through enhancement of protein inhibitor of STAT1 (PIAS1) [28]. The opposing roles of TGF-β1 and IFN-γ should be a topic of further investigation in the context of *Stat1*$^{-/-}$ susceptibility to rMWCNTs.

Others have shown that the same rMWCNTs used in the present study increase TGF-β1 in fibrotic foci within the lungs of mice exposed by oropharyngeal aspiration and TGF-β receptor-1 (TGF-βRI) has been implicated as a major regulator of MWCNT-induced fibrogenesis in mice exposed to rMWCNTs [29]. For example, rMWCNTs induced TGF-βRI in human lung fibroblasts *in vitro* and knock down or inhibition of TGF-βR1 or knock down of Smad2 resulted in decreased collagen production [22,29]. We were unable to detect TGF-βRI in the

present study, but observed that TGF-βRII levels were not changed by rMWCNT treatment or STAT1 deficiency. Nevertheless, it is possible that STAT1 could regulate levels of TGF-βRI. In addition to the collagen synthetic pathways induced by TGF-β1, it is also possible that inhibition of collagen-degrading proteases may be involved in the fibrogenic response to rMWCNTs.

Fibrogenesis stimulated by a foreign body insult (e.g., particles and fibers) is thought to be initiated at least in part by acute injury to epithelial cells. Increased epithelial proliferation marks an injury event where DNA synthesis and cell cycle progression are initiated as a homeostatic repair response, much like what is seen with chrysotile asbestos inhalation exposure [30]. In this study, we observed a significant increase in the proliferation of airway epithelial cells by BrdU uptake after exposure to rMWCNTs (Fig. 4). BrdU uptake at one-day was also induced by tMWCNTs but not to a significant extent. Furthermore, we observed that *Stat1*$^{-/-}$ mice exhibited significantly greater airway epithelial proliferation compared to vehicle-treated or tMWCNT-treated *Stat1*$^{-/-}$ mice. BrdU uptake in the airway epithelium of rMWCNT-treated *Stat1*$^{-/-}$ mice was twice that seen in rMWCNT-treated *Stat1*$^{+/+}$ mice, yet this difference was not statistically significant (Fig. 4). The increase in airway epithelial cell BrdU uptake could be mediated by growth factors (e.g., PDGF, EGF) produced by epithelial cells, macrophages, or other pulmonary cell types. We previously reported that primary *Stat1*$^{-/-}$ MLFs have enhanced proliferative responses to PDGF or EGF *in vitro* [19]. Therefore, it is

possible that airway epithelial cells from *Stat1*$^{-/-}$ mice might have enhanced proliferative responses to growth factors *in vivo*.

In the present study, we showed that rMWCNTs and tMWCNTs caused similar acute neutrophilic inflammation in the lungs of either *Stat1*$^{-/-}$ or *Stat1*$^{+/+}$ mice at one-day post-exposure, although only rMWCNTs caused sustained elevated neutrophil counts after 21 days in the BALF of mice (Fig. 2). We also observed that both rMWCNTs and tMWCNTs produced granulomas, although rMWCNTs produced significantly larger granulomas than tMWCNTs (Fig. 3). Other studies have documented granuloma formation after MWCNT exposure [4-6,20,29,31-33]. Granulomas centrally consist of epithelioid and multinucleated giant macrophages surrounded by activated lymphocytes, typically activated CD4+ T cells [34]. Granulomas resulting from MWCNT treatment have been found to contain CD3+ monocytes and CD4+ T cells, as well as increased levels of osteopontin (OPN) in the granulomatous foci in mouse lungs [35]. In our study, granuloma formation was generally independent of STAT1 as both *Stat1*$^{-/-}$ and *Stat1*$^{+/+}$ mice had a mean granuloma size that was not statistically different between genotypes. Moreover, OPN levels were similar between genotypes, albeit strongly induced by rMWCNTs (Appendix A.4). However, two out of six *Stat1*$^{-/-}$ mice exposed to rMWCNTs had at least one exaggerated granuloma, although these "super-granulomas" were rare and did not contribute significantly to differences in granuloma size between genotypes (data not shown). Other investigators have reported that *Stat1*$^{-/-}$ mice infected with *M. tuberculosis* have larger granuloma development compared their infected *Stat1*$^{+/+}$ counterparts [36].

Mucociliary clearance is an innate immune response that removes inhaled particles and fibers from the lungs, yet excessive mucous cell metaplasia and mucus hypersecretion contributes to airway obstruction. Mucous cell metaplasia has been observed previously in mice exposed to rMWCNTs [9,10]. Induction of Th2 cytokines such as IL-4 and IL-13, activation of STAT6, and transcription of mucin genes (*muc5ac* and *muc5b*) contribute to mucin formation in airway epithelial cells [37]. We did not observe significant differences in IL-4 or IL-13 mRNA levels between genotypes or treatment groups, although there was a trend for increased IL-4 mRNA in the lungs of *Stat1*$^{-/-}$ mice treated with rMWCNTs (Appendix A.2). However, others have shown that rMWCNTs cause increased IL-13 mRNA levels and allergic airway inflammation in female mice after inhalation exposure [9]. In addition, Hussain *et al.* observed mucous cell metaplasia after 21 days post-exposure to tMWCNTs in female mice [38]. This contrasts to most other studies performed in male mice. Therefore, sex differences could explain the difference in mechanism of mucous cell metaplasia observed in this study. It is also conceivable that an IL-13-independent mechanism could mediate mucous cell metaplasia in response to rMWCNTs. For example, STAT6 activation can also occur through an alternative mechanism involving STING and TBK1 activation [39].

STAT1 is an IFN-γ activated transcription factor driving the differentiation of naïve T cells to become Th1 cells. In the absence of a Th1 environment, there will more likely be a shift towards a Th2 response. In the present study, induction of a systemic Th2 immune response in

Stat1$^{-/-}$ mice was evident by increased levels of serum IgE. Serum IgE levels were especially high in *Stat1*$^{-/-}$ mouse serum and increased greatly following treatment of *Stat1*$^{-/-}$ mice with rMWCNTs after 21 days (Fig 2.6B). However, both *Stat1*$^{+/+}$ and *Stat1*$^{-/-}$ mice exhibited increased mucous cell metaplasia with rMWCNT treatment but not tMWCNTs. The reason for a differential systemic allergic response yet similar allergic lung responses between *Stat1*$^{+/+}$ and *Stat1*$^{-/-}$ remains to be elucidated.

In addition to genetic susceptibility, our study highlights the importance of nanotube rigidity. Physicochemical characteristics other than rigidity could also influence the allergic immune and fibrotic potential of MWCNTs. For example, length is an important determinant as intratracheal instillation of long, but not short, MWCNTs causes the formation of granulomas, up-regulation of ECM protease inhibitors, increased collagens, and TGF-β1 production in rats [21]. Thicker and longer MWCNTs induce the greatest DNA damage and induce transcriptional markers of fibrosis compared to thinner, shorter MWCNTs [33,34]. Finally, differences in residual metal catalysts (Fe in rMWCNTs and Ni in tMWCNTs) could influence toxicity and disease outcome. Collectively, these studies along with our observations in the present work emphasize that multiple physicochemical characteristics should be considered in the design of MWCNTs to reduce or prevent future disease.

Conclusions

In summary, MWCNT rigidity plays a substantial role in pulmonary toxicity. Moreover, STAT1 is an important protective factor and plays a role in suppressing the fibrogenic response to rMWCNTs by inhibiting TGF-β1 production, intracellular Smad2/3 phosphorylation, and collagen synthesis. Both rigidity and genetic susceptibility should be major considerations for risk assessment and development of MWCNTs.

Methods

MWCNT Materials and Preparation: tMWCNTs were obtained from Helix Material Solutions Inc. (Richardson, TX). rMWCNTs (XRNI MWNT-7 05072001K28) were obtained from Dale Porter at NIOSH and manufactured by Mitsui & Co (Tokyo, Japan). Pluronic F-68 Solution (#P5556) from Sigma (Saint Louis, MO) was diluted with DPBS to 0.1% and used to bring MWCNTs to a working concentration of 2 mg/mL. MWCNTs were sonicated in a cup horn sonicator for two minutes and were also vortexed vigorously immediately prior to dosing mice 4 mg/kg via oropharyngeal aspiration.

Rigidity Measurements: Measurements were taken as described in Method 3 by the International Standards Organization 11888:2011 [40,41]. Ten transmission electron microscope (TEM) images of tMWCNTs and ten of rMWCNTs taken at 10000X were used to perform length measurements of each MWCNT directly from end to end (R) and along the axis (*L*) of

each tube per image; these lengths were measured using the Adobe Photoshop C5S ruler tool to convert pixels to μm and trace the imaged MWCNTs. These measurements were averaged into a bending ratio (D_b) between the mean-squared end-to-end distance $<R^2>$ and squared contour length (L^2) to determine the approximate static bending persistence length (SBPL) using the equations:

$$D_b = <R^2>/L^2$$

$$SBPL = (D_b * L)/2$$

Animal Care: Pathogen free 6-8 week old adult SV129 male *Stat1*$^{+/+}$ and *Stat1*$^{-/-}$ mice were purchased from Taconic Laboratories (Germantown, NY) and housed in an IACUC approved and AALAC-accredited animal facility. Animals were acclimated for two weeks prior to treatments. Animals were housed 1-5 per cage and fed water and LabDiet 5001 rodent diet *ad libitum*.

Experimental Design and Collection of Mouse Samples: The experimental design is illustrated in Fig 2.2A. *Stat1*$^{+/+}$ and *Stat1*$^{-/-}$ mice were divided into 3 treatment groups (vehicle, tMWCNT, or rMWCNT) for one and 21 day sample collections. Mice were anesthetized with isoflurane and dosed with 4 mg/kg tMWCNTs (n=6), 4 mg/kg rMWCNTs (n=12), or equal volume pluronic vehicle (n=18) via oropharyngeal aspiration. Half the mice from each treatment group were euthanized via intraperitoneal injection of pentobarbital (Vortech Pharmaceuticals, LTD, Dearborn, MI #NDC 0298-9373-68) at one-day post exposure and the

rest at 21 days post exposure. Serum was collected immediately and extracted from clotting factors using a BD (Franklin Lakes, NJ) microtainer SST. Two 0.5 mL aliquots of phosphate buffered saline (PBS) were instilled via intratracheal cannulation and retrieved to collect bronchoalveolar lavage fluid (BALF) for cytokine and cellular content. The left lobe of the lung was inflated and fixed for histology with neutral buffered formalin (Azer Scientific, Morgantown, PA #NBF-4-G) and the right lobes were divided equally into RNAlater (Sigma #R0901) for mRNA or snap frozen in liquid nitrogen for protein analysis. Small intestine, heart, spleen, brain, and liver samples were also collected for histology and mRNA analysis.

Enzyme-Linked Immunosorbent Assay (ELISA): BALF was analyzed using DuoSet ELISA kits (R & D Systems, Inc., Minneapolis, MN) specific for mouse TGF-β1 (DY1679), Osteopontin (OPN) (DY441), and IL-1β (DY401). Serum IgE was assayed using a BD Pharmingen ELISA kit (557079, San Jose, CA). Sample concentrations in BALF or serum were derived from absorbance values and converted to concentration values based on standards provided with each. kit.

Cell Counts: Differential cell counts were obtained by cytospin centrifugation of 100 µL of BALF using a Single Cytology Funnel (Fisherbrand, Pittsburgh, PA, 10-354) onto a slide and once dry, stained with DiffQuik (Siemens, Munich, Germany, B4132-1A). Differential cell counts were taken by counting 500 cells per slide/animal to identify relative percentages of macrophages, neutrophils, eosinophils, and lymphocytes.

Quantitative Morphometry of Lung Granulomas: Granulomas in lung sections stained with Masson's Trichrome were analyzed by light microscopy (Olympus BX40 microscope). A granuloma was defined as a multi-cellular focal formation consisting of monocytes, macrophages, fibroblasts, and epithelial cells surrounding a MWCNT aggregate. Some granulomas also contained neutrophils and eosinophils. Photomicroscopic images were analyzed using Adobe Photoshop CS5 to determine the area of each granuloma formation by using the lasso tool and converting pixels to µm.

Airway Area to Perimeter Ratio: An area to perimeter (AP) ratio method was used to quantitatively assess airway fibrosis as previously described [7,11]. Briefly, light microscopic images of Masson's trichrome-stained airways were analyzed using Adobe Photoshop CS5; the lasso tool was used to outline the inside perimeter of the airway along the basal membrane of the airway epithelium and along the outside perimeter of the 'blue-stained' connective tissue surrounding the airway. The ratio of this inner to outer measurement circumference measurement is referred to as the area to perimeter ratio.

Bromodeoxyuridine (BrdU) Immunohistochemistry (IHC): Mice received an i.p. injection of 100 mg/kg BrdU in PBS one-hour prior to euthanasia with an i.p. injection of pentobarbital. Formalin-fixed, paraffin embedded blocks of lung or small intestine (positive control) were cut 5 µm with a microtome and mounted on a negatively charged slide and dried overnight. The sections were immunostained with anti-BrdU Pure (BD #347580) followed by the Vectastain

ABC kit (VectorLabs, Burlingame, CA, #PK-6102) and DAB buffer (BioGenex, San Ramon, CA, #HK542-XAK) as described per manufacturer protocol. BrdU-positive brown-stained nuclei stand out from the hematoxalin counterstain. Photomicroscopic images were analyzed in Adobe Photoshop CS5 using the count tool to measure numbers of BrdU-positive epithelial cells associated with each airway. BrdU-positive cells were normalized for the total number of airway epithelial cells in each airway section. Data are the average percent of BrdU positive cells per airway per mouse in each treatment group.

Mucin Quantification: Photomicroscopic images of Alcian Blue –Periodic Acid Schiff (AB-PAS) stained lung sections were analyzed using Image J software and the area of positive stained blue/purple mucin was quantified as previously described [11].

RT-PCR: Applied Biosystems high capacity cDNA reverse transcription kit (Fisher #4368814) was used to create cDNA from the mRNA isolated from the right lung lobes using Quick-RNA™ MiniPrep (Zymo Research, Irvine, CA, #R1058) according to the manufacturer's instructions. The FastStart Universal Probe Master (Rox) (Roche, Basel, Switzerland, #16881300) was then used to run Taqman qPCR on the Applied Biosystems OneStepPlus™ Real-Time PCR System Thermal Cycling Block (ABI, Foster City, CA, Cat#4376598) to determine the comparative C_T ($\Delta\Delta C_T$) fold change expression of IL-4, IL-13, PDGF-A, PDGF-B, Col1a1, and Col1a2 normalized for β2-microglobulin (B2M) as the endogenous control.

Collagen Analysis: Snap frozen right cranial lung lobes were thawed and 10-50 mg of tissue was prepared for the Sircol Assay (Biocolor Ltd., Carrickfergus, UK, #S1000). The tissues and samples were analyzed according to the manufacturer's instructions. Briefly, samples were sonicated for 6 min and then treated with Triton-X (Sigma #T8787) overnight. These samples were combined with Sirius Red dye and collagen hydroxyproline residues pelleted by centrifugation at full speed. The pellet was then washed twice with 99.9% cold denatured alcohol before resuspension in an alkali reagent. Absorbance was measured at 540 nm on a microplate reader to determine the concentration of collagen per lung. Samples were assayed in duplicate and collagen content was normalized to protein concentration of lung lysate and reported as µg of soluble collagen per mg of total protein. Collagen content in the lungs of mice was also measured by hydroxyproline assay according to the manufacturers' instructions (Sigma, St. Louis, MO).

Immunoblotting: Whole lung protein lysates were isolated from snap-frozen mouse left lung lobes and concentrations determined using the Pierce BCA Protein Assay Kit (ThermoFisher Scientific, Waltham, MA, #23225). Samples were diluted, loaded onto a Novex^{TM} 4-12% SDS-PAGE gel (Invitrogen, Carlsbad, CA, #XP04122BOX), and separated by electrophoresis as described previously [42]. Briefly, samples were transferred to PVDF membranes, blocked, and incubated in primary antibody (1:1000 dilution). Rabbit polyclonal pSmad2/3 (#8828), total Smad2/3, and β-actin (#4967) primary antibodies as well as anti-rabbit (#7074) secondary antibody were purchased from Cell Signaling Technology (Beverly, MA). Following primary

antibody incubation, the membranes were washed and then incubated with horseradish peroxidase-conjugated secondary antibody (1:2500 dilution). Enhanced chemiluminescence (ECL) (ThermoFisher Scientific #50-904-9326) was used to visualize immunoblot signals. Protein lysate was extracted from lung tissue of *Stat1*$^{+/+}$ mouse lungs after 21 day exposure to vehicle (n=9), tMWCNT (n=3), and rMWCNT (n=6) and *Stat1*$^{-/-}$ mouse lungs exposed to vehicle (n=9), tMWCNT (n=3), and rMWCNT (n=6). To quantify all immunoblot signals, densitometry was performed as described previously using Adobe Photoshop CS5 [43].

Statistics: Statistical analysis of the data was performed using GraphPad Prism version 5.0 (GraphPad Software Inc.). A one-way ANOVA with a *post hoc* Tukey test was used to determine significance between samples. A two-way ANOVA was used with a Bonferroni post-test to compare between genotypes.

List of Abbreviations:

Signal transducer and activator of transcription-1 (STAT1), carbon nanotubes (CNTs), multi-walled CNTs (MWCNTs), tangled MWCNT (tMWCNT), rod-like MWCNT (rMWCNT), wild type for STAT1 (*Stat1*$^{+/+}$), STAT1 knockout (*Stat1*$^{-/-}$), oropharyngeal aspiration (OPA), bronchoalveolar lavage fluid (BALF), transforming growth factor-β1 (TGF-β1), osteopontin (OPN), platelet derived growth factor-A (PDGF-A), platelet derived growth factor-B (PDGF-B), interleukin (IL), immunoglobulin E (IgE), static bending ratio (Db), static bending persistence length (SBPL), interferon (IFN), endothelial growth factor (EGF), transmission

electron microscope (TEM), bromodeoxyuridine (BrdU), enzyme linked immunosorbent assay (ELISA), TGF-β receptor I (TGF- βRI), TGF-β receptor II (TGF-βRII), mitogen activated protein kinase (MAPK), extracellular signal related kinase (ERK), extracellular matrix (ECM), type 1 T helper cell (Th1), type 2 T helper cell (Th2), portmanteau of mothers against decapentaplegic (MAD) and small body size (SMA) (Smad proteins)

Ethics Approval and Consent to Participate

Not applicable

Consent for Publication

Not applicable

Availability of Data and Materials

Not applicable

Competing Interests

The authors have no competing interests.

Funding

This work was supported by NIEHS R01ES020897 (JCB, GNP, KSD, MDI, ECN, KAS, AJT), and NIEHS Training Grant: T32 ES007046 (KSD, MDI). JCB was partially supported by NIEHS P30 ES025128.

Author Contributions

Conception and design: KSD, JCB; Experimentation analysis and interpretation: KSD, AJT, MDI, KAS, EAT, ECD, GNP, JCB; Drafting the manuscript for important intellectual content: KSD, JCB.

Acknowledgments

We thank Dr. Dale Porter at NIOSH for providing rMWCNT (Mitsui-7), Professor Il Je Yu at Hoseo University, South Korea for advice on the method for determining carbon nanotube bending ratio, and Dr. Debra Tokarz at NCSU College of Veterinary Medicine for advice on identity of inflammatory cell types in granulomas.

References

1. Donaldson K, Aitken R, Tran L, Stone V, Duffin R, Forrest G, et al. Carbon nanotubes: A review of their properties in relation to pulmonary toxicology and workplace safety. Toxicol. Sci. 2006;92:5–22.
2. Seaton A, Tran L, Aitken R, Donaldson K. Nanoparticles, human health hazard and regulation. J. R. Soc. Interface. 2010;7 Suppl 1:S119–29.
3. Donaldson K, Murphy F a, Duffin R, Poland C. Asbestos, carbon nanotubes and the pleural mesothelium: a review of the hypothesis regarding the role of long fibre retention in the parietal pleura, inflammation and mesothelioma. Part. Fibre Toxicol.2010;7:5.
4. Muller J, Huaux F, Moreau N, Misson P, Heilier JF, Delos M, et al. Respiratory toxicity of multi-wall carbon nanotubes. Toxicol. Appl. Pharmacol. 2005;207:221–31.
5. Dong J, Porter DW, Batteli LA, Wolfarth MG, Richardson DL, Ma Q. Pathologic and molecular profiling of rapid - onset fibrosis and inflammation induced by multi - walled carbon nanotubes. Arch Toxicol. 2015;89(4):621-33.
6. Mercer RR, Hubbs AF, Scabilloni JF, Wang L, Battelli L, Friend S, et al. Pulmonary fibrotic response to aspiration of multi-walled carbon nanotubes. Part. Fibre Toxicol. BioMed Central Ltd; 2011;8:21.
7. Ryman-Rasmussen JP, Cesta MF, Brody AR, Shipley-Phillips JK, Everitt JI, Tewksbury EW, et al. Inhaled carbon nanotubes reach the subpleural tissue in mice. Nat. Nanotechnol. 2009;4:747–51.
8. Mercer RR, Scabilloni JF, Hubbs AF, Wang L, Battelli L, McKinney W, et al. Extrapulmonary transport of MWCNT following inhalation exposure. Particle and Fibre Toxicology; 2013;10:38.
9. Rydman EM, Ilves M, Koivisto AJ, Kinaret PAS, Fortino V, Savinko TS, et al. Inhalation of rod-like carbon nanotubes causes unconventional allergic airway inflammation. Part. Fibre Toxicol. 2014;11:1–17.
10. Porter DW, Hubbs AF, Mercer RR, Wu N, Wolfarth MG, Sriram K, et al. Mouse pulmonary dose- and time course-responses induced by exposure to multi-walled carbon nanotubes. Toxicology. 2010;269:136–47.
11. Thompson EA, Sayers BC, Glista-Baker EE, Shipkowski KA, Ihrie MD, Duke KS, et al. Role of signal transducer and activator of transcription 1 in murine allergen-induced airway remodeling and exacerbation by carbon nanotubes. Am. J. Respir. Cell Mol. Biol. 2015;53:625–36.
12. Nagai H, Okazaki Y, Chew S, Misawa N, Yamashita Y, Akatsuka S, et al. Diameter and rigidity of multiwalled carbon nanotubes are critical factors in mesothelial injury and carcinogenesis. Proc National Acad Sci USA. 2011;108(49):E1330-8.
13. Aaronson DS, Horvath CM. A road map for those who don’t know JAK-STAT. Science. 2002;296:1653–5.
14. Simon AR, Takahashi S, Severgnini M, Fanburg BL, Cochran BH. Role of the JAK-STAT pathway in PDGF-stimulated proliferation of human airway smooth muscle cells. Am. J. Physiol. Lung Cell. Mol. Physiol. 2002;282:L1296–304.

15. Gorina R, Sanfeliu C, Galitó A, Messeguer A, Planas AM. Exposure of glia to pro-oxidant agents revealed selective Stat1 activation by H2O2 and Jak2-independent antioxidant features of the Jak2 inhibitor AG490. Glia. 2007;55:1313–24.
16. Horvath CM, Wen Z, Darnell JE. A STAT protein domain that determines DNA sequence recognition suggests a novel DNA-binding domain. Genes Dev. 1995;9:984–94.
17. Ramana CV, Gil MP, Han Y, Rasohoff RM, Schreiber RD, Stark GR. Stat1-independent regulation of gene expression in response to INF-γ. Proc. Natl. Acad. Sci. 2001. 98: 6674-9.
18. Bonner JC. Mesenchymal cell survival in airway and interstitial pulmonary fibrosis. Fibrogenesis Tissue Repair. 2010; 3: 15.
19. Walters DM, Antao-Menezes A, Ingram JL, Rice AB, Nyska A, Tani Y, et al. Susceptibility of signal transducer and activator of transcription-1-deficient mice to pulmonary fibrogenesis. Am. J. Pathol. 2005;167:1221–9.
20. Barna BP, Judson MA, Thomassen MJ. Carbon nanotubes and chronic granulomatous disease. Nanomater. 2014;4:508–21.
21. Wang P, Nie X, Wang Y, Li Y, Ge C, Zhang L, et al. Multiwall carbon nanotubes mediate macrophage activation and promote pulmonary fibrosis through TGF-β/smad signaling pathway. Small. 2013;9:3799–811.
22. Vietti G, Ibouraadaten S, Palmai-Pallag M, Yakoub Y, Bailly C, Fenoglio I, et al. Towards predicting the lung fibrogenic activity of nanomaterials: experimental validation of an in vitro fibroblast proliferation assay. Part. Fibre Toxicol. BioMed Central. 2013;10:52.
23. Bringardner BD, Baran CP, Eubank TD, Marsh B. The Role of Inflammation in the Pathogenesis of Idiopathic Pulmonary Fibrosis. Antioxid Redox Signal. 2008; 10:287-301.
24. Dimco G, Knight R a., Latchman DS, Stephanou A. STAT1 interacts directly with cyclin D1/Cdk4 and mediates cell cycle arrest. Cell Cycle. 2010;9:4638–49.
25. Jeong W Il, Park O, Radaeva S, Gao B. STAT1 inhibits liver fibrosis in mice by inhibiting stellate cell proliferation and stimulating NK cell cytotoxicity. Hepatology. 2006;44:1441–51.
26. Ramana C V, Chatterjee-Kishore M, Nguyen H, Stark GR. Complex roles of Stat1 in regulating gene expression. Oncogene. 2000;19:2619–27.
27. Massagué J, Ulloa L, Doody J. Inhibition of transforming growth factor-beta/SMAD signaling by the interferon-gamma/STAT pathway. Nature. 1999;397:710–3.
28. Reardon C, McKay DM. TGF-beta suppresses IFN-gamma-STAT1-dependent gene transcription by enhancing STAT1-PIAS1 interactions in epithelia but not monocytes/macrophages. J. Immunol. 2007;178:4284–95.
29. Mishra A, Stueckle TA, Mercer RR, Derk R, Rojanasakul Y, Castranova V, et al. Identification of TGF- β receptor-1 as a key regulator of carbon nanotube-induced fibrogenesis. Am J Physiol Lung Cell Mol Physiol. 2015;309:821–33.
30. Coin PG, Osornio-Vargas AR, Roggli VL, Brody AR. Pulmonary fibrogenesis after three consecutive inhalation exposures to chrysotile asbestos. Am. J. Respir. Crit. Care Med. 1996;154:1511–9.
31. Cesta MF, Ryman-Rasmussen JP, Wallace DG, Masinde T, Hurlburt G, Taylor AJ, et al. Bacterial lipopolysaccharide enhances PDGF signaling and pulmonary fibrosis in rats exposed to carbon nanotubes. Am. J. Respir. Cell Mol. Biol. 2010;43:142–51.

32. Manke A, Luanpitpong S, Dong C, Wang L, He X, Battelli L, et al. Effect of fiber length on carbon nanotube-induced fibrogenesis. Int. J. Mol. Sci. 2014;15:7444–61.
33. Jaurand M-CF, Renier A, Daubriac J. Mesothelioma: Do asbestos and carbon nanotubes pose the same health risk? Part. Fibre Toxicol. 2009;6:16.
34. Rosas LE, Snider HM, Barbi J, Satoskar AA, Lugo-Villarino G, Keiser T, et al. Cutting edge: STAT1 and T-bet play distinct roles in determining outcome of visceral leishmaniasis caused by Leishmania donovani. J. Immunol. 2006;177:22–5.
35. Huizar I, Malur A, Midgette YA, Kukoly C, Chen P, Ke PC, et al. Novel murine model of chronic granulomatous lung inflammation elicited by carbon nanotubes. Am. J. Respir. Cell Mol. Biol. 2011;45:858–66.
36. Sugawara I, Yamada H, Mizuno S. STAT1 knockout mice are highly susceptible to pulmonary mycobacterial infection. Tohoku J. Exp. Med. 2004;202:41–50.
37. Thai P, Chen Y, Dolganov G, Wu R. Differential regulation of MUC5AC/Muc5ac and hCLCA-1/mGob-5 expression in airway epithelium. Am. J. Respir. Cell Mol. Biol. American Thoracic Society. 2005;33:523–30.
38. Hussain S, Ji Z, Taylor AJ, Degraff LM, George M, Tucker CJ, et al. Multiwalled carbon nanotube functionalization with high molecular weight hyaluronan significantly reduces pulmonary injury. ACS Nano. 2016;10:7675–88.
39. Chen H, Sun H, You F, Sun W, Zhou X, Chen L, et al. Activation of STAT6 by STING is critical for antiviral innate immunity. Cell. 2011;147:436–46.
40. ISO/TS. TECHNICAL SPECIFICATION ISO / TS Nanotechnologies — Characterization of single-wall carbon nanotubes using. 2011.
41. Lee HS, Yun CH, Kim HM, Lee CJ. Persistence length of multiwalled carbon nanotubes with static bending. J. Phys. Chem. C. 2007;111:18882–7.
42. Shipkowski KA, Taylor AJ, Thompson EA, Glista-Baker EE, Sayers BC, Messenger ZJ, et al. An allergic lung microenvironment suppresses carbon nanotube-induced inflammasome activation via STAT6-dependent inhibition of caspase-1. PLoS One. 2015;10:6.
43. Sayers BC, Taylor AJ, Glista-Baker EE, Shipley-Phillips JK, Dackor RT, Edin ML, et al. Role of cyclooxygenase-2 in exacerbation of allergen-induced airway remodeling by multiwalled carbon nanotubes. Am. J. Respir. Cell Mol. Biol. 2013;49:525–35.

CHAPTER III

Susceptibility of p53 Heterozygous Mice to Granuloma Formation and Inducible Lymphoid Tissue after Chronic Pulmonary Exposure to Tangled or Rod-Like Multi-Walled Carbon Nanotubes

Katherine S. Duke[1], Elizabeth A. Ash[2], Mark D. Ihrie[1], Alexia J. Taylor[1], Elizabeth A. Thompson[1], Kelly A. Shipkowski[1], Mark F. Cesta[3], Debra A. Tokarz[4,5], Anne F. Hubbs[6,7], Robert C. Smart[1,4], Johnathan Hall[1], Linda M. Sargent[6,7], Dale W. Porter[6,7], and James C. Bonner[1,4*]

[1]*Toxicology Program, North Carolina State University, Raleigh, NC*

[2]*College of Veterinary Medicine, North Carolina State University, Raleigh, NC*

[3]*National Institute of Environmental Health Sciences, National Toxicology Program, Research Triangle Park, NC*

[4]*Center for Human Health and the Environment, North Carolina State University, Raleigh, NC,*

[5]*School of Veterinary Medicine, North Carolina State University, Raleigh, NC*

[6]*Center for Disease Control, Morgantown, WV*

[7]*National Institute for Occupational Safety and Health, Morgantown, WV,*

**Corresponding author*

Abstract

The production and use of multi-walled carbon nanotubes (MWCNTs) has increased substantially over the past decade. The fiber-like shape of MWCNTs are similar to asbestos and thus could pose similar health hazards and disease when inhaled, including pulmonary fibrosis and mesothelioma. Mice deficient in the tumor suppressor p53 are susceptible to pulmonary fibrosis and carcinogenesis. However, the chronic pathological effect of MWCNTs delivered directly to the lungs of p53 heterozygous ($p53^{+/-}$) mice has not been investigated. We hypothesized that exposure to tangled (t-) and rod-like (r-) MWCNTs by oropharyngeal aspiration followed by a 10 month recovery period would result in fibrogenic, immune and/or carcinogenic outcomes in the lungs of these mice. Wild type ($p53^{+/+}$) or $p53^{+/-}$ mice were exposed 1mg/kg/week MWCNTs over 4 weeks and sacrificed 11 months after the initial exposure to evaluate chronic pulmonary disease outcomes. Neither tMWCNTs nor rMWCNTs caused mesothelioma or lung cancer in $p53^{+/+}$ or $p53^{+/-}$ mice nor were there differences in pulmonary fibrosis between MWCNT-exposed mice of either genotype. However, increased granuloma size was observed in $p53^{+/-}$ mice compared to $p53^{+/+}$ mice exposed to either MWCNT type, and granulomas were significantly larger in rMWCNT exposed mice. However, there was no difference in the number of granulomas between genotypes after MWCNT exposure. Interestingly, MWCNT exposure increased inducible bronchus-associated lymphoid tissue (iBALT) formation and $p53^{+/-}$ mice had constitutively larger iBALT formations. The number of lymphoid aggregates significantly increased with rMWCNT exposure but not tMWCNT exposure. MWCNT exposure did not affect the proliferation of

immune cells within iBALT as measured by bromodeoxyuridine administration and immunohistochemistry, yet rMWCNTs but not tMWCNTs resulted in greater proliferation of granulomatous cells and epithelial cells at terminal bronchioles. These findings indicate that $p53^{+/-}$ mice are susceptible to MWCNT-induced formation of granulomas and tertiary lymphoid tissue, but not mesothelioma or fibrosis. However, we cannot rule out the possibility that $p53^{+/-}$ mice might be susceptible to these diseases upon exposure to other types of MWCNTs or under different exposure scenarios such as inhalation.

Introduction

The commercial use and incorporation of carbon nanotubes (CNTs) into products has been on the rise because of their unique optical, electrical and magnetic properties [1]; however, little is known about the risks of possible exposure to these materials. Multi-walled carbon nanotubes (MWCNTs) possess some characteristics that are similar to asbestos, a known human carcinogen. For example, MWCNTs have a fiber-like shape and contain trace metal catalysts (e.g., Fe, Ni, Co) from the manufacturing process [2]. Therefore, MWCNTs may pose similar toxicological risks to asbestos. Physicochemical characteristics of MWCNTs, including rigidity, can influence their carcinogenic potential. Therefore, both a tangled (t-) and rod-like (r-) MWCNTs were utilized for this study. Pulmonary disease states that are linked with asbestos exposure are fibrosis, granulomatous inflammation and mesothelioma. Studies with rodents show that MWCNTs delivered to the lungs by inhalation or oropharyngeal aspiration cause pulmonary fibrosis and granulomatous inflammation [3-6]. MWCNTs delivered to the lungs of mice by inhalation or oropharyngeal aspiration also reach the pleura and cause transient inflammatory lesions at the mesothelial lining or proliferation of mesothelial cells [7-9]. Recently, increased promotion of adenocarcinoma was reported in mice that were first exposed to tumor initiator methylcholanthrene (MCA) followed by exposure to MWCNTs [10]. This study also showed increased mesothelioma in mice co-exposed to MCA and MWCNTs and in one mouse from the MCA treatment group, but none resulting from MWCNT exposure alone [10].

The administration of fibers by intraperitoneal (i.p.) injection in mice is done as a surrogate to test mesothelioma development from the mesothelial cells on the diaphragm. Granulomatous formations have been shown to develop 7 days post i.p. exposure to either asbestos or MWCNTs [2]. At one month post exposure to MWCNTs or asbestos i.p. injections has resulted in chronic inflammation [11]. Administering an i.p. injection of asbestos (crocidolite or chrysotile) or an array of MWCNTs with varying lengths and properties has resulted in mesothelioma development in multiple studies. For example, mesothelioma formation has been shown at one year post i.p. exposure in tumor-susceptible heterozygous mice lacking one allele encoding the tumor suppressor p53, however no comparison was done to wild type p53 mice [12,13]. This induction of mesothelioma has been shown to be dose dependent and to develop MWCNT-induced mesothelioma faster than an equal dose of crocidolite asbestos [12-14]. This same development of mesothelioma has also been demonstrated in a wild type rat model after one and two years post MWCNT exposure [11,15]. Furthermore, an intrascrotal injection of MWCNTs has been shown to induce mesothelioma development in rats one year following exposure [16]. More recently, a study completed in Fisher 344 rats demonstrated the carcinogenic effect of a rod-like MWCNT inhalation exposure following 104 weeks, where rats developed bronchiolar-alveolar carcinoma and adenomas when treated with higher doses of rMWCNTs [17]. These studies provide evidence to support the development of MWCNT-induced mesothelioma and carcinomas in rodent models. However, they fail to address the pulmonary transport component of MWCNTs.

Genetic alterations also play a part in the development of pulmonary diseases like lung cancer, mesothelioma and fibrosis. The p53 tumor suppressor plays a key role in the regulation of the pulmonary carcinogenic and fibrotic processes by controlling cellular responses to stress like DNA repair, apoptosis and cell cycle progression [18]. Alteration of p53 function can lead to loss of function and proliferation control, potentially resulting in fibrosis or cancer. Disease states can further enhance the alteration of p53; for example, samples taken from patents with idiopathic pulmonary fibrosis (IPF) have high p53 mutation incidences [19,20]. Furthermore, the majority of IPF patients with overexpression of p53 have been found to have multiple point mutations in the *p53* gene [21]. Chronic exposure (12 weeks) of transformed human lung epithelial cells to single walled CNTs *in vitro* resulted in neoplastic marker development and resistance to apoptosis via decreased p53 activation [22]. Knock-down or knock-out *p53* studies have found an increase in tumor incidence and burden associated with decreased life span of the mice [23-25]. Knockdown or mutation of *p53* resulted in increased murine lung tumor cell motility not seen in p53 wild type or with rescued p53 expression *in vitro* [25]. Increased transcription of IL-6 and pro-inflammatory cytokines is initiated by activated p53 and function to regulate the immune response *in vivo* [26]. Therefore, p53 is a crucial regulator of cellular homeostasis, and alterations of this gene may result in the promotion of disease states in the lung. In this study, we used a p53 heterozygous/p53-deficient mouse model which systemically has only one functional p53 allele and is used as a susceptible model for p53 alterations and carcinogenesis [24].

As inhalation is the primary exposure route of particulate matter, work has been completed to address the translocation of MWCNTs to the pleural space, the anatomical location of mesothelioma. A recent study of whole body inhalation of a rod-like MWCNTs in male and female F344 rats for 104 weeks found bronchiolar-alveolar carcinomas and adenomas, but no pleural mesothelioma [17]. Studies conducted by exposing mice via inhalation or intrapulmonary spraying of MWCNTs were able to document sub-pleural translocation and induction of significant fibrosis at the pleural lining [7,9]. MWCNTs that reach the pleural space have a high retention and thus perturb sustained inflammation and progressive fibrosis at this location [27]. MWCNT size and shape have been determined as limiting factors of tube translocation and deposition long enough to cause mesothelial proliferation and fibrogenesis [28]. Studies have also shown the ability of inhaled asbestos can cause pleural injury through macrophage activation and recruitment [29]. Likewise, long MWCNTs induce macrophages to stimulate amplification of the inflammatory response in mesothelial cells [30]. Extra-pulmonary transport has also been demonstrated in a study showing MWCNTs present in the parietal pleura, respiratory musculature, liver, kidney, heart and brain of mice after one and 336 days post exposure [8]. No studies have been able to show long-term pulmonary MWCNT exposure to result in mesothelial tumors in the mouse lung.

Previous studies have demonstrated that MWCNTs do translocate to and stay in the pleura following pulmonary inhalation or intrapulmonary spray exposures. Inhalation of MWCNTs does result in pulmonary carcinomas, fibrosis and granulomas in the lungs of rodents. However

mesothelioma development from chronic MWCNT pulmonary exposure has never been demonstrated in mice. To address this we used a tumor susceptible mouse model that is heterozygous for the tumor suppressor p53, exposed them to tMWCNTs or rMWCNTs via oropharyngeal aspiration and assessed lung pathology at 11 months post initial exposure. In this study we sought to evaluate chronic effects of t- and r- MWCNTs; specifically the presence of fibrosis, granulomas, pre-neoplasia and mesothelioma.

Methods

Materials

tMWCNTs were purchased from Helix Material Solutions Inc., (Richardson, TX) and were characterized previously [7,31]. rMWCNTs (XNRI MWCNT-7 05072001 K28) were manufactured by Mitsui & Co (Tokyo, Japan) and are a kind gift from Dale Porter at NIOSH. These materials have been characterized for residual metal content, length, rigidity, and width and are previously reported [3]. MWCNTs were prepared in 0.1% Pluronic F-68 Solution (#P5556) from Sigma (Saint Louis, MO) diluted with DPBS.

Animal Care

Pathogen free wild type and $p53^{+/-}$ mice bred from a C57BL/6 background were housed in an IACUC approved and AALAC-accredited animal facility [32]. Animals were house 1-5 per cage and fed LabDiet 5001 rodent diet and water *ad libitum*. All animal procedures were approved by the NC State University IACUC.

Dosing of Mice

Wild type and $p53^{+/-}$ mice from the ages of 8-12 weeks were dosed once a week for 4 weeks with 1mg/kg tMWCNTs or rMWCNTs by oropharyngeal aspiration (OPA) under isoflurane anesthesia. A pictorial representation of the experimental design is shown in Appendix B.1A. These mice were divided into 4 groups with mixed genetic background, sex and treatment per group (Appendix B.2). The control wild type groups contained N=10, the wild type tMWCNT exposed group contained N=10, the wild type rMWCNT exposed group N=8, the $p53^{+/-}$ control group N=14, the $p53^{+/-}$ tMWCNT exposed group N=9, and the $p53^{+/-}$ rMWCNT exposed group N=8. Mice were exposed to tMWCNTs or rMWCNTs (1mg/kg) in 0.1% Pluronic surfactant solution (Sigma-Aldrich, Saint Louis, MO) by OPA under isoflurane anesthesia. Control mice received an equivalent dose of the vehicle 0.1% Pluronic surfactant solution.

Necropsy and Collection of Samples

Mice were euthanized utilizing pentobarbital fatal injection 11 months post initial exposure to tMWCNTs, rMWCNTs, or vehicle dose. Only two mice from the $p53^{+/-}$ rMWCNT group did not survive the entirety of the study, one died following the 4^{th} and final dose and the other was euthanized due to debilitating sarcoma development (Appendix B.2). Furthermore, two $p53^{+/-}$ mice, one exposed to tMWCNT and the other to rMWCNT, were excluded from analysis due to MWCNT independent development of adenocarcionoma and alveolar proteinosis respectively. Two 0.5mL aliquots of phosphate buffered saline (PBS) (Caisson Labs, Smithfield, UT) were lavaged to collect bronchoalveolar lavage fluid (BALF) for cytokine and

cellular content, the left lobe of the lung was inflated and fixed for histology with neutral buffered formalin (Azer Scientific, Morgantown, PA) and the right lobes were divided equally into RNAlater (Fisher Scientific, Waltham, MA) or a snap frozen cryotube for mRNA and protein analysis respectively. Small intestine, heart, spleen, and liver samples were also collected for histology; Heart, spleen and liver samples were stored in RNAlater for mRNA analysis as well.

Bromodeoxyuridine (BrdU) Immunohistochemical Staining (IHC)

To label cells actively synthesizing DNA, 100 mg/kg BrdU (Sigma, Saint Louis, MO) in PBS intraperitoneal injections were administered to mice one-hour prior to euthanasia. Lungs and small intestine (positive control) were sectioned using a 5µm microtome, mounted on a negatively charged slide and stained using a protocol described previously [3].

Granuloma Analysis

Masson's trichrome-stained lung sections containing granuloma formations were imaged with its respective scale bar. Each granuloma was characterized by the presence of MWCNT in the tissue with a reaction to them consisting of epithelioid macrophages and/or fibrosis. The presence of MWCNTs within alveolar macrophages (of which there were many) with no fibrosis or epithelioid macrophages was not considered a granuloma. Photoshop was utilized to measure granuloma area by using the ruler tool, under analysis, to measure and set a custom measurement scale by converting pixels to millimeters (µm). The lasso tool was used to

encompass the granuloma. A granuloma was defined as a mass of cells surrounding a foreign body and was bordered around the granuloma excluding the epithelial cells and contained to an easily defined border. Total lung area was measured by first configuring an image of the lung lobe by stitching using ImageJ with the Fuji plugin. The area of the lung was then measured using the lasso tool after being set to the dimensions of the image.

Lymphoid Tissue Quantification Analysis

Three lung sections from each mouse were cut, stained with bromodeoxyuridine (BrdU) and analyzed for inducible broncho-associated lymphoid tissue (iBALT) or ectopic lymphoid tissue (ELT) formations by scanning these sections for lymphoid structures. Each iBALT or ELT identified was imaged and the area was measured using the lasso tool in Photoshop from BrdU IHC stained slides. Total lung area was measured from BrdU IHC stained mouse lungs that were imaged at 40X and stitched together using the ImageJ plugin with unknown grid/collection [33]. The total lung area was quantitively measured in ImageJ as were all lymphoid aggregates of more than 10 mononuclear cells. These were put into categories of iBALT or ELT for further analysis. The number of iBALT or ELT lesions were also counted as were the total number of granulomas and the number containing BrdU positive cells. The number of granulomas adjacent to lymphoid tissue were also scored from the H&E stained sections.

Lymphoid Tissue Analysis

Three lung tissue blocks from each genotype and treatment group were selected and submitted for CD3 and CD45R/B220 IHC staining to assess lymphoid tissue structure.

Collagen Analysis

Snap frozen right lung lobes were weighed out to 10mg, homogenized and assayed for protein and soluble collagen. The Sircol soluble collagen kit (Biocolor, Carrickfergus, UK) was used to assay collagen content and Pierce BCA protein assay (Thermo Sicentific, Waltham, MA) was used to determine protein concentrations from each mouse lung. Area to perimeter ratio analysis was also conducted utilizing Masson's Trichrome stained mouse lungs by quantitively measuring collagen surrounding the airways as described previously [3].

Inflammatory Quantification

BALF was collected and 100µL was cytospun onto slides. Cells were stained with DiffQuik ® stain set (Dade Behring Inc, Newark, DE) and macrophages, eosinophils, neutrophils, and lymphocytes were counted to a total of 500 cells to determine respective abundance of each cell type per each animal. Total cell counts were completed by counting the total number of cells per three microscope views.

Cytokine Quantification

Cytokines (TGF-β1, Osteopontin, PDGF-BB) from BALF were measured by commercially available DuoSet enzyme linked immunosorbent assay (ELISA) kits (R & D Systems, Inc., Minneapolis, MN).

Transmission Electron Microscope (TEM)

As purchased tMWCNTs and rMWCNTs were imaged using a JEOL 2000FX scanning TEM and samples were prepared as described previously [34]. Paraffin blocks of lung tissue from mice exposed to either tMWCNTs or rMWCNTs were submitted to core TEM facilities for de-paraffinization and resin embedding.

Statistical Analysis

Statistical analysis was done by using GraphPad Prism software v. 5.0 (GraphPad Software, Inc., San Diego, CA). A one-way ANOVA with a Tukey post-hoc test was performed to determine statistical differences between treatments and genotypes.

Results

MWCNTs in the lung tissue of mice 11 months post-initial exposure. Transmission electron microscopy (TEM) of the bulk nanomaterials used in this study showed the contrasting rigidities between 'tangled' tMWCNTs and 'rod-like' rMWCNTs (Fig 3.1a,d). Singlet and agglomerated nanotube structures were present within pulmonary alveolar macrophages 11

months following the initial oropharyngeal aspiration exposure to either t- or r-MWCNTs (Fig 3.1b-c,e-f). tMWCNTs were present intracellularly and within close proximity to the Golgi apparatus and the nuclear membrane, but not within the nucleus. rMWCNTs were also present intracellularly 11 months following the initial exposure and are found in singlet and in condensed aggregates.

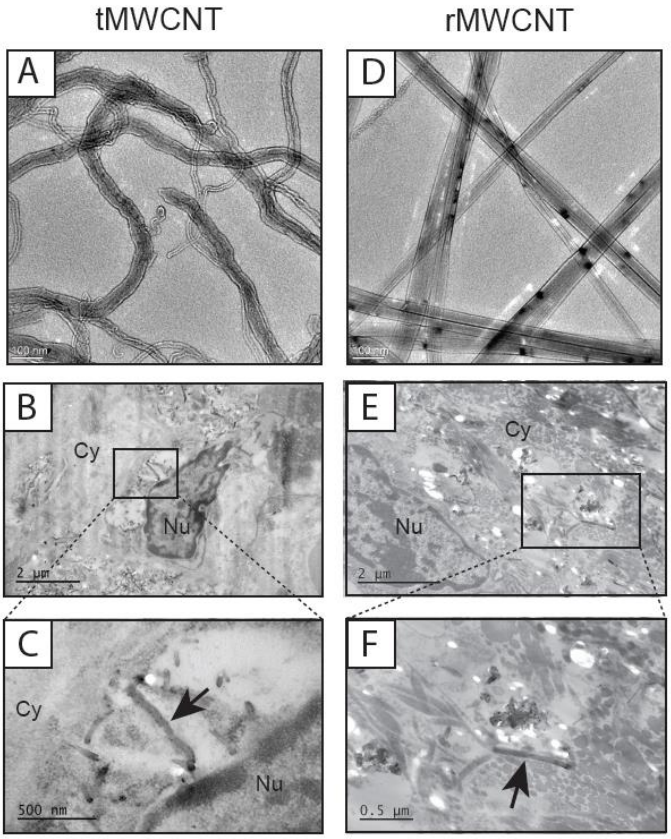

Figure 3.1. TEM images of t- and r-MWCNT. TEM images of A) tMWCNT and D) rMWCNT as purchased (scale bar equals 100 nm). TEM image of a $p53^{+/-}$ mouse lung 11 months following initial dose of B) tMWCNTs at 15000X and a $p53^{+/+}$ mouse 11 months following initial exposure to E) rMWCNTs at 20000X shown in respect to the nucleus (Nu) and cytoplasm (Cy). (scale bar equals 2 µm). Arrows in insets indicate the presence of intact singlet C) tMWCNT and F) rMWCNT within the cell imaged at 50000X (scale bar equals 500 nm).

Light microscopy of lung sections from mice showed aggregates of tMWCNTs or rMWCNTs present within granulomatous lesions as well as within singular alveolar macrophages (Fig 3.2a). Of note, the rMWCNTs, but not the tMWCNTs, protrude from macrophages indicating frustrated phagocytosis (Fig. 3.2b). Of interest, Charchot-Leyden like crystals were more prominent in the lungs of tMWCNT exposed mice compared to control or rMWCNT exposed lungs suggesting a prior eosinophilic inflammatory response (Fig. 3.2b arrows in tMWCNT panels). The Charchot-Leyden like crystals were only observed in mouse lungs exposed to tMWCNTs and generally associated with both macrophages and tMWCNTs. No crystals were observed in mouse lungs exposed to rMWCNTs, however macrophages in these lungs appeared to be larger than those found in the tMWCNT exposed lungs.

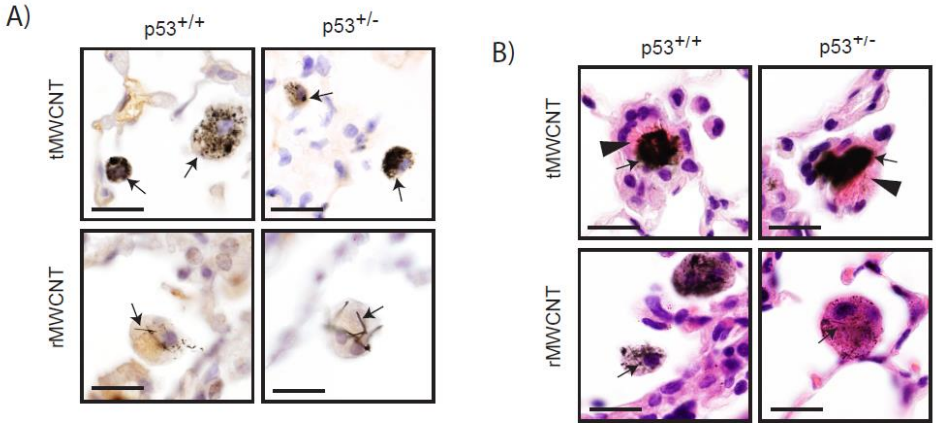

Figure 3.2. Pulmonary alveolar macrophages containing t- or r- MWCNT in the lungs of mice 11 months following initial exposure. A) Hematoxylin counterstained mouse lung tissue from both wild type and $p53^{+/-}$ with arrows indicating the enclosed foreign material within the alveolar macrophages in the lungs. Note: no positively stained nuclei are present, light counter staining allows for better visualization of foreign material. (scale bar equals 20 µm). B) Hematoxylin and Eosin (H&E) stained lung tissue from wild type and $p53^{+/-}$ mice with arrows indicating macrophages containing t- or r- MWCNT. Arrow heads indicate charchot-leyden like crystal presence (scale bars equal 20 µm).

Inflammatory cells and cytokines in BALF. Macrophages dominated the immune cells in the bronchoalveolar lavage fluid (BALF) from mouse lungs from both genotypes and treatment groups, and though there was a slight increase in neutrophil cell counts from the lungs of $p53^{+/+}$ mice with tMWCNT exposure, this increase was not significant (Appendix B.3). Analysis of the cellular makeup of the BALF revealed that, compared to total cell counts, tMWCNT or rMWCNT exposed mice contained similar total cell numbers as controls (data not shown). Differential cell counts conducted on the cytospins of the BALF revealed predominantly macrophage populated lungs with a slight, but not significant, increase in lymphocytes and neutrophils in lungs treated with rMWCNT (Appendix B.3). Cytokine levels of osteopontin (OPN), TGF-β1, and PDGF-BB in the BALF were not significantly increased by either MWCNT type or different between $p53^{+/+}$ and $p53^{+/-}$ mice at the chronic endpoint evaluated in this study (Appendix B.4; data not shown).

Granuloma formation in the lungs of $p53^{+/+}$ and $p53^{+/-}$ mice chronically exposed to tMWCNTs or rMWCNTs. Mice exposed to tMWCNTs had multiple, small granulomas mostly confined the distal terminal bronchioles and alveolar ducts in the centriacinar region near the alveolar-bronchiolar junctions (Fig. 3.3a). Granuloma size or frequency was not significantly different between $p53^{+/+}$ mice and $p53^{+/-}$ mice (Fig. 3.3b, c). The macrophages containing this material were enlarged with vacuolated cytoplasm, though the compacted agglomerates of tMWCNTs frequently obscured the macrophages. There were occasional multinucleated giant macrophages in the lungs of both $p53^{+/+}$ and $p53^{+/-}$ mice treated with either tMWCNTs or

rMWCNTs. The locations of the granulomas associated with rMWCNTs were similar to the location of the granulomas seen with tMWCNT exposed animals. The granulomas associated with rMWCNTs were larger with greater cellularity, containing numerous macrophages and often surrounded by lymphocytes (Fig. 3.3a). Rarely, there were rMWCNT-laden macrophages within the wall of an airway surrounded by increased numbers of fibroblasts (fibrosis). Foci of iBALT were observed near bronchioles with adjacent granulomas in the lungs of either $p53^{+/+}$ or $p53^{+/-}$ exposed to rMWCNTs but not tMWCNTs (Fig. 3.3d). rMWCNT exposure resulted in the formation of significantly larger granulomas with respect to lung area compared to tMWCNTs, and there was a trend for larger granulomas forming in $p53^{+/-}$ mice compared to $p53^{+/+}$ mice (Fig. 3.3b). Interestingly, the trend of increased granuloma area in $p53^{+/-}$ compared to $p53^{+/+}$ mouse lungs was mirrored by the number of granulomas resulting from the respective exposures, where more granulomas were observed in $p53^{+/-}$ mouse lungs compared to $p53^{+/+}$ mouse lungs treated with the same type of MWCNT (Fig 3.3b, c).

Effect of p53 deficiency and MWCNT treatment on lymphoid tissue formation. Bronchus-associated lymphoid tissue (BALT) is a tertiary lymphoid structure composed of lymphocytes (i.e. T- and B-cells) mainly along bifurcations of the upper airways and rarely forms in healthy human or mouse lungs. It can be induced (iBALT) during chronic inflammation, infection, or other disease states [35,36]. iBALT and non-bronchus-associated ectopic lymphoid tissue (ELT) structures were observed in mice from this study (Fig. 4c-d).

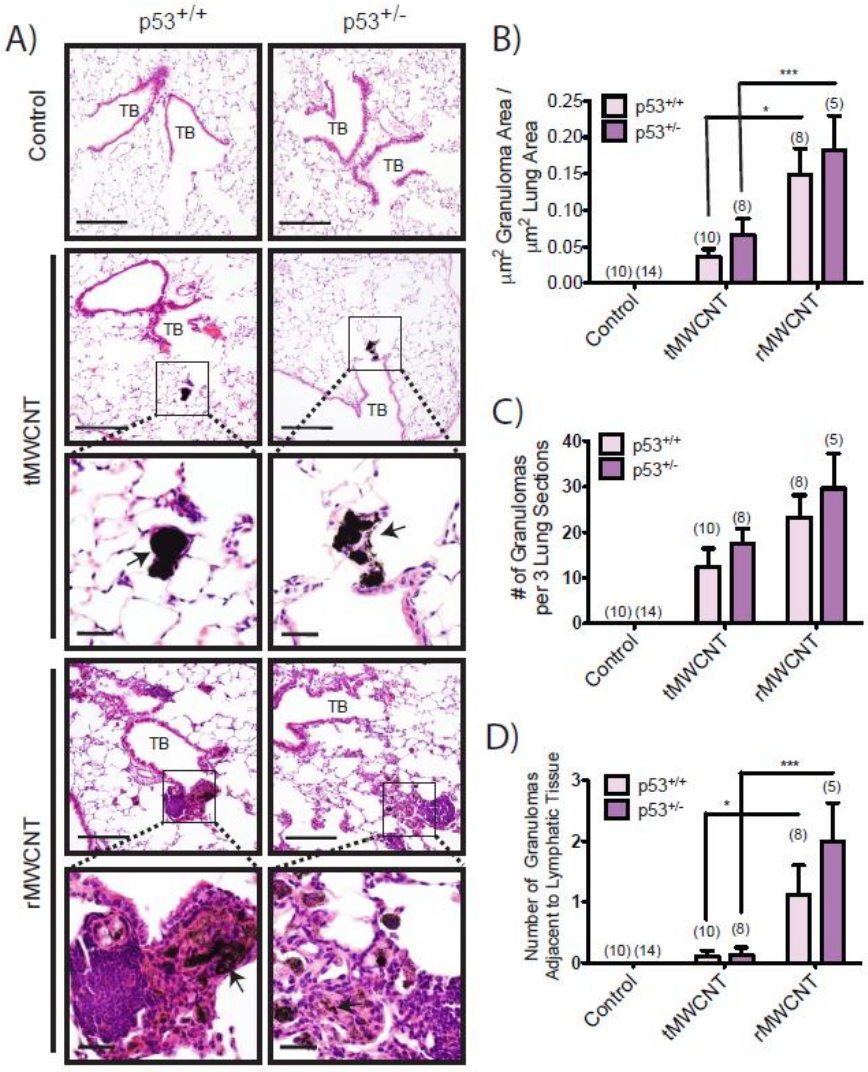

Figure 3.3. rMWCNT exposure results in significantly larger lung granuloma area and a higher association with lymphoid tissue compared to tMWCNT with a trend of larger formations in the lungs of p53$^{+/-}$ mice. A) H&E stained lung sections from wild type and p53$^{+/-}$ mouse lungs exposed to t- or r- MWCNTs near the terminal bronchioles (TB) of the lungs. Insets depict matured granuloma formations as indicated by arrows. (scale bar equal 200 μm, inset scale bars equal 50 μm). B) Average area of lung occupied by granuloma measured by quantitative morphometry (***p<0.001, *p<0.01 between tMWCNT and rMWCNT). C) Average number of granulomas per three lung sections per mouse. D) Average number of granulomas directly adjacent to lymphoid tissue per three lung sections per mouse (***p<0.001, *p<0.01 between tMWCNT and rMWCNT).

In the pluronic-exposed control animals, there was no foreign material consistent with either MWCNT. There were a few, scattered lymphocytes around blood vessels and airways. Nine animals had up to two (most have one) variably sized foci of iBALT. The iBALT and perivascular lymphocyte infiltration in tMWCNT exposed mice was similar to that seen in the control animals (Fig. 3.4a). The number of lymphoid aggregates significantly increased following rMWCNT but not tMWCNT exposure, but induction of lymphoid aggregates by rMWCNTs was not different between $p53^{+/+}$ and $p53^{+/-}$ genotypes (Fig 3.4a). However, the percent of the lung occupied by lymphoid tissue was significantly greater in control $p53^{+/-}$ mice compared to $p53^{+/+}$ but was not further increased by tMWCNT or rMWCNT treatment (Fig. 3.4b). Taken together this data suggests that while rMWCNTs increased the number of lymphoid aggregates, the lymphoid structures were significantly larger in $p53^{+/-}$ mouse lungs and this was primarily due to iBALT with minimal ELT (Fig 3.4 e-f). iBALT lesions contained proliferating cells as observed with bromodeoxyuridine (BrdU) immunohistostaining, yet the rate of proliferation was consistently around 10% for iBALT lesions in $p53^{+/+}$ and $p53^{+/-}$ mouse lungs with or without MWCNT treatment (data not shown). Overexpression of cytokines, like IL-6 are associated with inducing iBALT [37], yet we did not see increased levels of IL-6 mRNA from treated mouse lung samples (data not shown). We also did not observe increased transcription of chemokines CCL2, CXCL10 or CXCL9 at this time point (data not shown).

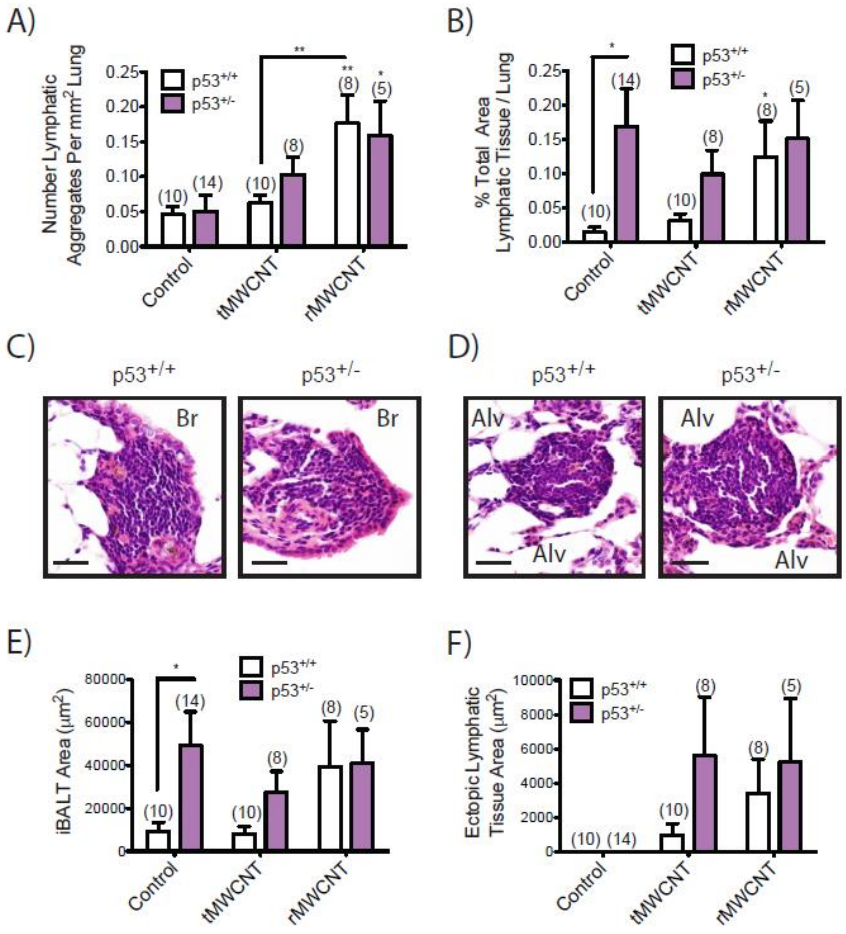

Figure 3.4. Formation of inducible lymphoid tissue in response to t- or r- MWCNT exposure. A) Average number of lymphoid aggregates as a function of square µm lung area (**p<0.01 between tMWCNT and rMWCNT, **p<0.01, *p<0.05 compared to control). B) Average percent of lung area occupied by lymphoid tissue measured by quantitative morphometry (*p<0.05 between genotypes, *p<0.05 compared to control). C) Inducible bronchioalveolar lymphoid tissue (iBALT) along the bronchial (Br) airway and D) ectopic lymphoid tissue (ELT) and surrounding alveolar (Alv) space of the lung of a wild type and p53+/- mouse lung (scale bars equal 50 µm). Lymphoid tissue area broken up into average area of E) iBALT and F) ectopic lymphoid tissue (*p<0.05 between genotypes).

Structural organization of inducible tertiary lymphoid tissue. To further characterize the lymphoid aggregates and granulomas, immunohistochemical (IHC) stains for T cells (CD3)

and B cells (CD45R/B220) were applied to serial lung sections. In all groups, T and B cells were evenly but thinly distributed throughout the parenchyma of the lungs. Development of both iBALT and ELT was evident. The immune cellular make-up of the inducible lymphoid tissues were classically ordered with a centrally-aggregated CD45R+ B cell population surrounded by more loosely distributed CD3+ T cells (Fig. 3.5). Despite non-specific staining of macrophage cytoplasm for CD3, close examination of the cellular morphology revealed that T and B cells were common in the periphery of both the r- and t-MWCNT-induced granulomas (data not shown). Prior studies of MWCNT exposure resulted in increased T cell and macrophage staining around granulomas as well [38,39]. Of note, there were significantly more granulomas adjacent to lymphoid tissue in the rMWCNT-exposed mouse lungs compared to the tMWCNT-exposed mouse lungs, and there was no notable difference between genotypes (Fig 3.3d).

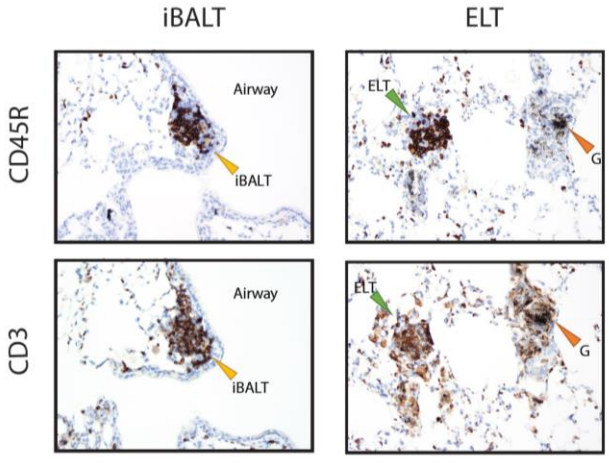

Figure 3.5. Structure of pulmonary inducible lymphoid tissue. Lung tissue from p53+/- mice exposed to rMWCNT for 11 months was immunohistochemically stained for the T cell marker CD3 and the B cell marker CD45R (B220) depicting a B cell germinal center with peripheral T cells in both the iBALT and ELT formations. For reference a granuloma (G) is indicated to show negative staining of cellular aggregates (scale bars equal 100 μm).

*rMWCNT exposure resulted in increased DNA synthesis in granuloma bearing cells***.** Lung tissue stained with BrdU was analyzed for brown-staining nuclei within granulomas that indicated proliferation (Fig. 3.6a arrows). Each granuloma counted was validated by the presence of foreign body nanomaterial (Fig. 3.6a arrow heads). About 25% of the $p53^{+/+}$ and 15% of the $p53^{+/-}$ rMWCNT-exposed lung granulomas included BrdU positive cells compared to only 5% of either $p53^{+/+}$ or $p53^{+/-}$ tMWCNT-exposed lung granulomas (Fig. 3.6b).

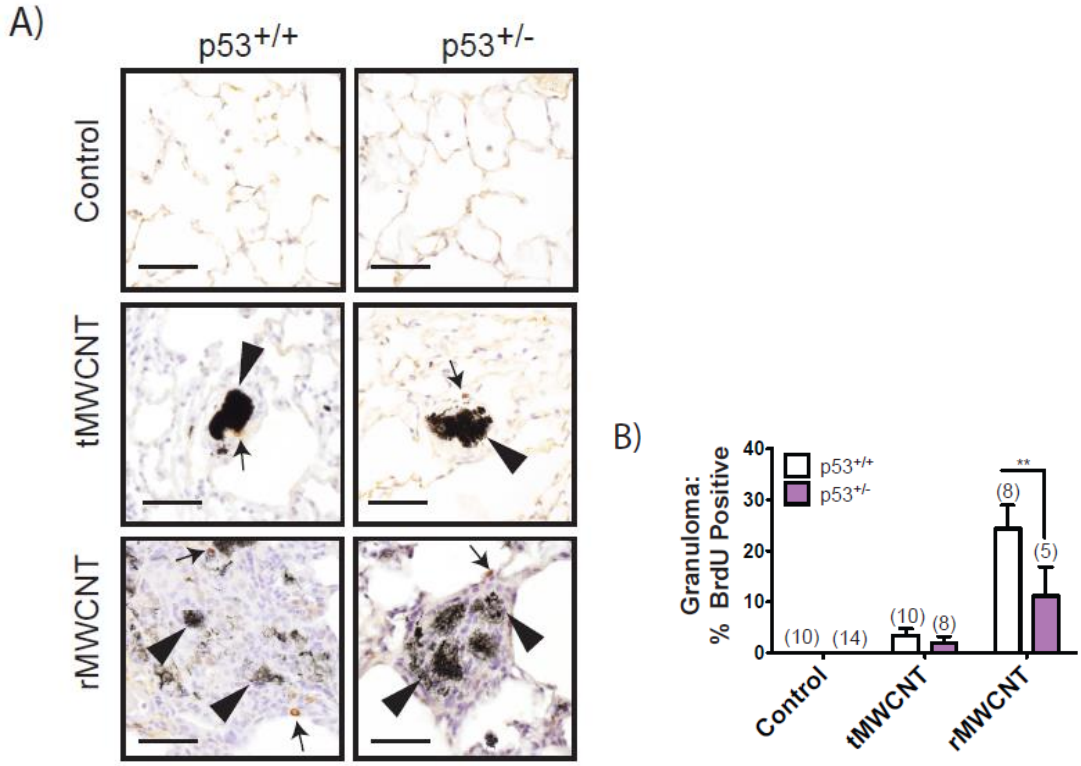

Figure 3.6. BrdU staining of granulomas show increased proliferation with rMWCNT exposure. A) Tissue from wild type and $p53^{+/-}$ mouse lungs exposed to t- or r- MWCNT for 11 months was stained with BrdU where a dark brown stain indicates DNA synthesis and is also indicated by arrows. Arrowheads indicate the nanomaterial within the granuloma (scale bars equal 50 µm). B) Average number of granulomas with BrdU positively stained nuclei (**p<0.01 between genotypes).

*Bronchiolar epithelial hyperplasia induced by MWCNT exposure***.** Some prominent bronchiolar epithelial hyperplastic lesions were observed in the lungs of either $p53^{+/+}$ or $p53^{+/-}$ mice exposed to rMWCNTs, but were observed rarely in tMWCNT-exposed mouse lungs (Fig. 3.7). Hyperplasia was defined by both the piling up of epithelial cells on the lateral surface of the basement membrane and BrdU positive staining of nuclei. There were also occasional aggregates of plasma cells near airways, which were not seen in the control or tMWCNT-exposed mouse lungs. In the animals exposed to rMWCNTs, there was markedly increased incidence of bronchiolar epithelial hyperplasia at terminal bronchioles and a few instances of alveolar hyperplasia. Interestingly, in times where hyperplasia is coupled with papillary hyperplasia and small fronds of epithelium projected into the lumen of the airway with simple connective tissue core present, this marks the transition towards neoplasia [40]. In a lung section from a rMWCNT-exposed $p53^{+/-}$ mouse a rare lesion of papillary hyperplasia was observed in the CD3 and CD45R lung sections, however it is important to note that there was no clear core present in the hyperplastic lesion to lend itself towards a neoplastic transition (Fig. 3.8). There was evident epithelial hyperplasia in rMWCNT-exposed mouse lungs, however there was no appreciable difference between genotypes observed.

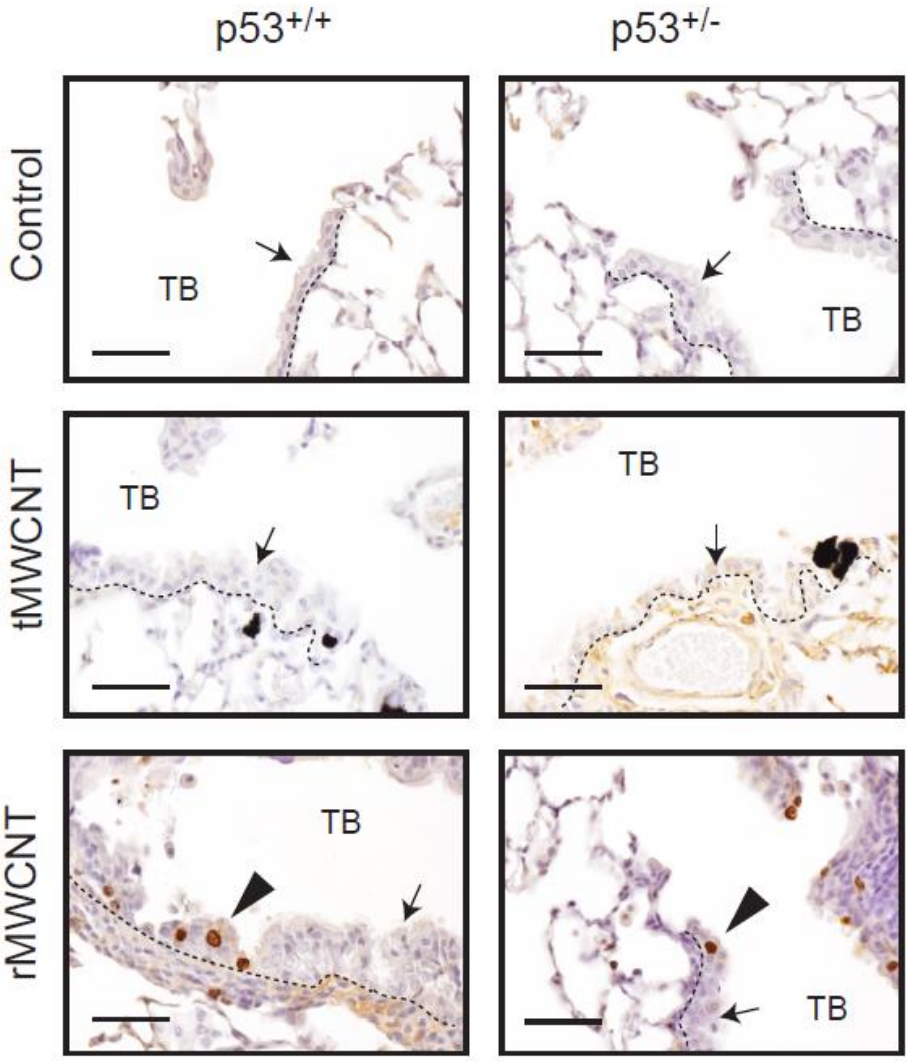

Figure 3.7. Alveolar hyperplasia. BrdU stained lung sections from control, tMWCNT and rMWCNT wild type and $p53^{+/-}$ mice were imaged to show the bronchial epithelium near a terminal bronchiole (TB) as indicated by arrows. Arrowheads indicate BrdU positive epithelial cells in the hyperplastic epithelium (scale bars equal 50 μm).

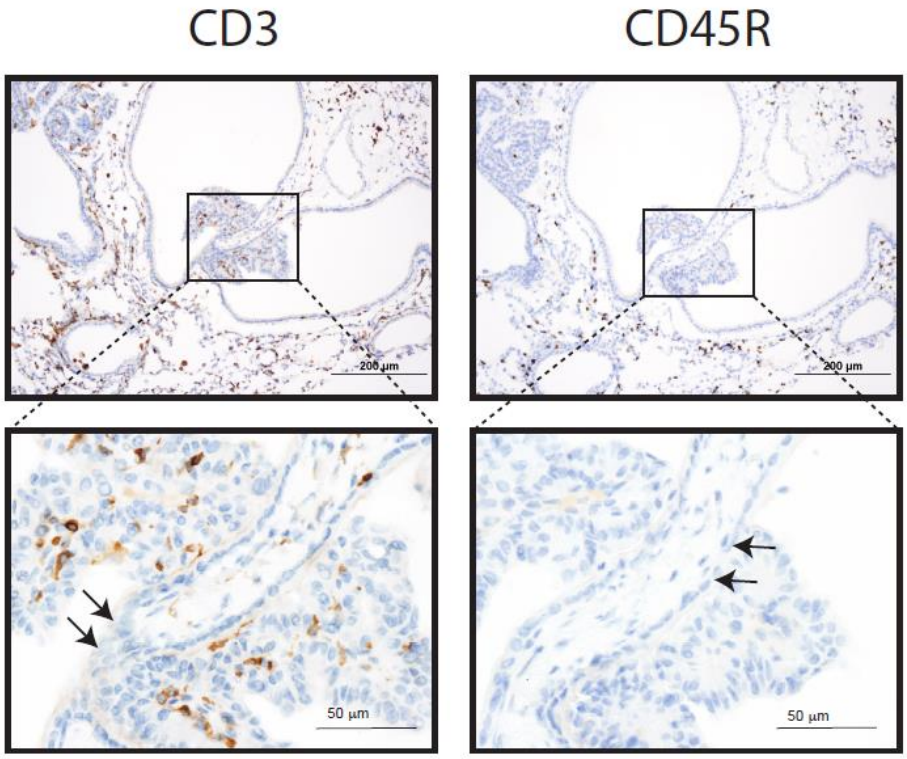

Figure 3.8. Papillary hyperplasia of the bronchiolar epithelium at alveolar duct bifurcation. Serial sections of papillary hyperplasia at the terminal bronchus in a $p53^{+/-}$ mouse following 11 months initial exposure to rMWCNTs. This rare pathology was captured in the IHC T cell marker CD3 and B cell marker CD45R sections. Arrows indicate location of papillary attachment to the bronchiole wall (scale bars equal 200 µm, inset scale bars equal 50 µm).

Pulmonary fibrosis after chronic exposure to tMWCNTs or rMWCNTs. To determine if significant collagen deposition occurred after exposure to either tMWCNTs or rMWCNTs, both a quantitative Sircol assay and semi-quantitative morphometric (area to perimeter ratio) analysis were performed. No observable difference was derived from the Masson's Trichrome stained lung sections in regards to collagen deposition (Fig. 3.9a). Total lung collagen levels remained consistent between genotypes regardless of exposure (Fig. 3.9b). Moreover, there

was no significant difference in area to perimeter ratio after quantitively measuring the collagen cuff around each airway in Masson's Trichrome stained lung sections (Appendix B.5).

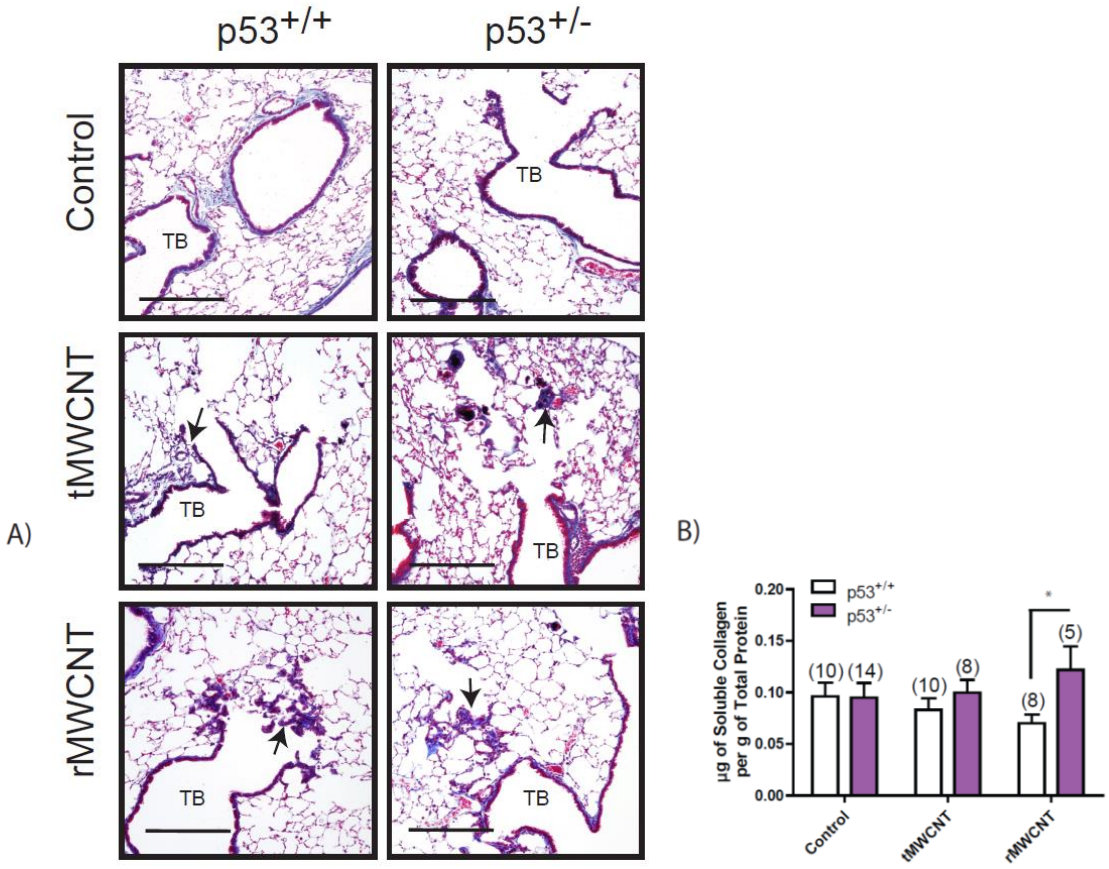

Figure 3.9. Collagen deposition 11 months following t- or r- MWCNT pulmonary exposure. A) Masson's Trichrome stained lung sections are imaged here depicting terminal bronchioles (TB). Arrows indicate fibrotic foci (scale bars equal 200 µm). B) Relative average µg of soluble collagen per mouse lung as determined using the Sircol assay (*$p<0.05$ between genotypes).

Discussion

The aim of this study was to examine the immunologic, fibroproliferative and neoplastic potential of two types of MWCNTs with different rigidities, tangled (t)MWCNTs and rigid (r)MWCNTs in the lungs of transgenic mice deficient in one allele encoding the tumor suppressor p53. A major goal was to determine if either tMWCNTs or rMWCNTs delivered to the lungs of $p53^{+/-}$ mice would cause mesothelioma 11 months after the initial oropharyngeal aspiration exposure. Because rMWCNTs have been classified as a Group 2B carcinogen by IARC [41], we postulated that rMWCNTs but not tMWCNTs would cause lung cancer or mesothelioma in $p53^{+/-}$ but not wild type $p53^{+/+}$ mice. While rMWCNTs caused focal bronchiolar epithelial hyperplasia and one observed incident of intraluminal airway papillary hyperplasia, no lung tumors or mesothelioma were observed in $p53^{+/-}$ mice. Moreover, we did not observe differences in pulmonary fibrosis between $p53^{+/+}$ and $p53^{+/-}$ mice exposed to either tMWCNTs or rMWCNTs. However, rMWCNTs caused more robust granuloma formation compared to tMWCNTs and granuloma size was exaggerated in $p53^{+/-}$ mice. In addition, we observed that rMWCNTs, but not tMWCNTs, stimulated iBALT formation in $p53^{+/+}$ mice and iBALT formation was spontaneously generated in the lungs of $p53^{+/-}$ mice. Also, $p53^{+/-}$ mice exhibited significantly larger lung area obscured by lymphoid aggregates compared to $p53^{+/+}$ mice and these tertiary lymphoid aggregates were more populated in lungs following tMWCNT exposure and even further following rMWCNT exposure. Of key interest to the study, there was a higher incidence of epithelial cell proliferation and hyperplasia following rMWCNT exposure compared to control or tMWCNT exposed mouse lungs. Overall, our

findings indicate that p53 plays a role in immunologic response to MWCNTs and highlights the importance of nanotube rigidity in the immune response to MWCNTs.

Our study revealed a role for p53 in regulating granuloma formation after exposure to MWCNTs. Notably, greater granulomas resulted from rMWCNTs, and $p53^{+/-}$ mice developed larger granulomas following exposure to either MWCNT type compared to $p53^{+/+}$. Granulomas are composed of epithelioid macrophages, multi-nucleated macrophages and lymphocytes (mainly T cells) and form in response to a foreign body or an immune reaction. Mature foreign body granulomas have fibrous tissue encapsulating and isolating the foreign material. The observation of increased BrdU positive cells in granulomas of rMWCNT exposed mouse lungs at the chronic 11 month post initial exposure time point evaluated was surprising. The proliferating cells could be monocytic or lymphocytic in origin; either cell type synthesizing DNA is indicative of chronic rMWCNT-induced cellular proliferative stimuli within the granuloma and may be a result of continual injury and/or immune stimulation. Infiltrating monocytes may be the main source of macrophage replacement, however it is unknown how often alveolar macrophages proliferate to sustain a resident population in the lung. Studies have indicated that alveolar macrophages have a half-life of over one-month and have been observed to have a stable unreplaced population after 8 months [42]. Resident alveolar macrophages self-replenish their population when the need arises [43]. The incidence of BrdU positive macrophages in granulomatous formations resulting from rMWCNT and not from tMWCNT exposure lends itself to suggest that, after 11 months post-initial exposure, the

rMWCNTs continue to elicit cellular damage and thus the need for macrophage replacement. We observed that T cells were integrated into the granulomas induced by rMWCNTs (Fig. 5) and this is indicative of previously described immune granulomas [44]. Previous studies have determined immune granulomas are positive for CD205 and absent in foreign body granulomas [44]. However, the observation of T cell infiltration within the rMWCNT foreign body granulomas and the frequency and proximity of tertiary lymphoid tissue to the t- or r-MWCNT-induced granulomas suggest that these foreign body granulomas are coupled with immune granulomas.

The development of tertiary lymphoid tissues (iBALT and ELT) were a result of p53 deficiency or rMWCNT exposure in the lung. These tertiary lymphoid organs form in response to chronic inflammation, infection or other disease states when the lungs are highly permissive to the formation of ELT or BALT [36,45]. The early development of this tissue is driven by IL-1α, and IL-1-receptor deficient mice fail to develop iBALT following exposure to either aluminum salts, silica, or viruses [46,47]. Interestingly, silica induced lymphoid neogenesis can result in the development of an induced autoimmune phenotype [48]. The lymphoid neogenesis exhibited in our study contained cellular elements organized into *de novo* formations of a B cell follicle surrounded by T cells [45]. Additionally, increased iBALT in the lung is observed in mice as they age, and is further exacerbated by cigarette smoke [49]. Previous examination of rMWCNT pulmonary exposure found that exposure resulted in the dilation of pulmonary lymphatics after 56 days as measured by indirect immunofluorescence of podoplanin, a

lymphatic endothelial marker [50]. Prior studies have observed MWCNTs deposited into BALT and have shown that these lymphoid tissues are a slower clearance method compared the mucociliary escalator in a rat model [51]. Also, the presence of MWCNTs in BALT increased over time and the lymphatic system, though slow, facilitates the clearance of CNTs from alveolar interstitium [51]. Interestingly, to date, there is no current literature available on p53 regulation or involvement of inducible lymphoid tissue development; however, p53 has been implicated in the immune response during development. For example, the co-regulatory function of NFκB and p53 increases IL-6 in primary human monocytes and macrophages and induce neutrophil chemoattractant chemokines [26]. In addition, p53 null or inhibited mice were able to clear the infection quickly compared to wild type mice upon pulmonary infection with gram negative bacteria [52]. This clearance is due to increased phagocytosis, degranulation and NOX-dependent oxidant generation by neutrophils, yet these mice also exhibited a high mortality following infection and clearance due to aggravated lung injury [52]. It is possible that the $p53^{+/-}$ mice with increased iBALT formation in the present study exhibited a heightened inflammatory response from t- or r-MWCNT exposure and this resulted in the increased granuloma sizes and number and size of induced lymphoid tissue neogenesis.

One of the pressing issues in this study was to determine if $p53^{+/-}$ mice, a mouse model that is susceptible to tumor development, would develop mesothelioma after pulmonary exposure to MWCNTs. Previous studies performed i.p. injections of $p53^{+/-}$ mice with asbestos or rMWCNTs and showed more rapid development of mesotheliomas compared to wild type [12,13].

We found that oropharyngeal aspiration of a total dose of 4mg/kg over 4 weeks did not result in mesothelioma or carcinogenic development 11 months following the initial dose in either the wild type nor $p53^{+/-}$ mice. However, to date, no study has shown mesothelioma development in rodent models following direct pulmonary exposure to asbestos, a known cause of mesothelioma in humans [17,29,53,54]. Therefore, it is not entirely surprising that MWCNTs did not cause mesothelioma in $p53^{+/-}$ mice and overall this may indicate that mice (even transgenic strains that are susceptible to tumor promotion) are poor models for assessing the carcinogenic potential of MWCNTs. We did observe epithelial hyperplasia resulting from rMWCNT pulmonary exposure and this concurs with previous studies of rodents exposed to this nanomaterial which have developed epithelial hyperplasia, adenocarcinoma and alveolar hyperplasia in the lung [10,17]. Comparisons between rodent models have been utilized as well where i.p. injection of C57BL/6 mice and Wistar rats with rMWCNTs or crocidolite asbestos resulted in mesothelioma coupled with an accumulation of monocytic cells that suppress polyclonal activation of lymphocytes 12 months following exposure [55]. The immune and proliferative effects of asbestos versus MWCNTs need to be carefully compared when determining potential pulmonary toxicity of such materials. The rodent model is limited by a short life span, and a latency period of over 15 years is common for asbestos-induced mesothelioma or fibrosis [56,57]. This truncated life span may be a reason that mesothelioma has not been observed *in vivo* to date in rodents from emerging fiber-like nanomaterials such as MWCNTs or known agents like asbestos that cause mesothelioma in humans decades after exposure.

To address the potential of mesothelial and epithelial cells to be transformed in the presence of MWCNTs, *in vitro* studies have exposed cell cultures to the nanomaterials continuously at each passage to address the chronic exposure response. Lohcharonkal's group exposed human mesothelial cells continuously to MWCNTs for 4 months, after which they documented increase proliferation and aggressive invasive behavior [58]. Other studies exposed epithelial cells *in vitro* for 2 or 6 months continuously to MWCNTs and showed that these epithelial cells had undergone malignant transformation and acquisition of neoplastic markers [22,59]. Little work has been done to bridge these *in vitro* studies with what may actually be going on in the pleural space to produce malignant cells.

Conclusions

The chronic presence of tangled (t-) or rod-like (r-) MWCNTs in the lungs of wild type or heterozygous $p53^{+/-}$ mice does not induce mesothelioma or lung tumors. However, $p53^{+/-}$ mice are susceptible to larger granuloma formation and the formation of tertiary lymphoid structures. These lymphoid structures are induced by rMWCNTs but not tMWCNTs in $p53^{+/+}$ mice. Moreover, rMWCNTs but not tMWCNTs induce hyperplasia in epithelial cells at terminal bronchioles in the lungs. Further studies should continue to address the differing physicochemical properties of MWCNTs along with genetic susceptibility in order to assess their potential to be carcinogenic, fibrogenic, or immunogenic.

Acknowledgments

We are grateful for the help of Dr. Erinn Needham-Dandley for her expertise in TEM imaging of the as purchased MWCNTs.

References

1. Kuick Research. Global Carbon Nanotubes Market and Patent Insight 2023; 2017.
2. Poland, C. a; Duffin, R.; Kinloch, I.; Maynard, A.; Wallace, W. a H.; Seaton, A.; Stone, V.; Brown, S.; Macnee, W.; Donaldson, K. Carbon Nanotubes Introduced into the Abdominal Cavity of Mice Show Asbestos-like Pathogenicity in a Pilot Study. Nat. Nanotechnol. 2008, 3, 423–428.
3. Duke, K. S.; Taylor-Just, A. J.; Ihrie, M. D.; Shipkowski, K. A.; Thompson, E. A.; Dandley, E. C.; Parsons, G. N.; Bonner, J. C. STAT1-Dependent and -Independent Pulmonary Allergic and Fibrogenic Responses in Mice after Exposure to Tangled versus Rod-like Multi-Walled Carbon Nanotubes. Part. Fibre Toxicol. 2017, 14, 26.
4. Chang, C.-C.; Tsai, M.-L.; Huang, H.-C.; Chen, C.-Y.; Dai, S.-X. Epithelial-Mesenchymal Transition Contributes to SWCNT-Induced Pulmonary Fibrosis. Nanotoxicology 2012, 6, 600–610.
5. Dong, J.; Porter, D. W.; Batteli, L. A.; Wolfarth, M. G.; Richardson, D. L.; Ma, Q. Pathologic and Molecular Profiling of Rapid - Onset Fibrosis and Inflammation Induced by Multi - Walled Carbon Nanotubes. Arch. Toxicol. 2014, 89, 621–633.
6. Shvedova, A. A.; Kisin, E.; Murray, A. R.; Johnson, V. J.; Gorelik, O.; Arepalli, S.; Hubbs, A. F.; Mercer, R. R.; Keohavong, P.; Sussman, N.; et al. Inhalation vs. Aspiration of Single-Walled Carbon Nanotubes in C57BL/6 Mice: Inflammation, Fibrosis, Oxidative Stress, and Mutagenesis. Am. J. Physiol. Lung Cell. Mol. Physiol. 2008, 295, L552-65.
7. Ryman-rasmussen, J. P.; Cesta, M. F.; Brody, A. R.; Shipley-, J. K.; Everitt, J.; Tewksbury, E. W.; Moss, O. R.; Wong, B. a; Darol, E.; Andersen, M. E.; et al. Inhaled Carbon Nanotubes Reach the Sub-Pleural Tissue in Mice. Nat. Nanotechnol. 2009, 4, 747–751.
8. Mercer, R. R.; Scabilloni, J. F.; Hubbs, A. F.; Wang, L.; Battelli, L. a; McKinney, W.; Castranova, V.; Porter, D. W. Extrapulmonary Transport of MWCNT Following Inhalation Exposure. Part. Fibre Toxicol. 2013, 10, 13.
9. Xu, J.; Futakuchi, M.; Shimizu, H.; Alexander, D. B.; Yanagihara, K.; Fukamachi, K.; Suzui, M.; Kanno, J.; Hirose, A.; Ogata, A.; et al. Multi-Walled Carbon Nanotubes Translocate into the Pleural Cavity and Induce Visceral Mesothelial Proliferation in Rats. Cancer Sci. 2012, 103, 2045–2050.
10. Sargent, L. M.; Porter, D. W.; Staska, L. M.; Hubbs, A. F.; Lowry, D. T.; Battelli, L.; Siegrist, K. J.; Kashon, M. L.; Mercer, R. R.; Bauer, A. K.; et al. Promotion of Lung

Adenocarcinoma Following Inhalation Exposure to Multi-Walled Carbon Nanotubes. Part. Fibre Toxicol. 2014, 11, 3.
11. Nagai, H.; Okazaki, Y.; Chew, S.; Misawa, N.; Yamashita, Y.; Akatsuka, S.; Ishihara, T.; Yamashita, K.; Yoshikawa, Y.; Yasui, H.; et al. Diameter and Rigidity of Multiwalled Carbon Nanotubes Are Critical Factors in Mesothelial Injury and Carcinogenesis. 2011.
12. Takagi, A.; Hirose, A.; Nishimura, T.; Fukumori, N.; Ogata, A.; Ohashi, N.; Kitajima, S.; Kanno, J. Induction of Mesothelioma in p53+/- Mouse by Intraperitoneal Application of Multi-Wall Carbon Nanotube. J. Toxicol. Sci. 2008, 33, 105–116.
13. Takagi, A.; Hirose, A.; Futakuchi, M.; Tsuda, H.; Kanno, J. Dose-Dependent Mesothelioma Induction by Intraperitoneal Administration of Multi-Wall Carbon Nanotubes in p53 Heterozygous Mice. Cancer Sci. 2012, 103, 1440–1444.
14. Kodama, M.; Tateno, H.; Tasak, S.; Soejima, K.; Asano, K.; Hayashi, Y. An Autopsied Case of Primary Malignant Pericardial Mesothelioma Diagnosed Antemortally. J. Japanese Respir. Soc. 2011, 49, 964–969.
15. Rittinghausen, S.; Hackbarth, A.; Creutzenberg, O.; Ernst, H.; Heinrich, U.; Leonhardt, A.; Schaudien, D. The Carcinogenic Effect of Various Multi-Walled Carbon Nanotubes (MWCNTs) after Intraperitoneal Injection in Rats. Part. Fibre Toxicol. 2014, 11, 59.
16. Sakamoto, Y.; Nakae, D.; Fukumori, N.; Tayama, K.; Maekawa, A.; Imai, K.; Hirose, A.; Nishimura, T.; Ohashi, N.; Ogata, A. Induction of Mesothelioma by a Single Intrascrotal Administration of Multi-Wall Carbon Nanotube in Intact Male Fischer 344 Rats. J. Toxicol. Sci. 2009, 34, 65–76.
17. Kasai, T.; Umeda, Y.; Ohnishi, M.; Mine, T.; Kondo, H.; Takeuchi, T. Lung Carcinogenicity of Inhaled Multi- Walled Carbon Nanotube in Rats. Part. Fibre Toxicol. 2016, 1–19.
18. Dai, C.; Gu, W. P53 Post-Translational Modification: Deregulated in Tumorigenesis. Trends Mol. Med. 2010, 16, 528–536.
19. Takahashi, T.; Munakata, M.; Ohtsuka, Y.; Nisihara, H.; Nasuhara, Y.; Kamachi-Satoh, A.; Dosaka-Akita, H.; Homma, Y.; Kawakami, Y. Expression and Alteration of Ras and p53 Proteins in Patients with Lung Carcinoma Accompanied by Idiopathic Pulmonary Fibrosis. Cancer 2002, 95, 624–633.
20. Vancheri, C.; Failla, M.; Crimi, N.; Raghu, G. Idiopathic Pulmonary Fibrosis: A Disease with Similarities and Links to Cancer Biology. Eur. Respir. J. 2010, 35, 496–504.
21. Hojo, S.; Fujita, J.; Yamadori, I.; Kamei, T.; Yoshinouchi, T.; Ohtsuki, Y.; Okada, H.; Bandoh, S.; Yamaji, Y.; Takahara, J.; et al. Heterogeneous Point Mutations of the p53 Gene in Pulmonary Fibrosis. Eur. Respir. J. 1998, 12, 1404–1408.
22. Wang, L.; Luanpitpong, S.; Castranova, V.; Tse, W.; Lu, Y.; Pongrakhananon, V.; Rojanasakul, Y. Carbon Nanotubes Induce Malignant Transformation and Tumorgenesis of Human Lung Epithelial Cells. Nano Lett. 2011, 11, 2796–2803.
23. Wang, Y.; Zhang, Z.; Lubet, R. a; You, M. A Mouse Model for Tumor Progression of Lung Cancer in Ras and p53 Transgenic Mice. Oncogene 2006, 25, 1277–1280.
24. Wang, Y.; Suh, Y. A.; Fuller, M. Y.; Jackson, J. G.; Xiong, S.; Terzian, T.; Quintás-Cardama, A.; Bankson, J. A.; El-Naggar, A. K.; Lozano, G. Restoring Expression of Wild-

Type p53 Suppresses Tumor Growth but Does Not Cause Tumor Regression in Mice with a p53 Missense Mutation. J. Clin. Invest. 2011, 121, 893–904.
25. Xu, B.; Guenther, J. F.; Pociask, D. a.; Wang, Y.; Kolls, J. K.; You, Z.; Chandrasekar, B.; Shan, B.; Sullivan, D. E.; Morris, G. F. Promotion of Lung Tumor Growth by Interleukin-17. AJP Lung Cell. Mol. Physiol. 2014, 307, L497–L508.
26. Lowe, J. M.; Menendez, D.; Bushel, P. R.; Shatz, M.; Kirk, E. L.; Troester, M. A.; Garantziotis, S.; Fessler, M. B.; Resnick, M. A. p53 and NF-κB Coregulate Proinflammatory Gene Responses in Human Macrophages. Cancer Res. 2014, 74, 2182–2192.
27. Murphy, F. a.; Poland, C. a.; Duffin, R.; Al-Jamal, K. T.; Ali-Boucetta, H.; Nunes, A.; Byrne, F.; Prina-Mello, A.; Volkov, Y.; Li, S.; et al. Length-Dependent Retention of Carbon Nanotubes in the Pleural Space of Mice Initiates Sustained Inflammation and Progressive Fibrosis on the Parietal Pleura. Am. J. Pathol. 2011, 178, 2587–2600.
28. Xu, J.; Alexander, D. B.; Futakuchi, M.; Numano, T.; Fukamachi, K.; Suzui, M.; Omori, T.; Kanno, J.; Hirose, A.; Tsuda, H. Size- and Shape-Dependent Pleural Translocation, Deposition, Fibrogenesis, and Mesothelial Proliferation by Multiwalled Carbon Nanotubes. Cancer Sci. 2014, 105, 763–769.
29. Choe, N.; Tanaka, S.; Xia, W.; Hemenway, D. R.; Roggli, V. L.; Kagan, E. Pleural Macrophage Recruitment and Activation in Asbestos-Induced Pleural Injury. Environ. Health Perspect. 1997, 105 Suppl, 1257–1260.
30. Murphy, F. a; Schinwald, A.; Poland, C. a; Donaldson, K. The Mechanism of Pleural Inflammation by Long Carbon Nanotubes: Interaction of Long Fibres with Macrophages Stimulates Them to Amplify pro-Inflammatory Responses in Mesothelial Cells. Part. Fibre Toxicol. 2012, 9, 8.
31. Ryman-Rasmussen, J. P.; Tewksbury, E. W.; Moss, O. R.; Cesta, M. F.; Wong, B. A.; Bonner, J. C. Inhaled Multiwalled Carbon Nanotubes Potentiate Airway Fibrosis in Murine Allergic Asthma. Am. J. Respir. Cell Mol. Biol. 2009, 40, 349–358.
32. Yoon, K.; Zhu, S.; Ewing, S. J.; Smart, R. C. Decreased Survival of C/EBPbeta-Deficient Keratinocytes Is due to Aberrant Regulation of p53 Levels and Function. Oncogene 2007, 26, 360–367.
33. Preibisch, S.; Saalfeld, S.; Tomancak, P. Globally Optimal Stitching of Tiled 3D Microscopic Image Acquisitions. Bioinformatics 2009, 25, 1463–1465.
34. Dandley, E. C.; Taylor, A. J.; Duke, K. S.; Ihrie, M. D.; Shipkowski, K. A.; Parsons, G. N.; Bonner, J. C. Atomic Layer Deposition Coating of Carbon Nanotubes with Zinc Oxide Causes Acute Phase Immune Responses in Human Monocytes in Vitro and in Mice after Pulmonary Exposure. Part. Fibre Toxicol. 2016, 13, 29.
35. Sminia, T.; van der Brugge-Gamelkoorn, G. J.; Jeurissen, S. H. Structure and Function of Bronchus-Associated Lymphoid Tissue (BALT). Crit. Rev. Immunol. 1989, 9, 119–150.
36. Foo, S. Y.; Phipps, S. Regulation of Inducible BALT Formation and Contribution to Immunity and Pathology. Mucosal Immunol. 2010, 3, 537–544.
37. Goya, S.; Matsuoka, H.; Mori, M.; Morishita, H.; Kida, H.; Kobashi, Y.; Kato, T.; Taguchi, Y.; Osaki, T.; Tachibana, I.; et al. Sustained Interleukin-6 Signalling Leads to the Development of Lymphoid Organ-like Structures in the Lung. J. Pathol. 2003, 200, 82–87.

38. Huizar, I.; Malur, A.; Patel, J.; Mcpeek, M.; Dobbs, L.; Wingard, C.; Barna, B. P.; Thomassen, M. J. The Role of PPAR γ in Carbon Nanotube-Elicited Granulomatous Lung Inflammation. Respir. Res. 2013, 14, 1.
39. Huizar, I.; Malur, A.; Midgette, Y. A.; Kukoly, C.; Chen, P.; Ke, P. C.; Podila, R.; Rao, A. M.; Wingard, C. J.; Dobbs, L.; et al. Novel Murine Model of Chronic Granulomatous Lung Inflammation Elicited by Carbon Nanotubes. Am. J. Respir. Cell Mol. Biol. 2011, 45, 858–866.
40. Renne, R.; Brix, A.; Harkema, J.; Herbert, R.; Kittel, B.; Lewis, D.; March, T.; Nagano, K.; Pino, M.; Rittinghausen, S.; et al. Proliferative and Nonproliferative Lesions of the Rat and Mouse Respiratory Tract. Toxicol. Pathol. 2009, 37, 5S–73S.
41. International Agency for Research on Cancer; IARC Working Group on the Evaluation of Carcinogenic Risks to Humans. Some Nanomaterials and Some Fibres; 2017.
42. Murphy, J.; Summer, R.; Wilson, A. A.; Kotton, D. N.; Fine, A. The Prolonged Life-Span of Alveolar Macrophages. Am. J. Respir. Cell Mol. Biol. 2008, 38, 380–385.
43. Hashimoto, D.; Chow, A.; Noizat, C.; Teo, P.; Beasley, M. B.; Leboeuf, M.; Becker, C. D.; See, P.; Price, J.; Lucas, D.; et al. Tissue-Resident Macrophages Self-Maintain Locally throughout Adult Life with Minimal Contribution from Circulating Monocytes. Immunity 2013, 38, 792–804.
44. Ohtani, H. Granuloma Cells in Chronic Inflammation Express CD205 (DEC205) Antigen and Harbor Proliferating T Lymphocytes: Similarity to Antigen-Presenting Cells. Pathol. Int. 2013, 63, 85–93.
45. Aloisi, F.; Pujol-Borrell, R. Lymphoid Neogenesis in Chronic Inflammatory Diseases. Nat. Rev. Immunol. 2006, 6, 205–217.
46. Kuroda, E.; Ozasa, K.; Temizoz, B.; Ohata, K.; Koo, C. X.; Kanuma, T.; Kusakabe, T.; Kobari, S.; Horie, M.; Morimoto, Y.; et al. Inhaled Fine Particles Induce Alveolar Macrophage Death and Interleukin-1α Release to Promote Inducible Bronchus-Associated Lymphoid Tissue Formation. Immunity 2016, 45, 1299–1310.
47. Neyt, K.; GeurtsvanKessel, C. H.; Deswarte, K.; Hammad, H.; Lambrecht, B. N. Early IL-1 Signaling Promotes iBALT Induction after Influenza Virus Infection. Front. Immunol. 2016, 7, 312.
48. Bates, M. A.; Brandenberger, C.; Langohr, I. Silica Triggers Inflammation and Ectopic Lymphoid Neogenesis in the Lungs in Parallel with Accelerated Onset of Systemic Autoimmunity and Glomerulonephritis in the Lupus-Prone NZBWF1 Mouse. 2015, 1–25.
49. John-Schuster, G.; Günter, S.; Hager, K.; Conlon, T. M.; Eickelberg, O.; Yildirim, A. Ö. Inflammaging Increases Susceptibility to Cigarette Smoke-Induced COPD. Oncotarget 2015.
50. Porter, D. W.; Hubbs, A. F.; Mercer, R. R.; Wu, N.; Wolfarth, M. G.; Sriram, K.; Leonard, S.; Battelli, L.; Schwegler-Berry, D.; Friend, S.; et al. Mouse Pulmonary Dose- and Time Course-Responses Induced by Exposure to Multi-Walled Carbon Nanotubes. Toxicology 2010, 269, 136–147.
51. Aiso, S.; Yamazaki, K.; Umeda, Y.; Asakura, M.; Kasai, T.; Takaya, M.; Toya, T.; Koda, S.; Nagano, K.; Arito, H.; et al. Pulmonary Toxicity of Intratracheally Instilled Multiwall Carbon Nanotubes in Male Fischer 344 Rats. Ind. Health 2010, 48, 783–795.

52. Madenspacher, J. H.; Azzam, K. M.; Gowdy, K. M.; Malcolm, K. C.; Nick, J. A.; Dixon, D.; Aloor, J. J.; Draper, D. W.; Guardiola, J. J.; Shatz, M.; et al. P53 Integrates Host Defense and Cell Fate During Bacterial Pneumonia. J. Exp. Med. 2013, 210, 891–904.
53. Muller, J.; Huaux, F.; Moreau, N.; Misson, P.; Heilier, J. F.; Delos, M.; Arras, M.; Fonseca, A.; Nagy, J. B.; Lison, D. Respiratory Toxicity of Multi-Wall Carbon Nanotubes. Toxicol. Appl. Pharmacol. 2005, 207, 221–231.
54. Mercer, R. R.; Hubbs, A. F.; Scabilloni, J. F.; Wang, L.; Battelli, L. a; Friend, S.; Castranova, V.; Porter, D. W. Pulmonary Fibrotic Response to Aspiration of Multi-Walled Carbon Nanotubes. Part. Fibre Toxicol. 2011, 8, 21.
55. Huaux, F.; d'Ursel de Bousies, V.; Parent, M.-A.; Orsi, M.; Uwambayinema, F.; Devosse, R.; Ibouraadaten, S.; Yakoub, Y.; Panin, N.; Palmai-Pallag, M.; et al. Mesothelioma Response to Carbon Nanotubes Is Associated with an Early and Selective Accumulation of Immunosuppressive Monocytic Cells. Part. Fibre Toxicol. 2015, 13, 46.
56. Frost, G. The Latency Period of Mesothelioma among a Cohort of British Asbestos Workers (1978-2005). Br. J. Cancer 2013, 109, 1965–1973.
57. Prazakova, S.; Thomas, P. S.; Sandrini, A.; Yates, D. H. Asbestos and the Lung in the 21st Century: An Update. Clin. Respir. J. 2014, 8, 1–10.
58. Lohcharoenkal, W.; Wang, L.; Stueckle, T. a.; Dinu, C. Z.; Castranova, V.; Liu, Y.; Rojanasakul, Y. Chronic Exposure to Carbon Nanotubes Induces Invasion of Human Mesothelial Cells through Matrix Metalloproteinase-2. ACS Nano 2013, 7, 7711–7723.
59. Luanpitpong, S.; Wang, L.; Castranova, V.; Rojanasakul, Y. Induction of Stem-like Cells with Malignant Properties by Chronic Exposure of Human Lung Epithelial Cells to Single-Walled Carbon Nanotubes. Part. Fibre Toxicol. 2014, 11, 22.

CHAPTER IV

Conclusions and Future Directions

4.1 General Conclusions

These studies have highlighted some major pathologic and mechanistic differences between tangled (t-) and rod-like (r-) multi-walled carbon nanotubes (MWCNTs). The tMWCNTs cause acute neutrophilia one-day post exposure which resolves after 21 days and 11 months. Granulomas were relatively small and condensed in the lungs of mice after 21 days and 11 months showing negligible fibrosis or chronic inflammation and no goblet cell metaplasia or epithelial hyperplasia in mice. In contrast, the rMWCNTs, which were found to be 7-fold more rigid than the tMWCNTs, resulted in both acute and chronic inflammation persisting at least 21 days post exposure, and in significantly greater airway fibrosis, TGF-β1 levels and Smad2/3 activation in the lungs of exposed mice compared to tMWCNT treatment. This was found to be through a mechanism in which STAT1 negatively regulates TGF-β1 levels and downstream signaling activation of Smad2/3. rMWCNT exposure resulted in significantly larger granulomas than tMWCNTs in both experimental protocols of one bolus dose or four consecutive doses given over four weeks. Granulomas in mice with a C57Bl/6 background are frequently associated with inducible ectopic lymphoid tissue in the lung. Interestingly, rMWCNT exposure resulted in epithelial cell hyperplasia and one rare instance of papillary hyperplasia in $p53^{+/-}$ mice after 11 months. However, no neoplasia was observed in these mice. The negative findings in this study are equally important. The lack of MWCNT-induced neoplasia or fibrosis 11 months following initial exposure may result from using a mouse

model instead of a rat model. Also, the length of this study may have limited our observations of hyperplastic and neoplastic events. A study published recently reported that direct pulmonary exposure of MWCNTs over 104-109 weeks in rats to resulted in adenoma and adenocarcinoma development [1,2]. These studies were over twice as long as our 11 month, or roughly 44 week exposure. These studies highlight the importance of CNT physicochemical differences (i.e. rigidity) in susceptible mouse models that result in differential pulmonary pathologic outcomes.

The question of how relatable MWCNTs are to asbestos appears to be a bigger question than anticipated. As MWCNTs are not all made alike, they may need to be analyzed on a case-by-case basis with a full understanding of their intrinsic physicochemical properties. The body of literature is growing on these materials, but the number of types of manufactured MWCNTs available is growing faster. From these two *in vivo* studies completed in *Stat1*$^{-/-}$ mice and p53$^{+/-}$ mice, it is clear that the two MWCNTs evaluated result in drastically different disease states in mice. The rMWCNTs resulted in significantly greater fibrosis compared to tMWCNT and this process was regulated by STAT1. While the rMWCNT have been classified by the International Agency for Research on Cancer (IARC) as group 2B possible human carcinogens, the carcinogenic potential of a variety of different types of carbon nanotubes remains elusive and represents a challenge for assessing the hazard of these emerging materials on human health.

Further investigation into the mechanism of MWCNT-induced pulmonary fibrosis is key to understanding how this disease develops, what biomarkers to measure in humans exposed to MWCNTs, and how to best treat this disease. The mechanism of pulmonary fibrosis in this study was derived from total lung protein from 129SvJ background mice 21 days post t- or r-MWCNT exposure. The densitometry analysis was completed on immunoblots of total and activated Smad2/3 protein. To thoroughly investigate STAT1 regulation of fibroblast activation and fibrogenesis in response to MWCNT in *Stat1*$^{-/-}$ mouse lungs compared to *Stat1*$^{+/+}$, primary mouse lung fibroblasts were isolated from these mice and exposed to t- or r-MWCNTs *in vitro*. Previously published work from Wang *et al*. showed increased TGF-β1-receptor, Smad2, and phosphorylated Smad2 in 3T3-L1 fibroblasts exposed to MWCNTs *in vitro* [3]. Unfortunately, in my study the MWCNTs seemed to float above the cellular layer and did not interact with the fibroblasts nor did they elicit a fibrogenic response. MWCNTs were administered in conjunction with pro-fibrogenic growth factors TGF-β1 or PDGF-BB, however there was only a growth factor response observed in the primary fibroblasts and no tube difference. Macrophage cell lines offered a much more robust response to MWCNT *in vitro*. Primary bone marrow derived macrophages (BMDM) were isolated from *Stat1*$^{+/+}$ and *Stat1*$^{-/-}$ mice and exposed to increasing doses of t- or r- MWCNTs as shown in Appendix C.1. Total mRNA was collected and run through qPCR for fibrogenic targets TGF-β1 and PDGF-BB. Interestingly, *Stat1*$^{-/-}$ BMDMs had significantly higher transcription of these targets in a dose responsive manner for TGF-β1 (Appendix C.2) and PDGF-BB (Appendix C.3). A murine immortalized macrophage line, RAW264.7 was also exposed to the same MWCNTs using this

method and was found to have a time course related increase in TGF-β1 production with tMWCNT exposure, and was exaggerated with rMWCNT exposure (Appendix C.4). The mechanism of MWCNT-induced fibrosis is poorly understood, and there are some practical barriers to teasing out its mechanism. However, this mechanism seems to be macrophage mediated, where *Stat1*$^{-/-}$ macrophages produce significantly greater TGF-β1 and PDGF-BB mRNA 24 hours following MWCNT exposure *in vitro*, and RAW264.7 macrophages produce greater TGF-β1 over a matter of days after exposure to either t- or r- MWCNT. We have shown in prior studies that primary fibroblasts isolated from *Stat1*$^{-/-}$ mice produce significantly more collagen mRNA and protein than *Stat1*$^{+/+}$ primary mouse lung fibroblasts with TGF-β1 stimulation [4]. A better understanding of the mechanism of MWCNT-induced pulmonary fibrosis will help to provide alternate understanding to the progression of this disease state.

The neoplastic potential of these materials seems to lie in the mouse model as well as the choice of tumor suppressor chosen. While p53 is arguably the most mutated gene found in cancers, the *CDKN2A-CDKN2B* locus is frequently deleted in cancers, and is the most common genetic aberration found in mesothelioma from both humans and rodents [5-10]. The cyclin-dependent kinase inhibitor 2A (CDKN2A)-CDKN2B locus encodes three tumor-suppressor proteins $p15^{INK4B}$, $p14^{ARF}$ ($p19^{ARF}$ in mice), and $p16^{INK4A}$ which have been extensively reviewed [11]. The protein products of these sequences inhibit cyclin D-dependent CDK4 and CDK6, thereby inhibiting activation of retinoblastoma protein (RB). ARF binds MDM2 E3 ubiquitin ligase and prevents p53 degradation by ubiquitylation and facilitates p53 activation. Notably, in one

of the intraperitoneal injection exposures of rats to MWCNTs where mesothelioma developed, these tumors were tested for genomic alterations by comparative genomic hybridization and homozygous deletions were found in Cdkn2a/2b in almost all the tumors tested [10]. Future work may focus on susceptibility in models more relevant to cancers observed from asbestos related disease states.

This work in Chapter II has elucidated a novel mechanism of STAT1 regulation of TGF-β1 and downstream activation of signaling molecules in MWCNT-induced fibrosis. Chapter II and III have found novel immunologic effects of MWCNTs not reported previously. These studies highlight the need for expanding our understanding of MWCNT physicochemical properties to better asses the risk of pulmonary toxicity. Future work should focus on coupling characterization of MWCNT characteristics with toxicologic and mechanistic studies to better compare tube types and understand how these physicochemical properties influence toxicity.

4.2 Future Directions

Future work investigating MWCNTs should focus on characterizing physicochemical characteristics to better categorize materials for a proper risk assessment. Length, rigidity, metal content, CNT coating and other properties have been linked to severity of disease and could be exceptionally useful for novel MWCNTs safety assessments. These properties could also be useful in the research and development steps of designing new MWCNTs as well. While safe handling and production of CNTs is key to protecting individuals, exposure does

happen and we, as a society need to best understand what the risks are from this exposure. Further studies are needed to better understand the potential for these materials to cause fibrosis in other sub populations who have co-exposure to other materials or allergens, co-morbidities like asthma, sarcoidosis, autoimmune diseases, or obesity, and in susceptible populations accounting for age and genetic predispositions.

4.3 References

1. Suzui, M.; Futakuchi, M.; Fukamachi, K.; Numano, T.; Abdelgied, M.; Takahashi, S.; Ohnishi, M.; Omori, T.; Tsuruoka, S.; Hirose, A.; et al. Multiwalled Carbon Nanotubes Intratracheally Instilled into the Rat Lung Induce Development of Pleural Malignant Mesothelioma and Lung Tumors. Cancer Sci. 2016, 107, 924–935.

2. Kasai, T.; Umeda, Y.; Ohnishi, M.; Mine, T.; Kondo, H.; Takeuchi, T. Lung Carcinogenicity of Inhaled Multi- Walled Carbon Nanotube in Rats. Part. Fibre Toxicol. 2016, 1–19.

3. Wang, P.; Nie, X.; Wang, Y.; Li, Y.; Ge, C.; Zhang, L.; Wang, L.; Bai, R.; Chen, Z.; Zhao, Y.; et al. Multiwall Carbon Nanotubes Mediate Macrophage Activation and Promote Pulmonary Fibrosis through TGF-B/smad Signaling Pathway. Small 2013, 9, 3799–3811.

4. Thompson, E. A.; Sayers, B. C.; Glista-Baker, E. E.; Shipkowski, K. A.; Ihrie, M. D.; Duke, K. S.; Taylor, A. J.; Bonner, J. C. Role of Signal Transducer and Activator of Transcription 1 in Murine Allergen-Induced Airway Remodeling and Exacerbation by Carbon Nanotubes. Am. J. Respir. Cell Mol. Biol. 2015, 53, 625–636.

5. Cheng, J. Q.; Jhanwar, S. C.; Klein, W. M.; Bell, D. W.; Lee, W. C.; Altomare, D. A.; Nobori, T.; Olopade, O. I.; Buckler, A. J.; Testa, J. R. p16 Alterations and Deletion Mapping of 9p21-p22 in Malignant Mesothelioma. Cancer Res. 1994, 54, 5547–5551.

6. Illei, P. B.; Rusch, V. W.; Zakowski, M. F.; Ladanyi, M. Homozygous Deletion of CDKN2A and Codeletion of the Methylthioadenosine Phosphorylase Gene in the Majority of Pleural Mesotheliomas. Clin. Cancer Res. 2003, 9, 2108–2113.

7. Krasinskas, A. M.; Bartlett, D. L.; Cieply, K.; Dacic, S. CDKN2A and MTAP Deletions in Peritoneal Mesotheliomas Are Correlated with Loss of p16 Protein Expression and Poor Survival. Mod. Pathol. 2010, 23, 531–538.

8. Altomare, D. A.; Vaslet, C. A.; Skele, K. L.; De Rienzo, A.; Devarajan, K.; Jhanwar, S. C.; McClatchey, A. I.; Kane, A. B.; Testa, J. R. A Mouse Model Recapitulating Molecular Features of Human Mesothelioma. Cancer Res. 2005, 65, 8090–8095.

9. Jean, D.; Thomas, E.; Manié, E.; Renier, A.; de Reynies, A.; Lecomte, C.; Andujar, P.; Fleury-Feith, J.; Galateau-Sallé, F.; Giovannini, M.; et al. Syntenic Relationships between Genomic Profiles of Fiber-Induced Murine and Human Malignant Mesothelioma. Am. J. Pathol. 2011, 178, 881–894.

10. Nagai, H.; Okazaki, Y.; Chew, S.; Misawa, N.; Yamashita, Y.; Akatsuka, S.; Ishihara, T.; Yamashita, K.; Yoshikawa, Y.; Yasui, H.; et al. Diameter and Rigidity of Multiwalled Carbon Nanotubes Are Critical Factors in Mesothelial Injury and Carcinogenesis. 2011.

11. Sharpless, N. E.; Sherr, C. J. Forging a Signature of in Vivo Senescence. Nat. Rev. Cancer 2015, 15, 397–408.

REFERENCES

[Insert your References here. Format and location depends on your style guide.]

APPENDICES

APPENDIX A

Supplemental Tables and Figures: Chapter II

Physicochemical parameters of tangled (t) and rigid(r) multi-walled carbon nanotubes (MWCNTs).

MWCNT	Manufacturer	Bending ratio (D_b)	Catalyst	Trace catalyst	Length	Width
tMWCNT	Helix Material Solutions Inc., Richardson, TX	0.162620909	Nickel	5.3%[a]	0.3-50 µm[a]	30-50 nm[a]
rMWCNT	Mitsui & Co, Ltd., Tokyo Japan	0.899625693	Iron	0.32%[b]	3.86 µm[b]	49 ±13.4 nm[b]

[a] Ryman-Rassmussen et al., 2009 (Ref. 7)
[b] Porter *et al.*, 2010 (Ref.10)

Appendix A.1. Physicochemical parameters of tangled (t) and rigid(r) multi-walled carbon nanotubes (MWCNTs).

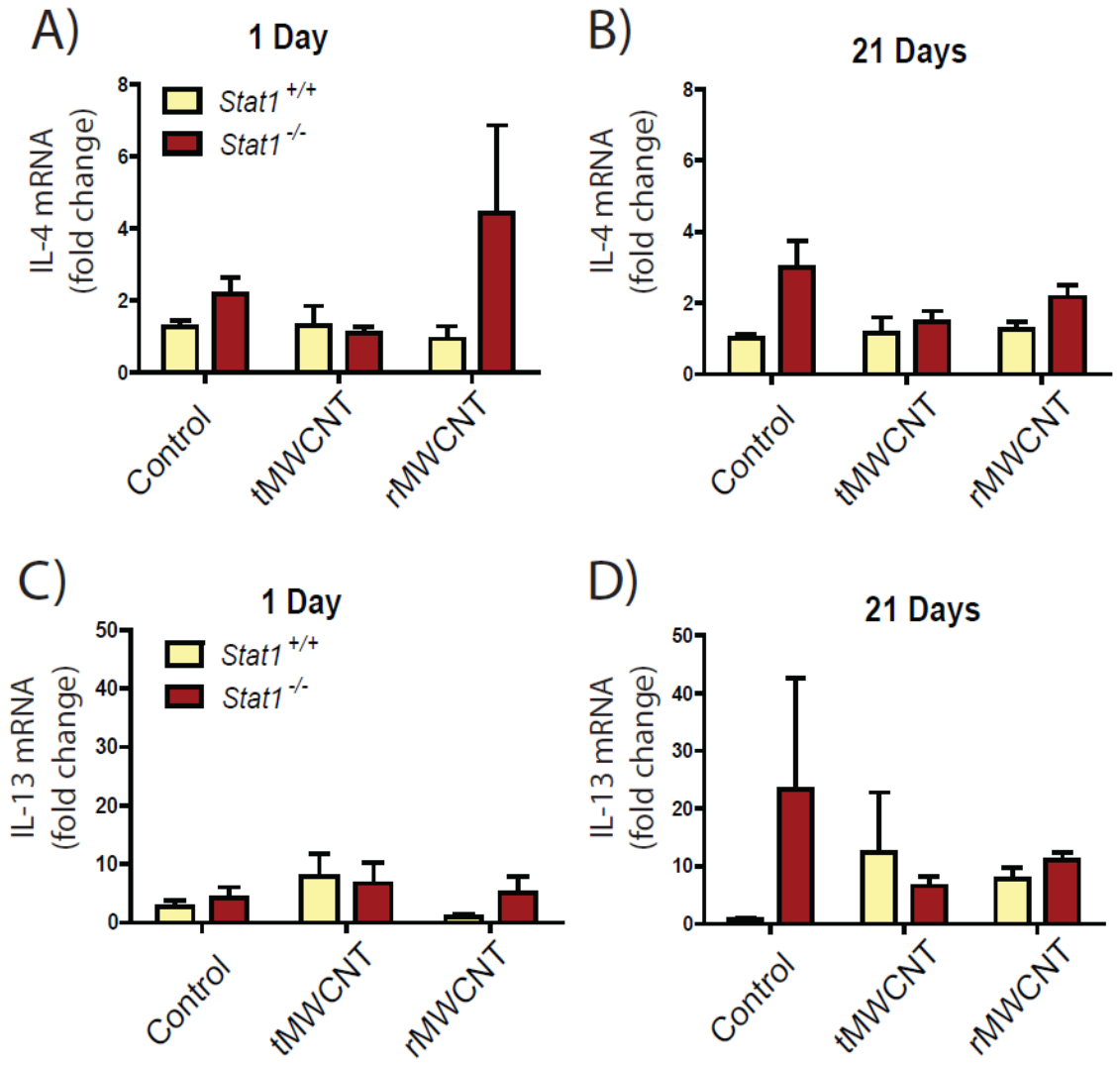

Appendix A.2. Interleukin-4 (IL-4) and IL-13 mRNA expression in *Stat1*$^{+/+}$ and *Stat1*$^{-/-}$ mouse lungs after exposure to tMWCNTs or rMWCNTs. **A)** Fold change in IL-4 mRNA at one and **B)** 21 days post exposure. **C)** Fold change in IL-13 mRNA expression at one and **D)** 21 days post exposure. Expression of mRNA normalized to β2-microglobulin (B2M).

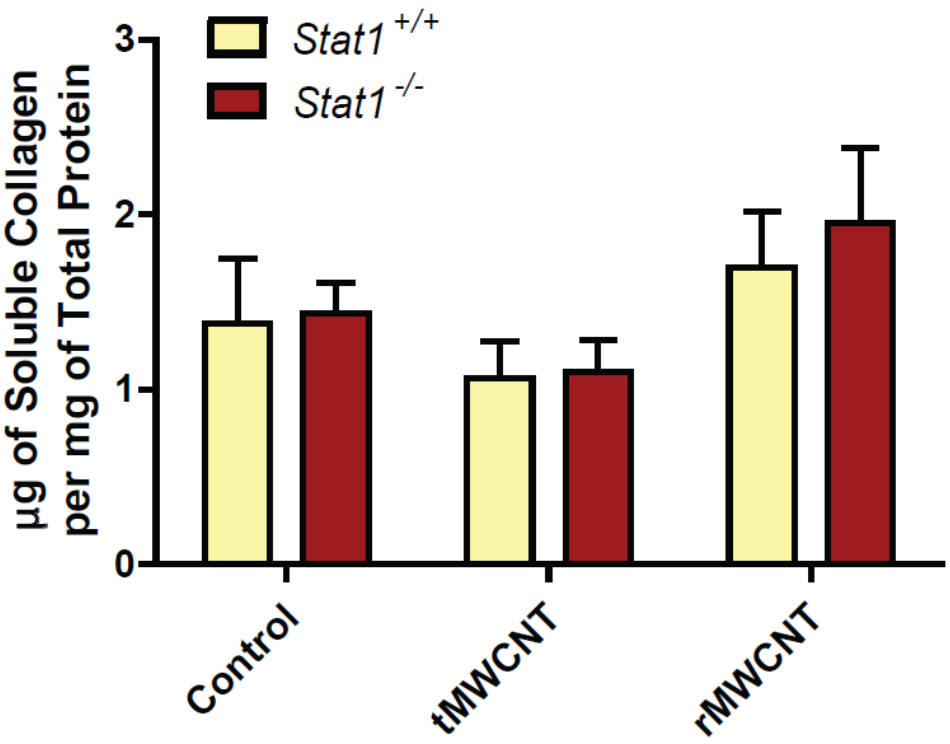

Appendix A.3. Soluble collagen content measured from mouse lungs 21 days post exposure. Average soluble collagen concentration per lung in each respective treatment after 21 days of exposure to control, tMWCNTs, or rMWCNTs normalized to protein content of sample.

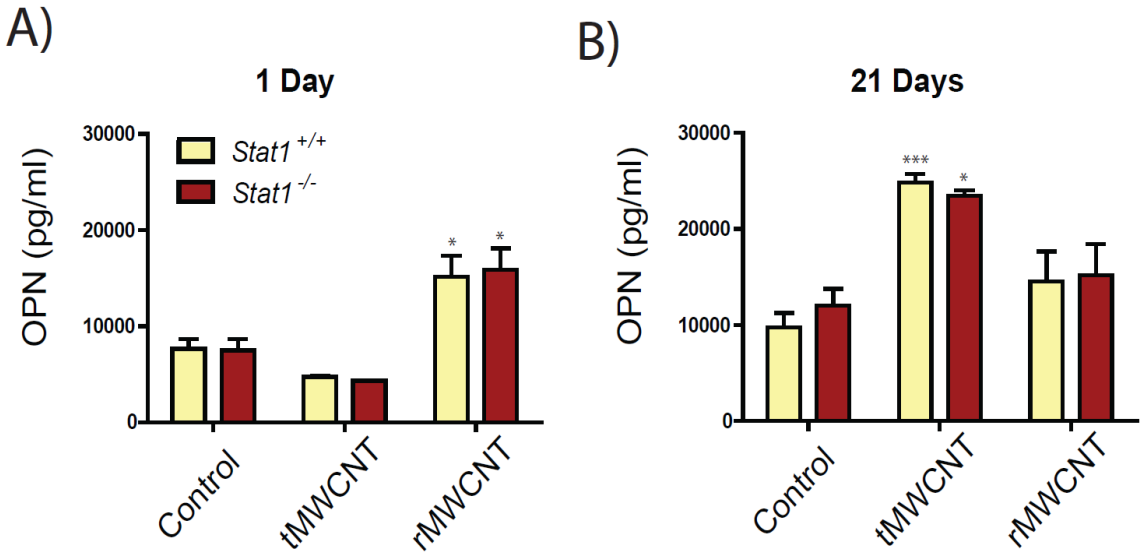

Appendix A.4. Osteopontin (OPN) protein levels in lungs from *Stat1*$^{+/+}$ and *Stat1*$^{-/-}$ mice after one and 21 days of exposure to tMWCNTs or rMWCNTs. **A)** OPN protein in BALF after one and **B)** 21 days exposure to vehicle, tMWCNTs, or rMWCNTs as measured by ELISA (*$p<0.05$ or ***$p<0.001$ compared to control).

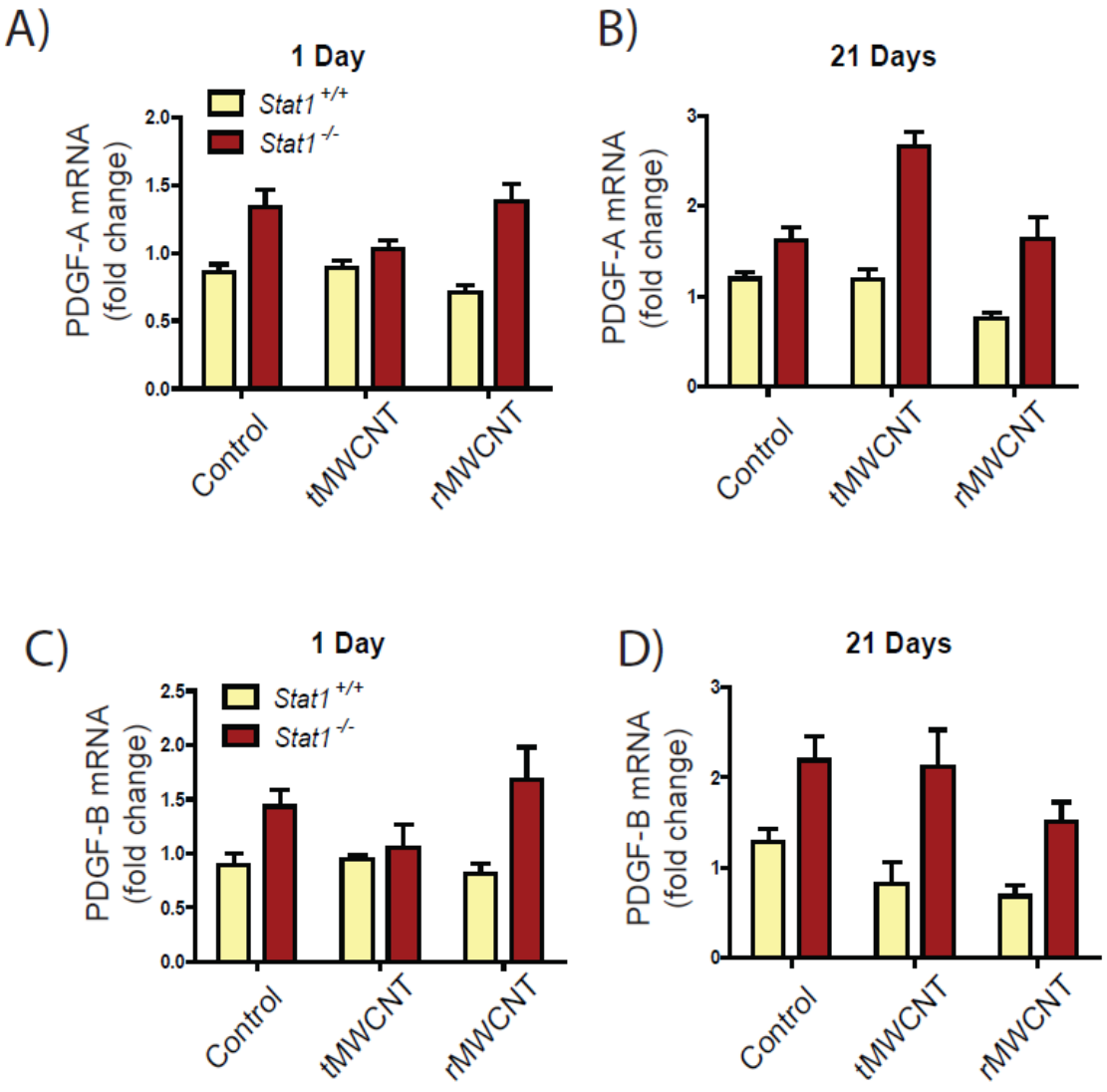

Appendix A.5. Platelet derived growth factor (PDGF) -A and -B expression in *Stat1*$^{+/+}$ and *Stat1*$^{-/-}$ mouse lungs after exposure to tMWCNTs or rMWCNTs. **A)** Fold change in PDGF-A mRNA at one and **B)** 21 days post exposure. **C)** Fold change in PDGF-B mRNA expression at one and **D)** 21 days post exposure. Expression of mRNA normalized to B2M.

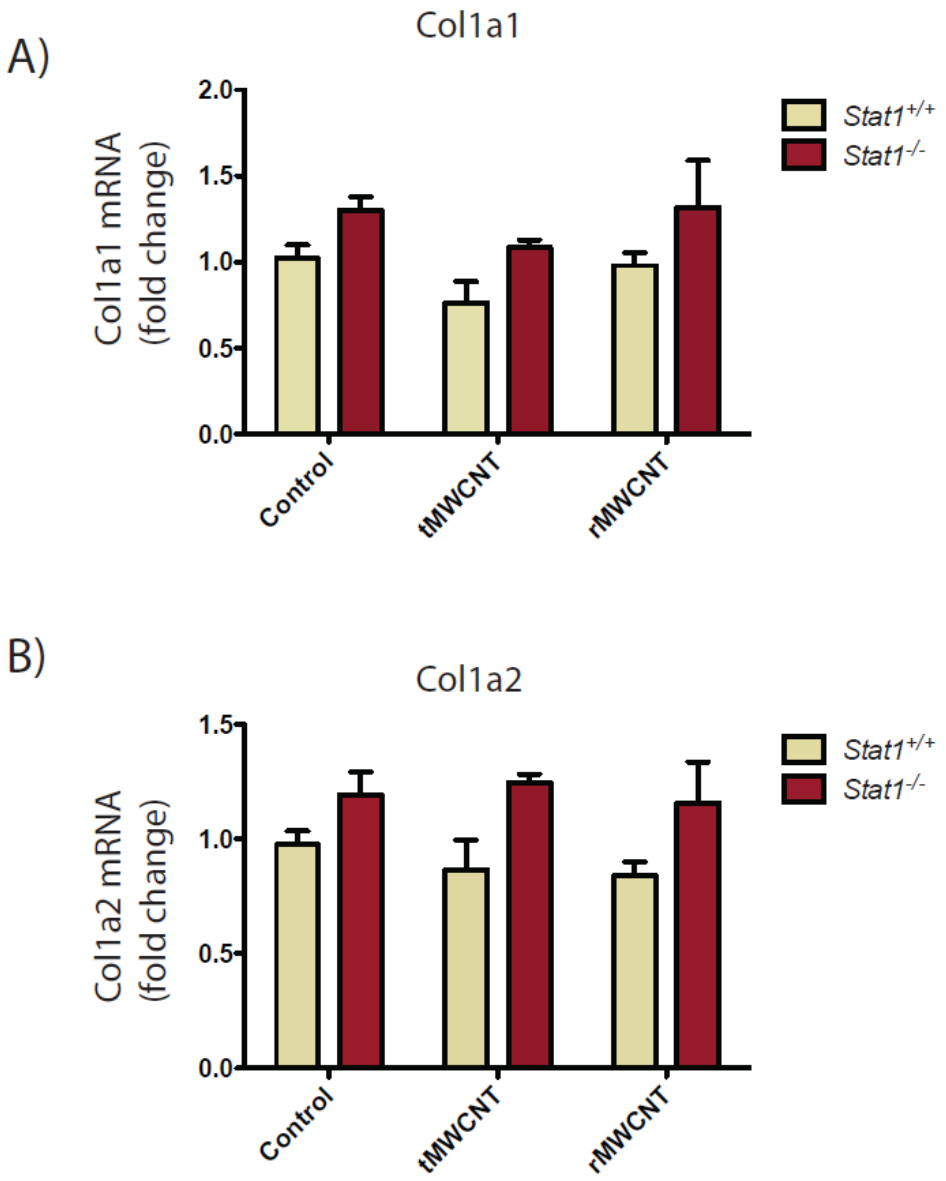

Appendix A.6. Expression levels of collagen mRNAs determined via Taqman qRT-PCR of RNA isolated from mouse lungs 21 days post exposure. **A)** Fold change in Col1a1 and **B)** Col1a2 mRNA expression after 21 days post exposure. Expression of mRNA levels normalized to B2M.

APPENDIX B

Supplemental Tables and Figures: Chapter III

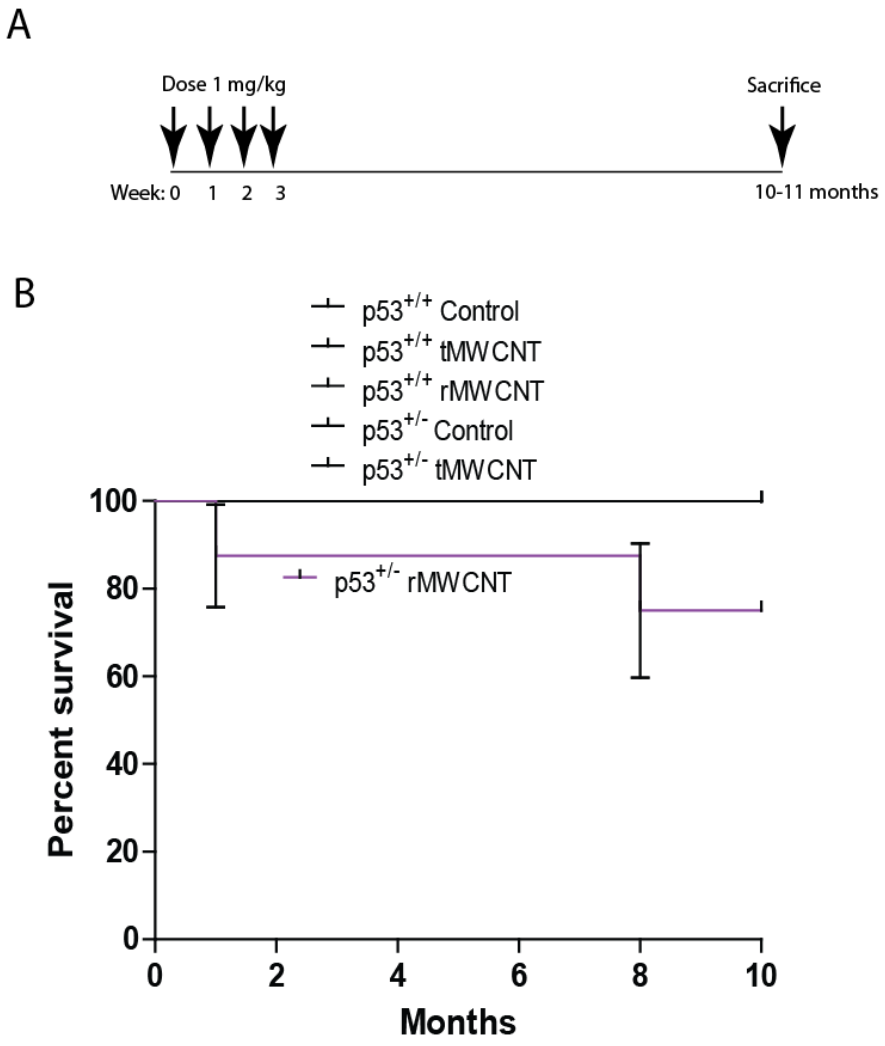

Appendix B.1. Experimental design and survival curve from animal exposures. A) Depiction of experimental set up and dosing indicating that one dose of 1 mg/kg t- or r- MWCNTs was given once a week for four weeks and sacrificed 11 months following the initial dose. B) Survival curve of all mouse groups where the $p53^{+/-}$ group exposed to rMWCNTs were the only to suffer unplanned casualties.

Genotype	Treatment	Number per Sex		Excluded Mice
		M	F	
C57 Wildtype	0.1% Pluronic	9	1	N/A
C57 Wildtype	tMWCNT	10	0	N/A
C57 Wildtype	rMWCNT	8	0	N/A
p53 $^{+/-}$ Het	0.1% Pluronic	9	5	N/A
p53 $^{+/-}$ Het	tMWCNT	3	5/6	1 Female: Lymphoma
p53 $^{+/-}$ Het	rMWCNT	5/8	0	3 Males: 2 early termination, 1 Pulmonary alveolar proteinosis

Appendix B.2. Table of mouse treatments, sex, and exclusions. Animal number and biological makeup per treatment group.

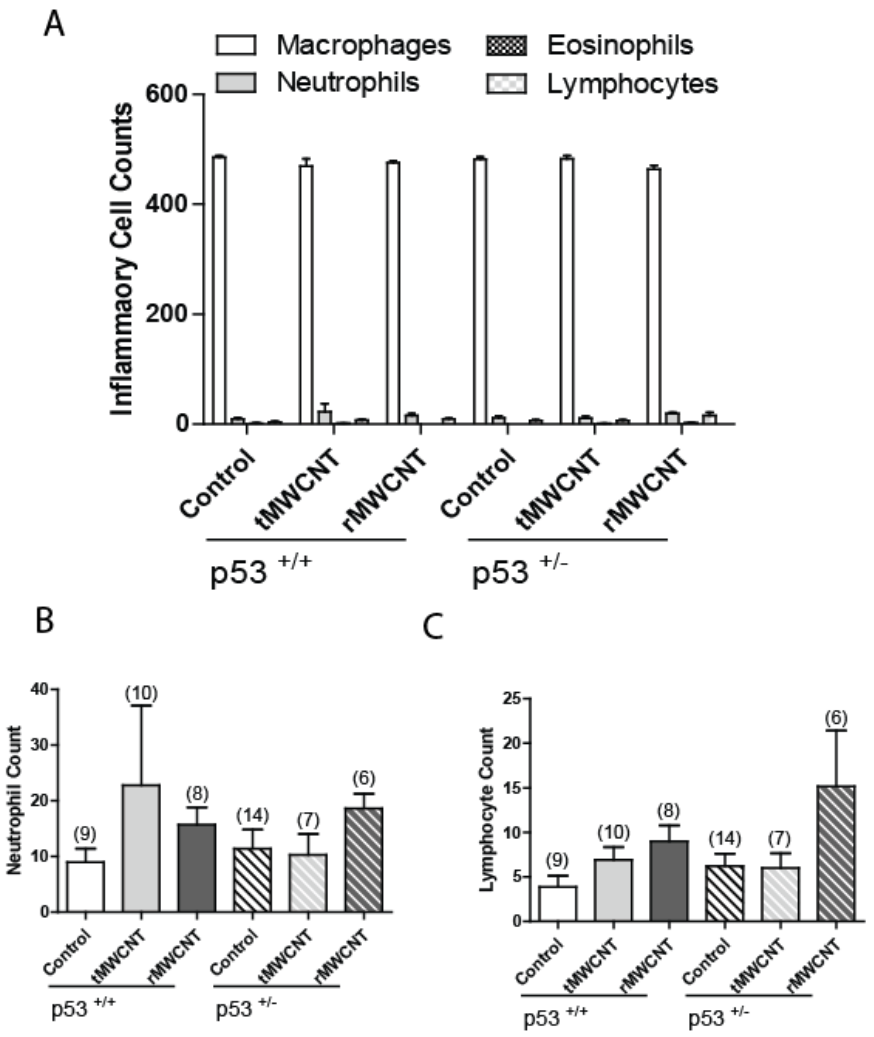

Appendix B.3. Differential cell counts. A) Differential cell counts were made by counting 500 cells and categorizing them as a macrophage, neutrophil, eosinophil or lymphocyte. B) Number of neutrophil and C) lymphocytes in the differential cell counts.

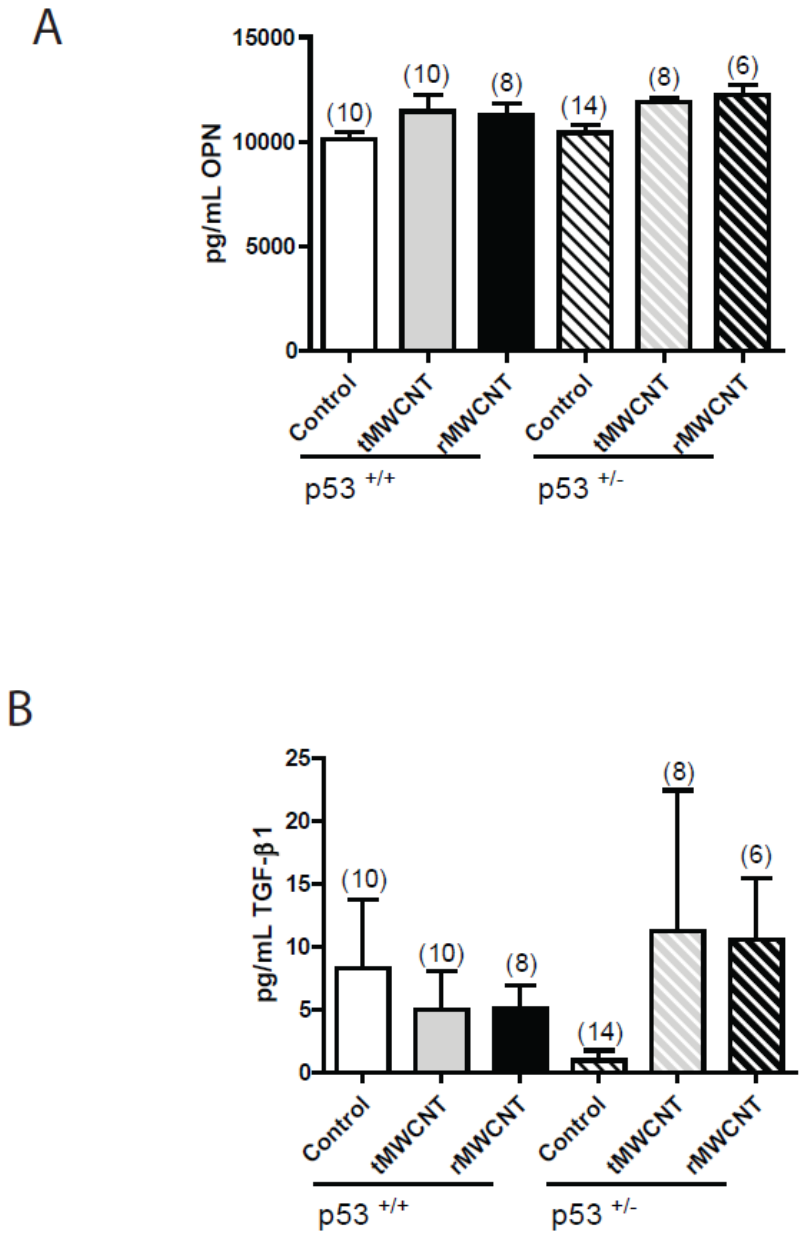

Appendix B.4. Inflammatory cytokine levels. Bronchiolo-alveolar lavage fluid was run through an ELISA to measure levels of A) osteopontin (OPN) and B) TGF-β1.

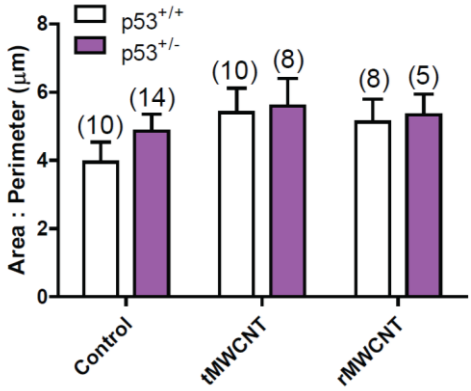

Appendix B.5. Airway fibrosis. Average area to perimeter ratios of airways as measured by quantitative morphometry and averaged per mouse. Graphed here are average values per group of mice in each treatment group.

APPENDIX C

Supplemental Figures: Chapter IV

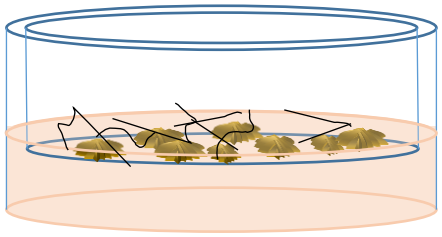

Appendix C.1. Experimental set-up of bone marrow derived macrophage (BMDM) experimentation. BMDMs were grown submerged in media on a porous insert until confluent. Upon confluence, media was removed and only replaced below insert, MWCNT were applied directly to cell layer insert and incubated at 37^{o}C for 24 hours before supernatant and mRNA collection.

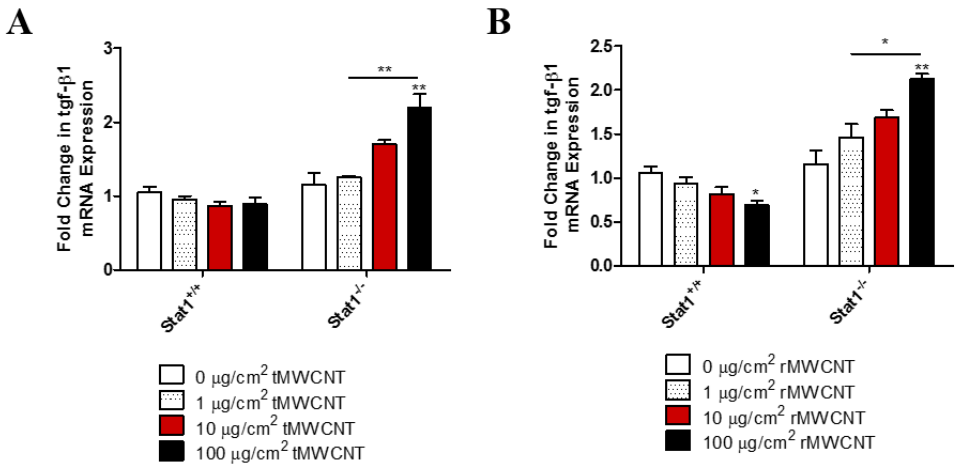

Appendix C.2. TGF-β1 mRNA levels measured from bone marrow derived macrophages (BMDM). BMDM were isolated from *Stat1*$^{+/+}$ and *Stat1*$^{-/-}$ mice. These cells were grown on inserts and exposed to minimal supernatant, tMWCNTs or rMWCNTs. After 24 hours exposure total mRNA was collected and tested for TGF-β1 by qRT-PCR.

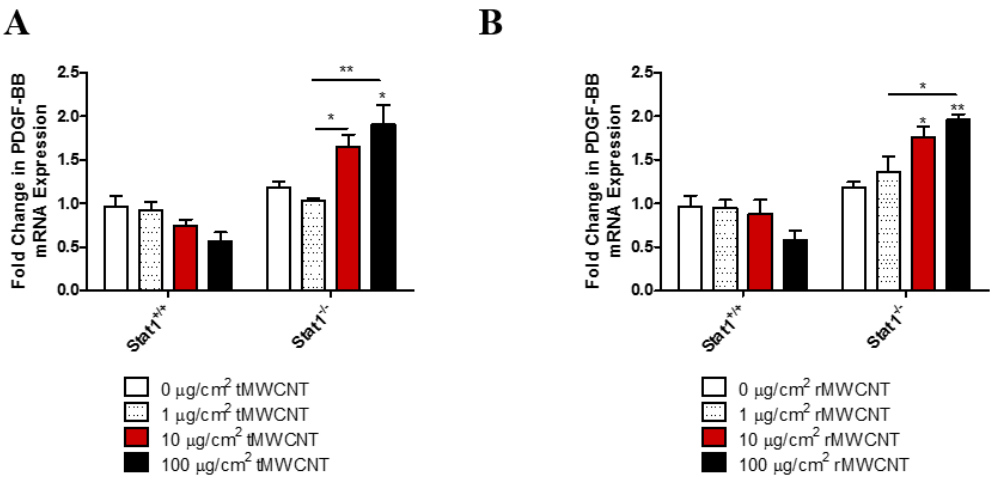

Appendix C.3. PDGF-BB mRNA levels measured from bone marrow derived macrophages (BMDM). BMDM were isolated from *Stat1*$^{+/+}$ and *Stat1*$^{-/-}$ mice. These cells were grown on inserts and exposed to minimal supernatant, tMWCNTs or rMWCNTs. After 24 hours exposure total mRNA was collected and tested for PDGF-BB by qRT-PCR.

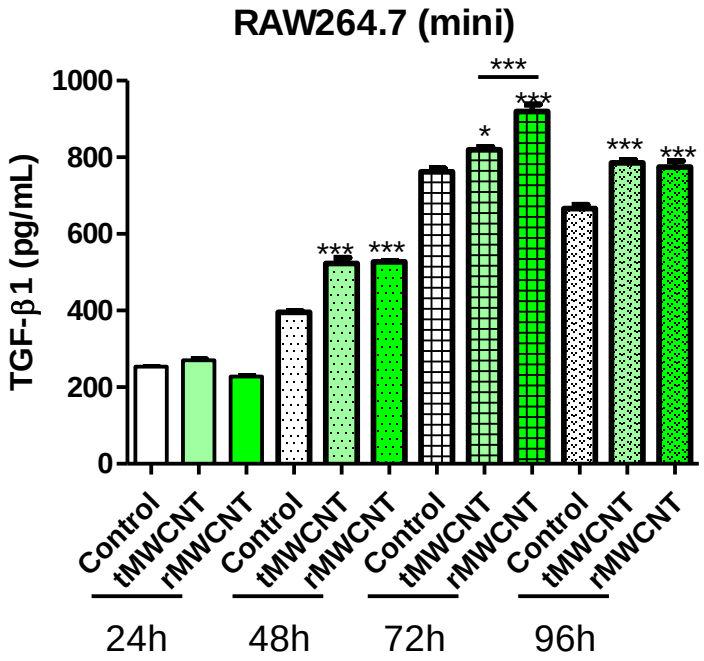

Appendix C.4. TGF-β1 levels measured using supernatant from RAW264.7 macrophages. RAW264.7 macrophages were grown to confluence in an insert, once confluent they were kept in serum free media prior to treatment with 10 µg/µL t- or r- MWCNT or vehicle. Supernatant was collected after 24, 48, 72, and 96 hours and run on a TGF-β1 ELISA.